The Institute of Paper Chemistry

Appleton, Wisconsin

Doctor's Dissertation

The Role of Particle Size and Molecular Weight on the Adsorption and Flocculation of Polystyrene Latex With Poly (1,2-Dimethyl-5-Vinylpyridinium Bromide)

Alan R. Eggert

June, 1976

THE ROLE OF PARTICLE SIZE AND MOLECULAR WEIGHT ON THE ADSORPTION AND FLOCCULATION OF POLYSTYRENE LATEX WITH POLY(1,2-DIMETHYL-5-VINYLPYRIDINIUM BROMIDE)

A thesis submitted by

Alan R. Eggert

B.A. 1971, Ripon College

M.S. 1973, Lawrence University

in partial fulfillment of the requirements
of The Institute of Paper Chemistry
for the degree of Doctor of Philosophy
from Lawrence University,
Appleton, Wisconsin

June, 1976

TABLE OF CONTENTS

	Page
SUMMARY	1
INTRODUCTION	4
GENERAL ASPECTS OF COLLOIDAL STABILITY	6
DLVO THEORY	10
Adsorption-Bridging	12
Electrostatic Patch Model	14
Flocculation by Polyelectrolytes of Opposite Sign to the Particle	14
Effect of Particle Size	16
Adsorbed Polymer Configuration	16
PRESENTATION OF THE PROBLEM AND THESIS OBJECTIVES	21
GENERAL APPROACH	22
EXPERIMENTAL MATERIALS, EQUIPMENT AND PROCEDURES	23
Adsorption-Flocculation Experiments	24
POLYMER ADSORPTION — RESULTS AND DISCUSSION	27
Rate of Polymer Adsorption	27
Effect of Poly(DMVPB) Concentration	27
Saturation Adsorption	30
Molecular Weight Effect	31
Effect of Ionic Strength	33
Effect of Particle Size	34
Equilibrium Adsorption Isotherms	36
Adsorption Configuration	38
Nonequilibrium Adsorption Configuration	38
Polymer Configuration at Saturation Adsorption	40
FLOCCULATION RESULTS	44
Description of Flocculation Curve	44
Results	46

Page

Effect of PSL Concentration 46

Critical Flocculation Concentration 46

Effect of Molecular Weight 49

Effect of Salt Concentration 50

Effect of Surface Charge Density and Particle Size 50

Optimum Flocculation Concentration 55

Effect of Molecular Weight 55

Effect of Salt Concentration 58

Effect of Surface Charge Density and Particle Size 59

Point of Charge Neutralization 61

Restabilization Concentration 64

Flocculation Curves 65

Summary of Flocculation 69

DISCUSSION OF FLOCCULATION RESULTS 70

The Bridging Model 70

The Charge Neutralization Model 77

The Electrostatic Patch Model 77

Existence of Electrostatic Patch 78

Effect of Electrostatic Patches on DLVO Theory 79

Effect of Patch Size 83

Recapitulation 88

ACKNOWLEDGMENTS 89

NOMENCLATURE 90

LITERATURE CITED 92

APPENDIX I. THE CHARACTERIZATION OF POLYSTYRENE LATEX PARTICLES 97

APPENDIX II. POLYMER SYNTHESIS AND CHARACTERIZATION 111

Page

APPENDIX III. ADSORPTION DATA 150

APPENDIX IV. ADSORPTION AND FLOCCULATION DATA 151

APPENDIX V. DUPLICATED FLOCCULATION RUNS 187

APPENDIX VI. THE CFC AND OFC VALUES FOR THE CONSTANT PARTICLE EXPERIMENT 190

SUMMARY

The objective of this thesis was to determine the interrelationship between polymer molecular weight and colloidal particle size in the ability of a cationic polyelectrolyte to initiate flocculation in an anionic colloidal dispersion. This interrelationship was evaluated in a poly(1,2-dimethyl-5-vinylpyridinium bromide)-water-polystyrene latex (PSL) system under various conditions of ionic strength. The experimental program was divided into three sections: 1) the characterization of polystyrene latex particles, 2) the characterization of poly(DMVPB), and 3) the investigation of the adsorption and subsequent flocculation of polystyrene latex by poly(DMVPB).

Dow Uniform Latex Particles were obtained from the Dow Chemical Company having particle diameters of 0.109, 0.234, 0.481, 0.794, and 1.101 μm. Emulsifier was removed from the particle surface by a mixed bed ion exchange method. An additional PSL, particle size 0.330 μm prepared without emulsifiers, was also used in this study. The electric charge carried by the PSL particles was characterized by standard potentiometric and electrophoretic mobility methods. Surface charge density increased with increasing particle size, which is characteristic of the Dow Uniform Latex Particle.

Poly(DMVPB) was synthesized via a free radical pathway. Two narrow molecular weight fractions of poly(DMVPB) were obtained by gel permeation chromatography using Bio-Glas as the fractionating bed. The polymer molecular weights were determined by light scattering and sedimentation equilibrium techniques and found to be 3.3×10^4 and 10^6. The solution size of poly(DMVPB) was calculated from light scattering data, from intrinsic viscosity and diffusion coefficient determinations using the Einstein-Stokes and Stokes equation.

Adsorption isotherms showed that up to the point of charge neutralization, all of the polymer added is adsorbed onto the PSL particle surface. At higher concentrations the amount adsorbed increased only slightly with polymer concentration, and a plateau region was reached. The saturation adsorption data indicated that the amount of poly(DMVPB) adsorbed onto PSL particles increased with ionic strength but only slightly with increasing polymer molecular weight. Also the radius of curvature was found to have little, if any, effect on the amount of polymer adsorbed per unit area. Equilibrium adsorption isotherms of both polymer molecular weights showed that the adsorption behavior could be adequately described by Langmuir type adsorption. Based on an empirical equation, the equilibrium adsorption configuration in the plateau region was concluded to be relatively flat with small loops but no loops or dangling ends extending far out into the solution.

The flocculation of the poly(DMVPB)-water-PSL system was followed by a turbidity method. Along the flocculation curve, four points were determined: 1) the critical flocculation concentration (CFC), 2) the optimum flocculation concentration (OFC), 3) the point of charge neutralization, and 4) the restabilization concentration (RSC).

The CFC occurred at a relatively low adsorption level (1-10% based on saturation adsorption) and highly negative zeta potential values. The CFC was found to decrease with increasing polymer molecular weight and salt concentration. Also the CFC decreased as the particle size and surface charge density decreased.

Optimum flocculation occurred after 7-17% adsorption. Zeta potential values at OFC were negative. There was no dependence of polymer molecular weight in both salt concentrations, indicating polymer charge is the

important factor. Again, the OFC decreased with decreasing particle size and surface charge density.

The point of charge neutralization and RSC were also independent of polymer molecular weight. A characteristic of the flocculation curves was the broad flocculation zone which increased with polymer molecular weight.

The findings from the adsorption-flocculation study were consistent with an electrostatic patch flocculation mechanism. However, at high PSL particle concentrations, nonequilibrium bridging flocculation may occur with high molecular weight polymers.

INTRODUCTION

The main use for polymeric flocculants is to facilitate the separation of colloidal suspended solids from water. The size of the dispersed particles commonly ranges from the submicroscopic (clay particles down to 0.01 μm) through the micron range (bacteria and algae), up to silts and slimes containing particles 20 μm or more. Conventional separation methods of filtration, settling, or centrifugation fail with colloidal suspensions because of their stability due to surface charges, which keep the particles separate and discrete. It has long been known that the only practical way of treating colloidal suspensions is first to operate on their surface chemistry in order to induce aggregation, and then, when the flocs have grown as large as possible, to separate them off by settling or filtration. An "optimum dosage" of the flocculant produces the largest flocs, greatest sediment volume, minimum residual turbidity, and most permeable filter-cake. If more than the optimum quantity of polymer is added the efficiency of flocculation is reduced, and with great excess, the system may pass into a permanently stabilized condition.

Today polymeric flocculants have wide application in a variety of fields, although a detailed understanding of their flocculation mechanism has not yet been achieved. The choice of polymer in any particular case still has to be made largely on an empirical basis. Three mechanisms of aggregation of colloidal particles have been postulated: 1) charge neutralization by the use of inorganic electrolytes, allowing the attractive Van der Waals forces to implement aggregation, 2) bridging by the use of large polymeric materials, where the physical interaction of polymer and colloidal particles lead to aggregation, and 3) the patch model, where electrostatic charge

interactions initiate flocculation. The concept of bridging between particles is now well established when polyelectrolytes have the same sign as the particles or with nonionic polymers. Where colloidal particles are flocculated by oppositely charged polymers, charge neutralization or electrostatic attraction may play a significant or even dominant part. This makes LaMer's (1) distinction between "coagulation" and "flocculation" difficult to apply; therefore, only the latter term will be used.

GENERAL ASPECTS OF COLLOID STABILITY

Colloidal suspensions are thermodynamically unstable since the free energy of the aggregated state is lower than the free energy of the dispersed state. Nonaggregating suspensions generally are the result of electrostatic repulsion barriers which cause the particles to exist in metastable states. The distance of closest approach between colloidal particle surfaces can also be physically hindered by the degree of hydration of the colloidal surfaces; however, this mechanism is important only when considering extremely short-range particle interactions since the adsorbed layer of water is only a few molecules thick (2).

Colloidal systems remain in metastable, dispersed states if the repulsion barrier is large with respect to the kinetic (or thermal) energy of the particles. To account for this repulsion barrier, an electrical double layer model was proposed. In 1879, Helmholtz (3) described a capacitor model, consisting of a charged surface with a parallel layer of counterions in the liquid phase near the interface. Later, Gouy (4) and Chapman (5) independently proposed a model which described a diffuse layer of immobile counterions. Stern (6) modified the Gouy-Chapman model to include an immobile, inner region of adsorbed ions with finite ionic sizes. Stern's model, with an immobile, inner layer of adsorbed ions (Stern layer) and a mobile, diffuse outer layer of counterions and coions (Gouy-Chapman or diffuse layer), is the basis for the present day concept of the electrical double layer.

Figure 1 shows the Gouy-Chapman-Stern model of the electrical double layer. The electrically charged surface acquires its charge from either direct surface ionization, preferential adsorption of certain ions from solution at specific sites on the surface or by isomorphous lattice

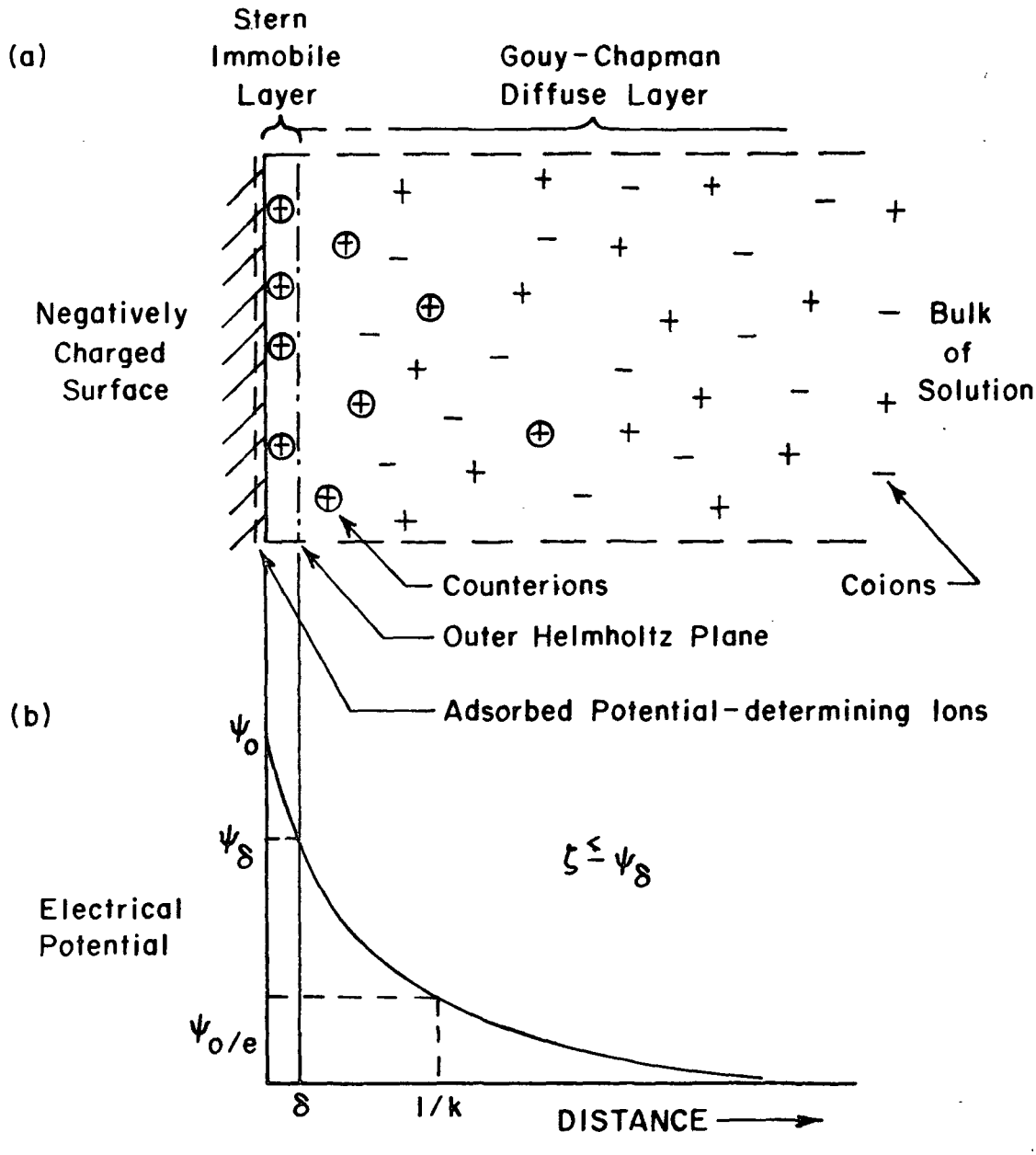

Figure 1a. Model of the Electric Double Layer. The Marked Counterions Represent the Ions in Excess Compared to the Bulk Phase. The Number of Counterions Equals the Number of Negative Charges on the Surface. The Coions are the Nonadsorbed Ions That Have the Same Charge as the Potential-Determining Ions

Figure 1b. Potential Distribution in the Electric Double Layer

substitution. The adsorbed ions (Stern layer) plus the counterions in the diffuse layer cause the surface potential to decrease rapidly with distance away from the surface.

The following terms are normally employed to describe the double layer:

ψ_o = the surface potential

ψ = the electrostatic potential at some distance $\underline{X}$ from the surface

δ = the thickness of the immobile Stern layer

ψ_δ = the potential drop across the diffuse layer

ζ = the experimentally determined potential at the hydrodynamic plane of shear

κ = the Debye-Huckel parameter; $1/\kappa$, an approximation of double layer thickness

For a 1:1 electrolyte,

$$\kappa = (8\pi\ e^2NC/\varepsilon\ kT)^{1/2}, \qquad (1)$$

where $\underline{e}$ = electronic charge

$\underline{N}$ = Avogadro's number

$\underline{C}$ = concentration in moles/liter

ε = dielectric constant

$\underline{k}$ = Boltzmann constant

$\underline{T}$ = absolute temperature

In the special case of a 1:1 electrolyte in water at 25°C,

$$1/\kappa = 3.04/\sqrt{C} \qquad (2)$$

The direct consequence of the electrical double layer is an energy barrier that must be overcome before collision between two similar particles can occur.

If the electrical double layer is sufficiently reduced, "slow flocculation," controlled by the kinetics of collision through a potential energy barrier, sets in. Destruction of the double layer potential causes the sol to undergo rapid coagulation, the rate being controlled by the frequency of Brownian collision, as in the classical theory of Smoluchowski (7).

DLVO THEORY

The relationship of the double layer theory to the stability of lyophilic colloids is referred to as the Derjaguin, Landau, Verwey and Overbeek (DLVO) theory. The basic concept of the DLVO theory states that the total potential energy of interaction between suspended particles is equal to the sum of the repulsive potential energy and the attractive potential energy.

$$V_T = V_R + V_A \tag{3}$$

The source of the repulsive potential energy is the interaction of the double layers. This potential predominates at intermediate distances. The attractive potential energy arises solely from Van der Waals interactions and because of their nature decrease rapidly with increasing distance between particles. The attraction at great distances is still finite, such that the attractive potential is more effective than the repulsive potential. At very small distances, the attractive potential completely dominates the system. The calculation of V_R and V_A has been reviewed by others (8-10).

If essentially all of the colloid particles in a suspension are repelled from each other due to a large repulsive potential energy, the system is said to be stable. If the particles are able to approach each other with sufficient kinetic energy to exceed the repulsive energy barrier, then the attractive forces cause the particles to flocculate. Figure 2 shows sample curves of the potential energy of interaction versus the distance between particles. Reduction of the repulsion potential allows flocculation.

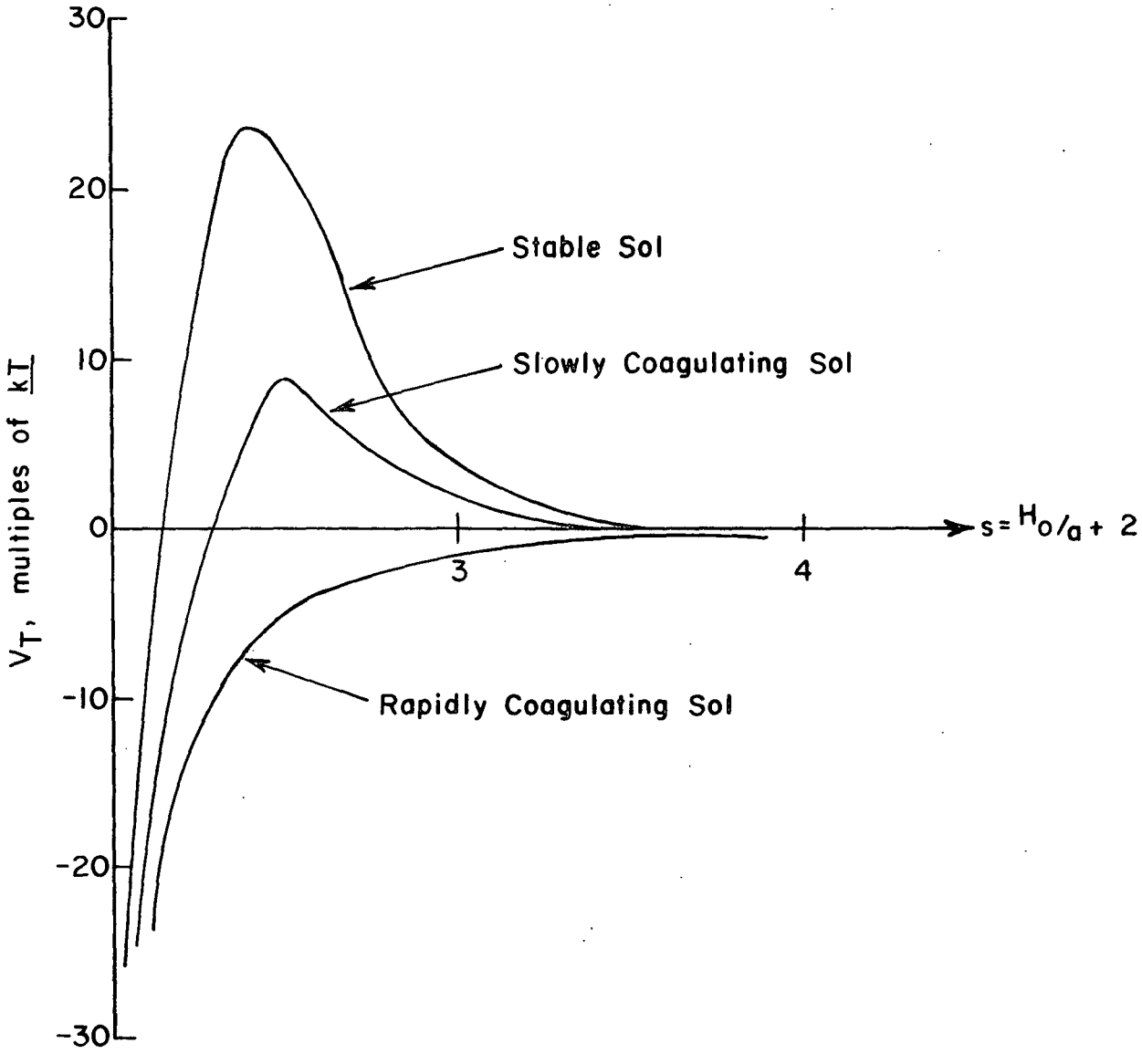

Figure 2. Total Potential Energy of Interaction Versus Unitless Distance

Since the attractive potential is independent of electrolyte concentration whereas the repulsive potential is not, reduction of the energy barrier may be accomplished by addition of electrolyte to the solution. If the interactions between the solute and particles are weak (no adsorption), this will result in reduction of the potential of the diffuse layer and concurrently compress it. An example of this interaction would be the addition of simple nonhydrolyzed ions such as sodium and calcium. If the interactions between solute and particle are strong, ions of opposite charge to the particle will be adsorbed, reducing the potential at the surface and compressing the double layer. Charge reversal can occur if enough ions are adsorbed. This second type of interaction can occur with addition of highly charged, hydrolyzed polymeric species, e.g., the hydrolysis products of aluminum and iron ions.

The result of both types of interactions is for the electrolytes to reduce the height of the repulsive energy barrier such that the attractive forces then cause flocculation of the system.

ADSORPTION-BRIDGING

A second mechanism of flocculation postulated is an adsorption-bridging mechanism. This theory is based on the physical interactions between colloidal particles and polymer, neglecting the electrostatic interactions. Audsley (11) views bridging as that process of adsorbing a macromolecule on a particle in suspension in which only a fraction of the polymer is adsorbed onto the particle, while the unattached part freely penetrates into the solution and can adsorb onto other particles. A particle with extending polymer chains can be considered formally to behave in collisions as if it had a much larger radius (particle radius plus extended polymer chain), but its mass and

mobility will be close to that of a particle without adsorbed polymer. With this concept, the longer the polymer chain, the more effective the flocculant.

The first step of this mechanism entails the attachment of part of the polymer to the particle surface at one or more adsorption sites, leaving part of the polymer extending out into the bulk of the solution. Bridges are then formed when the extended polymer segments can attach themselves to an available site on other particles (in most systems the rate of polymer adsorption is fast in comparison to the flocculation rate). The size of the floc is limited by the shear gradient imposed by the conditions of agitation in the system and the availability of adsorption sites. After formation of the bridges, the particles cannot approach each other more closely because electrostatic repulsion between the particles still exists. The requirements for flocculation by bridging are: 1) that adsorption sites are available and 2) that the configuration of adsorbed polymer is such that sufficient polymer segments exist which extend farther than the interaction distances of the repulsive forces.

The bridging theory has found wide appeal to explain certain phenomena in many types of polymer-colloid systems. Kitchner (12) cites the following characteristics as evidence that bridging occurs:

1) Polymers produce larger, tougher flocs than do simple electrolyte coagulants.

2) The effectiveness of polymers of a given chemical type increases greatly with increasing molecular weight.

3) Highly branched polymers are less effective than linear polymers of comparable molecular weight and chemical type.

4) Highly charged particles are not flocculated by polymer until their zeta potential has been reduced either by use of a polyelectrolyte of opposite charge or by addition of simple salts in conjunction with a nonionic polymer.

Most of this evidence applies to nonionic polymers. Recalling that a polyelectrolyte has properties of both polymers and electrolytes, flocculation could result from bridging, charge neutralization, or a combination of both.

ELECTROSTATIC PATCH MODEL

The third flocculation mechanism postulated is an electrostatic patch model. This theory is based on the electrostatic attraction forces that exist between positive and negative patches. This effect arises when highly charged cationic polymers are adsorbed onto particles of fairly low negative surface charge density. In such cases the particle charge cannot be uniformly neutralized by the adsorbed polymer charges; therefore, the particle surface will have an array of positive and negative patches. For flocculation to occur, the total net charge of the particle need not be zero because the net interaction force is weighted heavily by certain localized charges. The fact that particle mobility need not be zero for flocculation to occur has been shown experimentally (13,14). Kasper (15) first recognized the importance of the patch model in flocculation, and it was also invoked later by Gregory (16) and Lindquist (17) in their work.

FLOCCULATION BY POLYELECTROLYTES OF OPPOSITE SIGN TO THE PARTICLE

Flocculation and charge reversal of inorganic colloidal particles by organic polymers has been studied by numerous investigators; the literature has been reviewed and theories formulated by LaMer and Healy (1), Kitchner (12), and others (13,15). It can be postulated that charge neutralization, bridging or electrostatic attraction will play a dominant role in flocculation of particles by oppositely charged polyelectrolytes.

Gregory (13) has indicated that optimum flocculation occurred when the electrophoretic mobility of the colloidal particles had been reduced to near zero. The same conclusion has been reached by Teot (14) for polystyrene latex, by Dixon and Zielyk (18) for bacteria, and by LaMer, et al. (19) for silica dispersions by low molecular weight polyethylenimines. It can be concluded that charge neutralizations play a dominant role in these works.

On the other hand, LaMer, et al. (19) found that as the polymer molecular weight increased, the optimum flocculation was reached before the point of charge neutralization. This point was well illustrated by Brown, et al. (20) who found that at polymer molecular weights above 50,000, the optimum flocculation concentration decreased with increasing molecular weight. Gregory and Sheiham (21) found that at particle concentrations of 10^{11} cm^{-3} or greater, bridging could take place before the adsorbed polymer reached its equilibrium configuration.

Kasper (15) found that with low molecular weight polymers, the optimum dosage decreases with increasing molecular weight. However, with higher molecular weight polymers, the optimum dosage was independent of molecular weight. Kasper proposed an electrostatic patch mechanism to account for this phenomena. The magnitude of the attractive force is dependent upon the number, size and charge density of the patches, the solution composition, size of the particle, and the average interparticle distance. When any one of these factors increases the attractive forces sufficiently, flocculation occurs. This mechanism was also invoked by Gregory (16) to account for the enhanced rate of flocculation observed with cationic polymers of moderately high molecular weight.

EFFECT OF PARTICLE SIZE

Little research has been carried out to study the role of particle size in polymeric flocculation. In investigating the flocculation of polystyrene latex particles from 0.088 to 3.490 μm in diameter, Black and Vilaret (22) found that the amount of a linear quaternary ammonium substituted type of polymer required for optimum flocculation was proportional to the surface area of the particles. They also found that optimum flocculation took place well before the point of zero zeta potential and that the smaller size particles always produced larger masses of floc. Iler (23) found the same dependence on particle size for small particles (<0.040 μm in diameter) but that with larger diameter particles, the optimum polymer concentration varied inversely with the square of the particle diameter. Iler concludes that several of the small particles may be bridged by one polymer molecule ($\underline{M}_{\underline{w}}$ = 200,000), whereas with the larger particles each pair of particles may be bridged by several polymer chains. There is thus a fundamental difference between the structures of flocculates of large and small particles, the difference depending on the molecular length of the linear flocculating polymer. He also reports that no free polymer exists in solution at concentrations below optimum flocculation. With excess polymer the large particles are restabilized, whereas those particles smaller than 0.040 μm are not restabilized. Only at saturation does Iler find that the free polymer concentration in solution builds up.

ADSORBED POLYMER CONFIGURATION

The flocculation mechanism for a particular suspension is determined by the physical and electrostatic surface characteristics of the particles and of the polymer. In Fig. 3, examples of adsorbed configurations of

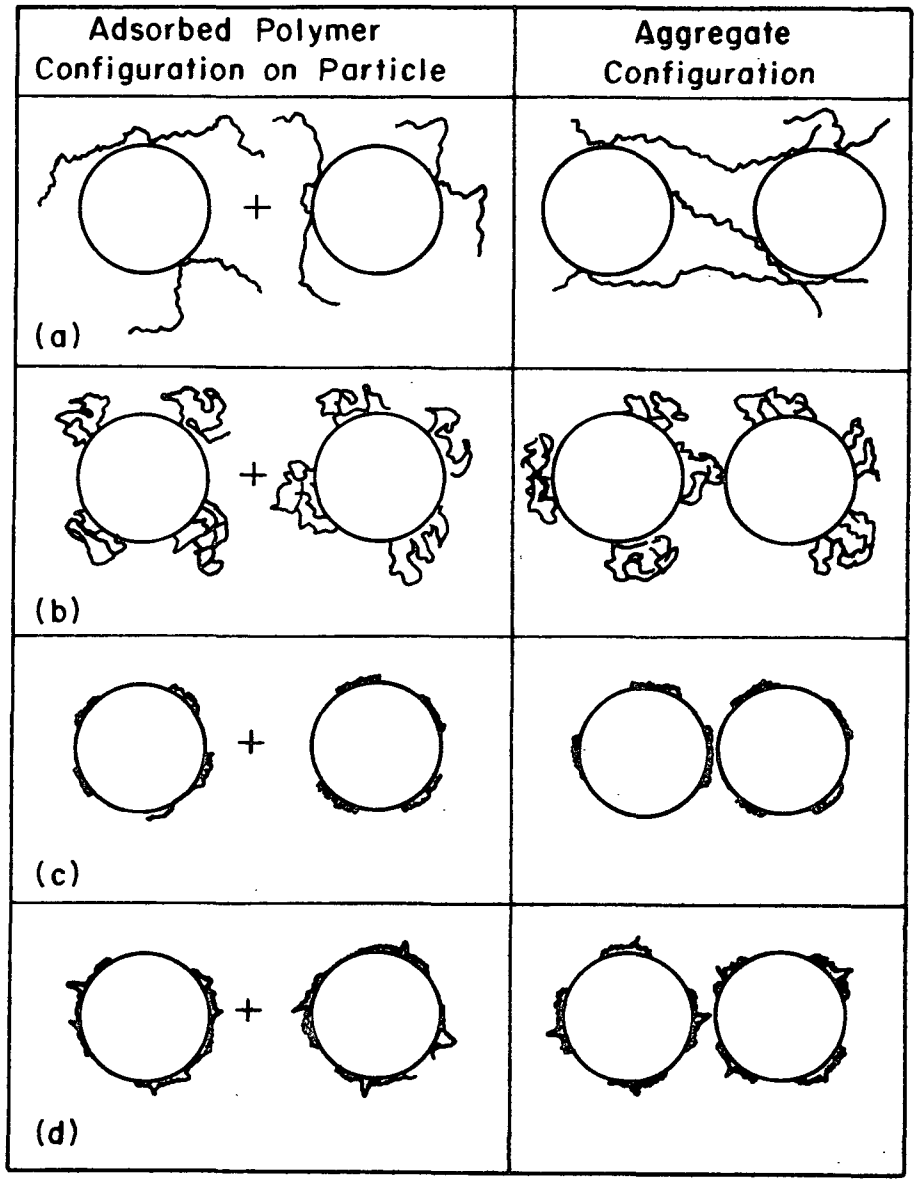

Figure 3. Polymer Adsorption Configuration and the Resulting Aggregate Configuration

polymer and corresponding flocculation configurations are illustrated. In Fig. 3a and 3b polymer molecules absorb with "dangling" ends and extending "loops" on the surface of colloidal particles. The interaction energies between the polymer and particles are weak as characterized by the attachment of relatively few polymer segments on the particles. Collisions between particles result in aggregation if an extended polymer segment of one particle can attach to an available site on another particle. In the aggregated state the particles cannot approach each other more closely because electrostatic repulsion between the like-charged particles still exists. Requirements for this bridging mechanism are: 1) the "loops" and/or "dangling" ends must extend farther than the interaction distances of the repulsive forces, and 2) adsorption sites must be available for attachment. The effectiveness of this mechanism is dependent on the size or molecular weight of the polymer.

In Fig. 3c, oppositely charged polyelectrolyte molecules adsorb in a flat configuration on colloidal particles. The polymer size is small compared to the particle size and the interaction energies between the polymer and particle are strong. The adsorbed polymer "shields" the surface charge from the other particles. When sufficient polymer is adsorbed to reduce the particle's surface potential, aggregation occurs from Van der Waal's attractive force or when a polymer coated "patch" comes in contact with an uncoated, oppositely charged surface. The effectiveness of this mechanism is dependent on polymer charge.

In Fig. 3d oppositely charged polyelectrolyte molecules adsorb in a relatively flat configuration with small loops on colloidal particles. The loops are not effective for bridging until the repulsive forces between the particles have been reduced. This illustrates flocculation by the combination of charge neutralization and bridging.

From the above illustration it is apparent that an understanding of the adsorbed configuration of the polymer would be of great value in assessing the mechanism of flocculation. In recent years sophisticated theories of polymer adsorption have been developed (24-26). The major complicating factor in studying polymer adsorption is that the configuration that a particular macromolecule adopts at a given interface can be different from its configuration in bulk solution, and moreover, varies with the degree of adsorption. In the case of adsorption from very dilute solutions, the adsorbed polymer is likely to unfold into a flat configuration with a certain fraction of its segments in contact with the surface and the unattached segments remaining as loops or dangling ends extending into bulk solution. In more concentrated polymer solutions adjacent sites will become occupied by other polymer molecules and thus will restrict the unfolding into this particular equilibrium configuration. There will be fewer adsorbed segments and the loops will extend further out into the solution. In general, the actual equilibrium configuration at the interface will be dependent on the number of polymer molecules adsorbed per unit area.

Experimentally, Fleer (27) found in the adsorption of polyvinyl alcohol onto silver iodide that the adsorbed layer thickness increased with the molecular weight of the polymer. Fontana and Thomas (28), adsorbing poly-(alkyl methacrylate) onto silica, found that at 70-90% of surface coverage approximately 36% of the polymer segments were attached. As the surface coverage decreased, the percent of segments attached increased (40-54%). They also found that as the molecular weight increased (3×10^5-1×10^6), the thickness of the adsorbed layer remained constant. In the adsorption of narrow molecular weight fractions of poly(vinyl alcohol) at the polystyrene/water interface, Garvey, et al. (29) found the adsorbed layer

thickness to increase linearly with $\underline{M}_{\underline{w}}^{1/2}$. The volume occupied by each polymer molecule in the adsorbed state was found to be approximately the same as that occupied by the effective hydrodynamic sphere in bulk solution. However, the adsorbed layer thickness was found to be greater than the effective hydrodynamic diameter of the polymer coils in solution. The adsorption was interpreted in terms of a possible deformation of the random coil but with no interpenetration with adjacent adsorbed molecules.

It is important to note that the findings of the three previously mentioned works were based on adsorption with a nonionic polymer. It is not clear at this time how this type of adsorption is related to that of polyelectrolytes where electrostatic interaction plays a dominant role. One approach that has been employed in obtaining a configuration of an adsorbed polyelectrolyte has been through the utilization of statistical mechanical treatments. Numerous investigators have used various models to account for the effect of molecular weight, polymer concentration and degree of surface coverage. However, no one model has considered all of the above parameters. In general, it can be concluded (30-32) for molecules which have strong adsorption energies (polyelectrolytes and oppositely charged surfaces) that: 1) 95% of their segments are attached, 2) there are no free tails, 3) there are no loops greater than ten segments, and 4) the adsorbed configuration is independent of molecular weight. In these statistical mechanical models, it is assumed that the surface is infinitely larger than the dimensions of the polymer molecule. Where the polymer is of the same magnitude as the particle, these treatments would not apply.

PRESENTATION OF THE PROBLEM AND THESIS OBJECTIVES

In the flocculation of a colloidal dispersion by an oppositely charged polyelectrolyte, studies have found increasing polymer molecular weight to be beneficial in some cases (13,15,18,20) and in others, to have little effect (16,17,21). The solution properties of pH and ionic strength have also been shown to be important (15,17,27). However, little research (22,23) has been conducted which bears on the role that colloidal particle size plays in the flocculation of a colloidal dispersion. It is likely that the adsorbed polymer configuration could vary as the particle size/polymer size ratio increases and thus influence the mechanism of flocculation. The role of particle size can only be properly assessed when the polymer and colloidal particles are fully characterized.

The objective of this thesis was to determine the interrelationship between polymer molecular weight and colloidal particle size in the ability of a cationic polyelectrolyte to initiate flocculation in an anionic colloidal dispersion. This interrelationship will be evaluated by using well characterized polyelectrolyte and colloidal material.

GENERAL APPROACH

The role of particle size in the ability of a cationic polyelectrolyte to initiate flocculation in an anionic colloidal dispersion was evaluated in a system of polystyrene latex and poly(1,2-dimethyl-5-vinylpyridinium bromide) (DMVPB) under various conditions of ionic strength. The particle size/polymer size ratio was varied by employing different particle sizes and different polymer molecular weights. Narrow molecular weight fractions were used to reduce the effect of polymolecularity.

The experimental program was divided into three sections:

1. Characterization of polystyrene latex particles.
2. Characterization of poly(DMVPB).
3. The investigation of the adsorption and subsequent flocculation of polystyrene latex by poly(DMVPB).

EXPERIMENTAL MATERIALS, EQUIPMENT AND PROCEDURES

The polar solvent water was used throughout this investigation. It was deionized and distilled and had a conductivity less than 1.5×10^{-6} mho/cm.

The characterization of poly(DMVPB) and PSL and the adsorption-flocculation work was done in aqueous media containing analytical reagent grade 10^{-2}M NaCl and 5×10^{-4}M NaCl in separate solutions. The solvent was filtered through 0.2 μm pore size Millipore cellulose ester filters prior to use.

To eliminate the adsorption of poly(DMVPB) on the glassware, all glassware was treated with a 1% solution of polyethylene glycol (20,000 M_w) (33). The treated glassware was washed exhaustively with distilled water prior to use to remove excess polyethylene glycol.

Polystyrene latex particles were picked as a representative colloidal particle for the following reasons: 1) the particle size and particle size distribution can be accurately controlled within a narrow range, 2) the particles are spherical, 3) the particles are nonporous (34), and 4) the particles are stable over a wide pH range.

These latexes are prepared by either conventional emulsion polymerization or by seeded emulsion polymerization. The emulsifier was removed as completely as possible by a mixed-bed ion exchange method (35). The electric charge carried by the PSL particles was characterized by standard potentiometric and electrophoretic mobility methods. A complete description of the particles, the experimental procedure and discussion of the results of the characterization is presented in Appendix I.

Poly(DMVPB) was chosen as a representative cationic flocculant. This polymer was synthesized by free radical polymerization (see Appendix II). The polymerization took place in an oxygen-free atmosphere to prevent secondary reactions. Conversion of monomer to polymer was kept under 20% to minimize branching or cross-linking. Since this polymer is an ammonium salt, the extent of cationic charge on the polymer is not dependent upon the pH of the solution.

Narrow molecular weight fractions were obtained by gel permeation chromatography using Bio-Glas as the fractionating bed. The polymer molecular weight was determined by light scattering and sedimentation equilibrium techniques. Poly(DMVPB) was further characterized by standard intrinsic viscosity and diffusion techniques. The experimental procedures and discussion of characterization results are found in Appendix II.

ADSORPTION-FLOCCULATION EXPERIMENTS

The equipment employed by Lindquist (17) was used in this work. The method of agitation was identical to Lindquist's with the exception of an agitation rotation of 5.5 rpm.

The following procedure was set up to: 1) determine the efficiency of flocculation, 2) determine zeta potentials of PSL particles with adsorbed polymer, and 3) follow the adsorption of poly(DMVPB) into PSL. All adsorption studies were done in duplicate. In all cases, the solutions were at pH 6.

1. Fifteen ml of PSL at the desired concentration, pH and ionic strength was placed into each tube of a series of treated (with polyethylene glycol) 50 ml screw cap centrifuge tubes. Since the PSL particles varied

in particle size and surface charge density, three experiments were run. The concentration of the PSL particles was varied to obtain data on the factors of constant surface area, constant number of particles and constant charge.

2. Ten ml of polymer solution at the desired concentration, pH, and ionic strength was added with a pipet to each tube. The ionic strengths and pH of the polymer solution and PSL suspensions were adjusted at least one-half hour prior to use. The polymer concentration ranged from 0.001 to 40 mg/liter in all experiments.

3. The centrifuge tubes were sealed with caps lined with polyethylene film, shaken vigorously and mounted at the periphery of two 12-inch notched wheels in a constant temperature bath. The tubes were then agitated at 5.5 rpm at 25°C.

4. After one hour of agitation, the pH of the suspension in each tube was measured using a Markson No. 808 test tube electrode. Little change in pH (<0.100 pH units) was found during the initial adsorption-flocculation studies. Therefore this step was eliminated in the remaining experiments.

5. After a twenty minute settling period, the turbidity at an angle of 90° of the suspension was measured on a Brice Phoenix Light Scattering Photometer at a wavelength of 5460 A. A 24 × 24 mm turbidity cell was used to hold the sample when measuring turbidity. In a similar manner, a PSL suspension without polymer which was not agitated for one hour and did not settle for twenty minutes was measured for turbidity. The term relative turbidity used in this work is defined as the turbidity of a PSL suspension with polymer/PSL suspension without polymer. Due to the above conditions, the relative turbidity of the stable, dispersed PSL suspension is not 100%.

6. Electrophoretic mobilities of the suspension were determined on a Zeta Meter.

7. Duplicate suspensions were centrifuged to obtain a clear supernatant. Samples analyzed for poly(DMVPB) by UV adsorption were obtained in the following manner:

A. Particle sizes 1.101, 0.794, and 0.481 μm were centrifuged at 19,000 g for twenty minutes. A portion of the suspension was withdrawn from the Sorvall Centrifuge by a syringe equipped with a 10-inch stainless steel needle. It is imperative to remove the same suspension layer from each centrifuge tube. The adsorption was corrected for polymer sedimentation (<5%).

B. Particle sizes 1.101, 0.794, 0.481, 0.234, and 0.109 μm were centrifuged at 80,000 g for 30 minutes in a Beckman Ultracentrifuge. The entire suspension was carefully poured from the centrifuge tube.

In both methods, the samples were analyzed 12 hours after centrifugation. Two methods were employed due to the varying sedimentation ability of the PSL particles.

POLYMER ADSORPTION — RESULTS AND DISCUSSION

The purpose of this section is threefold: 1) to present the probable adsorption mechanism of poly(DMVPB) onto PSL, 2) to indicate the effects of polymer molecular weight, salt concentration and PSL particle size on the adsorption of poly(DMVPB) onto PSL, and 3) to suggest a probable configuration of the adsorbed polymer molecule in the equilibrium state. All data presented in this section are taken from the constant surface area experiment.

RATE OF POLYMER ADSORPTION

A preliminary adsorption experiment was undertaken to determine the rate of poly(DMVPB) adsorption up to the charge neutralization point on PSL. The results are presented in Appendix III. The results indicate almost complete adsorption after 18 minutes of contact time. There was no significant increase in adsorption after 30 minutes of contact time. This rapid adsorption is characteristic of systems where strong attractive electrostatic interaction is present between polymer and nonporous colloidal particles (15,17,36). It can be concluded that the adsorption of poly(DMVPB) on PSL up to the point of charge neutralization is rapid and that little adsorption occurs after 30 minutes of contact time.

EFFECT OF POLY(DMVPB) CONCENTRATION

The adsorption of poly(DMVPB) on PSL particles has been examined during the flocculation studies. A comparison of the two centrifuge speeds used in this work revealed that the results obtained by both methods were not significantly different. Figures 4 and 5 indicate the adsorption trend of F_1-6 ($\underline{M}_w = 10^6$) and F_2-7 ($\underline{M}_w = 3.3 \times 10^4$) under two salt conditions for particle size 1.101 and 0.234 μm. These same trends are observed for the remaining three particle sizes. Complete data are found in Appendix IV.

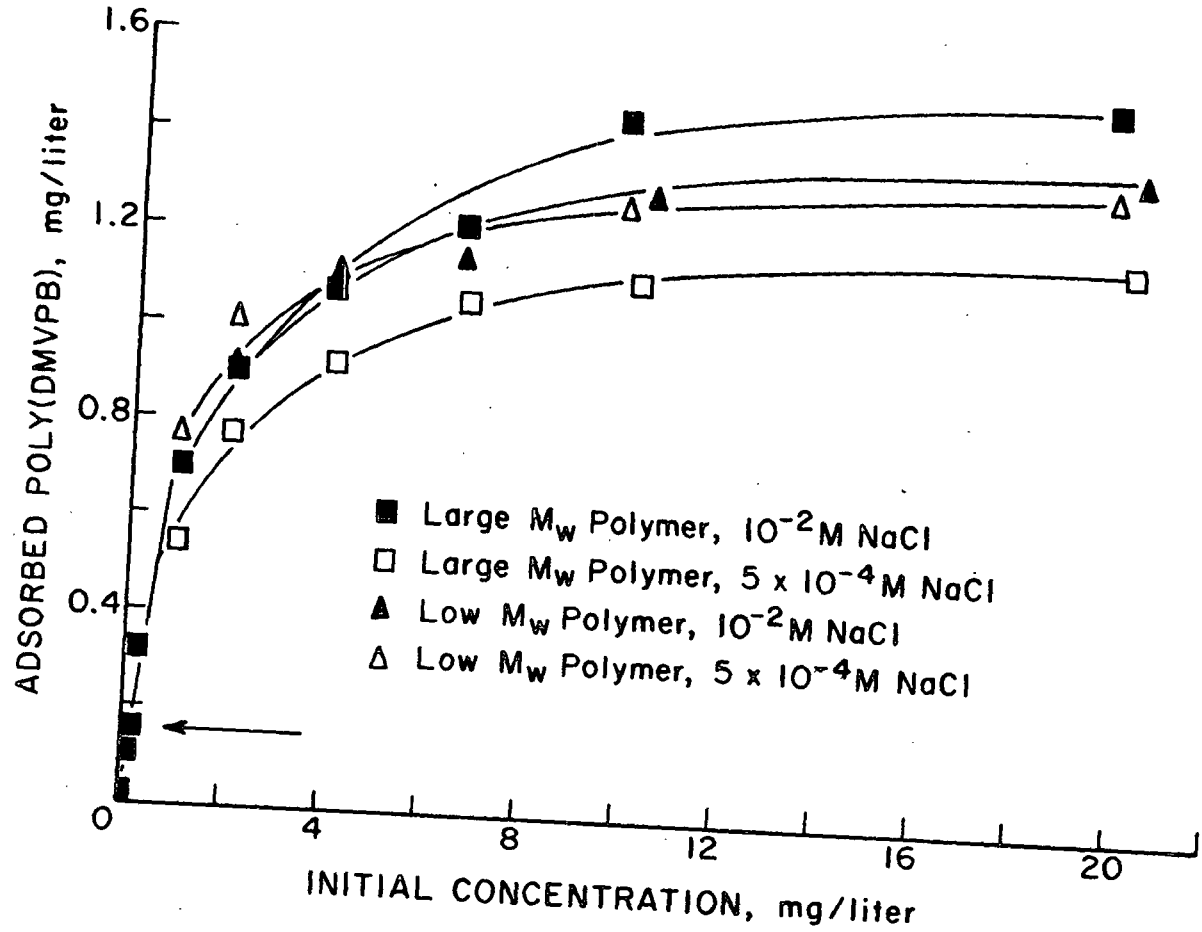

Figure 4. Adsorption of Poly(DMVPB) on PSL; Particle Size 0.234 μm, 73 mg/Liter. The Arrow Indicates the Approximate Point of Charge Neutralization for all Four Experimental Runs

In all cases, the adsorption isotherms show a high affinity character; at low concentrations all of the polymer is adsorbed. At higher concentrations the amount adsorbed increases only slightly with polymer concentration and a plateau region is reached.

For discussion, the curved portion of the adsorption isotherms will be referred to as the "knee" of the isotherm. In all cases, zeta potential data indicates that the neutralization point and the beginning of the knee occur at the same concentration. Up to the knee, the polymer is adsorbing on a net

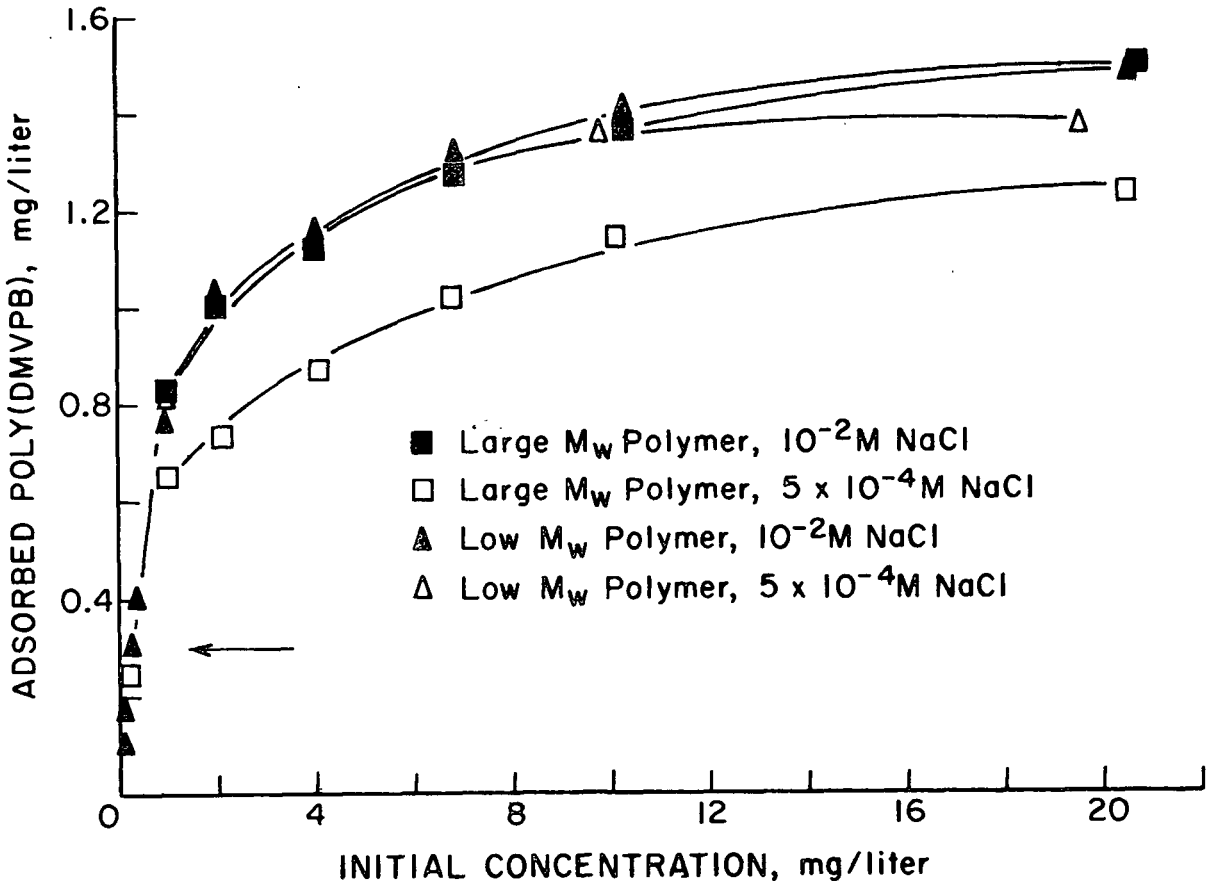

Figure 5. Adsorption of Poly(DMVPB) on PSL; Particle Size 1.101 μm, 341 mg/Liter. The Arrow Indicates the Approximate Point of Charge Neutralization for all Four Experimental Runs

negative surface; above the knee the polymer is adsorbing on a net positive surface. The data suggest that the neutralization point acts as a pivot between two different adsorption conditions. Therefore the description of the adsorption process of poly(DMVPB) on PSL particles is separated into two steps.

In the first step, polymer adsorption up to the knee is complete. The cationic polymer is adsorbed on a negative surface. It can be assumed that the

dominant ionic interaction is between the cationic pyridinium ring and the anionic surface sulfate groups. Theoretically both electrostatic and chemical associations could contribute to the interaction. Conner (37) studied the adsorption of n-alkyltrimethylammonium ions on polystyrene surfaces. His infrared studies indicate that the ionic interaction up to the knee of the isotherm is a purely electrostatic one and that formation of a chemical bond does not occur. It is reasonable to assume from this work that the dominant, if not only, contributor to the ionic interaction up to the neutralization point is an electrostatic association. Up to the knee position, approximately the same amount of material is adsorbed irrespective of polymer molecular weight and salt conditions. The adsorption after the point of charge neutralization is, however, dependent on polymer molecular weight and the salt concentration.

In the second step, a more gradual adsorption occurs with the poly(DMVPB) chains adsorbing onto a surface with a net positive charge. In this case, the electrostatic contribution to the free energy of adsorption would not favor adsorption. Rather the adsorption process in this region must be driven by the decrease in free energy which occurs upon removing the polymer chain from the solution and onto a PSL particle site. Evidence to support this argument is found in the work of Connor and Ottewill (38) who found that the form of the adsorption isotherm (n-alkyltrimethylammonium ions on polystyrene surfaces) above the knee closely resembled that obtained on a polystyrene surface having no ionic groups.

SATURATION ADSORPTION

The values of polymer adsorption at saturation were determined in duplicate after 16 hours of contact time. The saturation values are not

necessarily equilibrium values since attainment of equilibrium may require several days (15). Nevertheless, the saturation adsorption data are useful in quantitatively and qualitatively describing the effect of polymer molecular weight, salt concentration and particle size.

MOLECULAR WEIGHT EFFECT

The saturation adsorption data after 16 hours of contact time is shown in Table I. The data points are averages of duplication runs. The saturation adsorption of poly(DMVPB) in 10^{-2}M NaCl increases with molecular weight while no molecular weight dependence on adsorption is found in 5×10^{-4}M NaCl.

TABLE I

SATURATION VALUES OF POLY(DMVPB) ADSORPTION AFTER 16 HOURS OF CONTACT TIME IN 10^{-2}M NaCl (A) AND 5×10^{-4}M NaCl (B) FOR THE CONSTANT SURFACE AREA EXPERIMENT

Particle Size, μm	Fraction	Saturation Adsorption, mg/liter (A)	(B)
1.101	F_1-6	1.67	1.52
	F_2-7	1.50	1.38
0.794	F_1-6	1.69	1.43
	F_2-7	1.54	1.40
0.481	F_1-6	1.69	1.38
	F_2-7	1.54	1.38
0.234	F_1-6	1.69	1.38
	F_2-7	1.47	1.43
0.109	F_1-6	1.77	1.36
	F_2-7	1.47	1.42

It is generally found that the adsorption of polymers on surfaces increases with molecular weight. Modern theories (39,40) predict that under θ conditions the maximum adsorption increases linearly with the

square root of the molecular weight for degrees of polymerization lower than several thousand. For very high molecular weights the amount adsorbed tends to a limiting value. In athermal solvents a much less pronounced dependence on molecular weight exists.

These theories apply to the adsorption of nonionic polymers where the interaction energy between polymer and particle is intermediate or weak compared to the predicted interaction energy of the system. Experimental and theoretical works in the literature (15,17,18) where the polymer-particle interactions are strong find adsorption to have little dependence on molecular weight.

The slight increase in adsorption with molecular weight in the system could therefore be a result of incomplete equilibrium, nonequilibrium conditions or the strong interaction energy between polymer and particle. Shyluk (41), studying the adsorption of poly(DMVPMS) onto crystalline silica, found that when the polymer molecular weight is large, only a portion of the polymer is immediately adsorbed, and adsorption continued for weeks. A lower saturation level for the higher molecular weight polymer as compared to that for the low molecular weight polymer is found after ten days. In comparison, Kasper (15), adsorbing poly(DMVPB) onto PSL, found no dependence of molecular weight in 10^{-2}M NaCl solutions at saturation. However, in 5×10^{-4}M NaCl solutions, he found an increase in adsorption with a decrease in molecular weight. This latter phenomenon is predicted theoretically only for a porous surface where the high molecular weight polymer cannot enter the pores.

EFFECT OF IONIC STRENGTH

In Table I, the dependence of the adsorption on the concentration of salt is shown. The adsorption increases only slightly as the concentration of salt increases. This increase can be influenced by two factors: 1) the ability of the counterion (Cl^-) to mask or screen the charges on the poly(DMVPB) molecule, and 2) a change in the solvent quality.

As the salt concentration increases, the fixed polymer charges become shielded from each other by the additional byions. The repulsion between the fixed charges is less, resulting in a more compact configuration. Experimentally this is found and the results are presented in the polymer characterization section (Appendix II). A more compact configuration would allow greater amounts of polymer to adsorb per unit surface area.

Not only does increasing salt concentration result in a decrease in electrostatic repulsion between fixed polymer charges, but also between previously adsorbed macroions and those approaching the surface. This diminished repulsion would seemingly allow more polyelectrolytes to adsorb before the surface became positively charged to the point where additional adsorption is prevented.

The last factor which may account for increased polymer adsorption with increasing salt concentration is a reduction in solvent quality. The added electrolyte requires a certain degree of hydration and thus reduces the amount of water available to the poly(DMVPB) molecule. This reduction in solvent power facilitates adsorption. Experimental studies have confirmed that the adsorption of polymers and polyelectrolytes is greater from poor solvents than good solvents (42,43). In summary, the increase in poly-(DMVPB) adsorption with increased ionic strength can be explained by reduced

molecular size, decreased intermolecular interactions and reduced solvent quality.

EFFECT OF PARTICLE SIZE

The complete saturation adsorption data and the effect of particle size is shown in Table I and Fig. 6. The slopes in Fig. 6 were calculated by the least-squares method. The results indicate that only in the case of the large molecular weight polymer in 5×10^{-4}M NaCl is the slope of the plot statistically significantly different from zero. A zero slope indicates that the radius of curvature has no effect on the amount of polymer absorbed per unit area. The reason for both positive and negative slopes in Fig. 6 is most likely explained by the fact that the data points were determined by an average of only two experimental runs.

It can be argued deductively that the radius of curvature should have no effect on the amount of polymer adsorbed per unit area in this system. The main criteria for adsorption in a high interaction system is the availability of an adsorption site. Theory (44) predicts that the polymer segment density normal to a flat surface falls exponentially with distance for nonionic polymer. If one assumes that the segment density of adsorbed polymer molecules at a given distance from the surface is constant for both flat and curved surfaces, then the area per particle covered by adsorbed polymer molecules is also independent of radius of curvature. Therefore, the number of adsorption sites available per unit area is independent of radius of curvature. This argument is a thermodynamically favorable one; a decrease in the area covered per molecule with decreasing radius of curvature would increase the free energy of the system. The work of Tadros (45) further strengthens the argument. A consequence of the initial assumption is

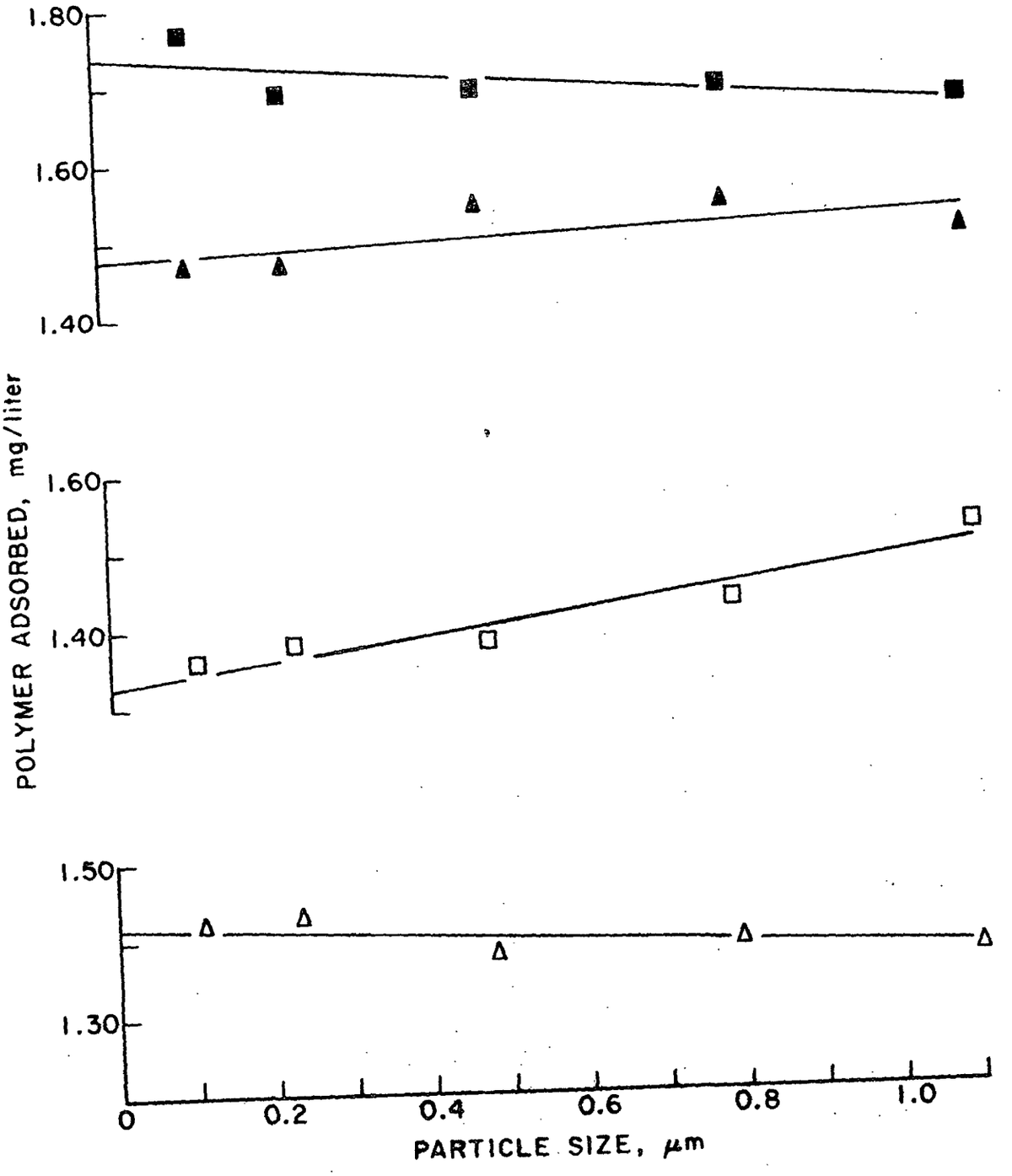

Figure 6. The Effect of Particle Size on the Saturation Adsorption of Fractions F_1-6 (□) and F_2-7 (Δ) in 10^{-2}M NaCl (Shaded Figures) and 5×10^{-4}M NaCl (Open Figures)

that the adsorbed layer thickness should increase with increasing particle radius. Tadros found this trend, thus supporting the validity of this assumption.

Although the argument presented is based on nonionic polymer theory and data, it is felt this reasoning would be valid in a system where high interaction energy exists between particle and polymer. In summary, the low values of the slopes in Fig. 6 suggest that the radius of curvature has little effect on the amount of polymer adsorbed per unit area.

EQUILIBRIUM ADSORPTION ISOTHERMS

From the adsorption data, equilibrium adsorption isotherms (EAI) were constructed to determine whether monolayer or multilayer adsorption was occurring. The Langmuir equation (46) was employed to determine if the polymer adsorption was strictly monolayer;

$$\Gamma = K \Gamma_M Ce/(1 + KCe), \tag{4}$$

where Γ = specific adsorption at the equilibrium concentration Ce

K = Langmuir constant

Γ_M = specific adsorption at surface saturation

Figure 7 illustrates the shape of EAI for fractions F_1-6 and F_2-7 under both salt concentrations with PSL particle size 0.234 μm. The adsorption form illustrated in Fig. 7 is the Langmuir type. The EAI for the other four particle sizes are similar and complete data are available in Appendix IV. Equation (4) can be rearranged in the following manner:

$$Ce/C_* = 1/C_M K + Ce/C_M, \tag{5}$$

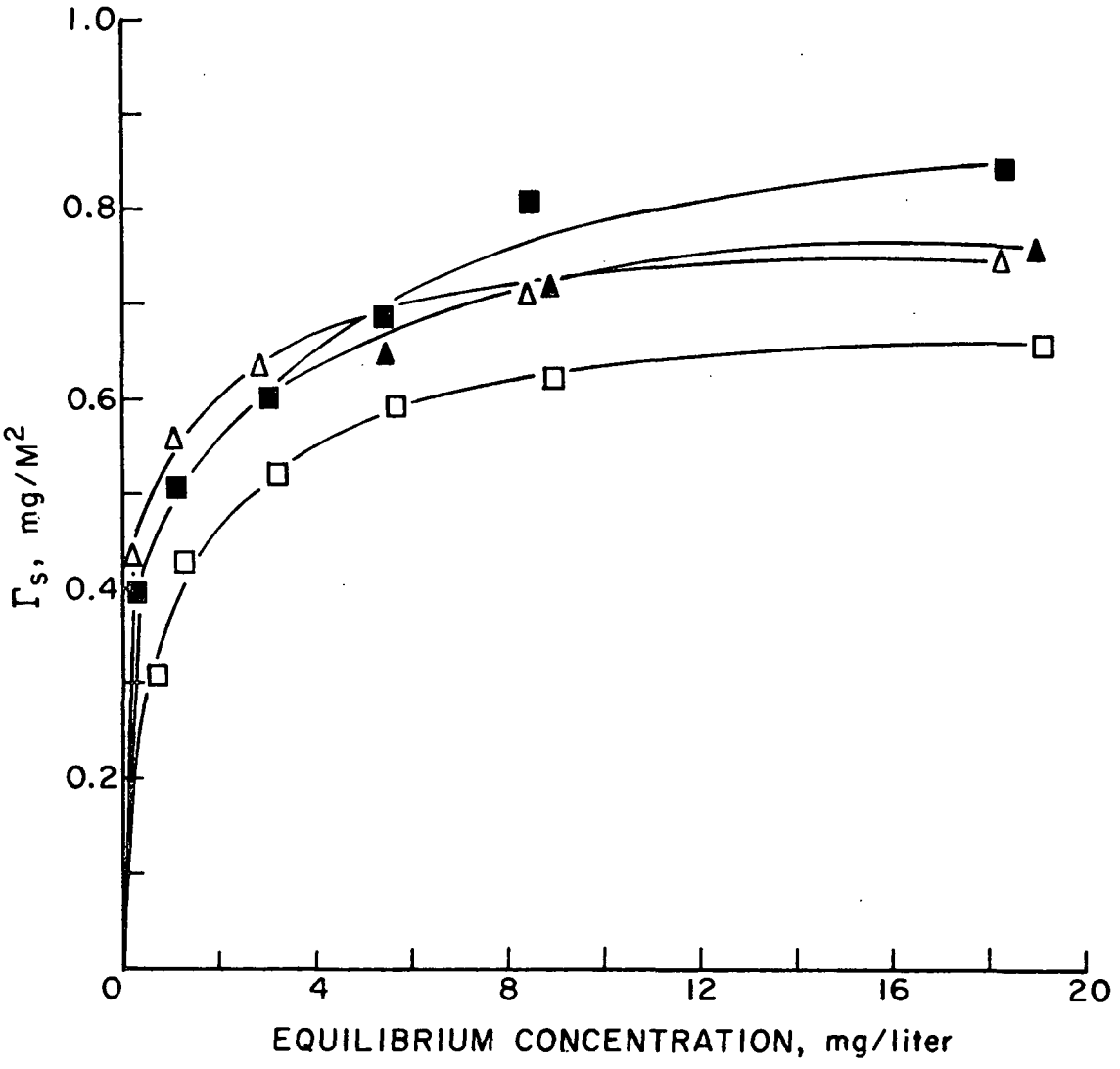

Figure 7. Equilibrium Adsorption Isotherm. Fraction F_1-6 (□) and Fraction F_2-7 (Δ) in 10^{-2} M NaCl (Solid Figures) and 5×10^{-4} M NaCl (Open Figures). Particle Size 0.234 μm, 73 mg/Liter

where C_* is the specific adsorption at equilibrium concentration Ce and C_M is the maximum amount adsorbed, both expressed in mg/liter. A plot of Ce/C_* versus Ce has a slope of $1/C_M$ and an intercept of $1/KC_M$. The values of C_M and K are obtained by regression analysis. These EAI are seen in Fig. 8. The relationship is found to be linear, which is a characterization of Langmuir type behavior. However, this does not prove "monolayer" adsorption. It can be said that over this concentration range a limiting adsorption level is reached which is of the Langmuir type. This relationship is also found with the other four particle sizes.

In summary, the EAI constructed follow the form of Langmuir type adsorption. This indicates that multilayer formation is not occurring and the data will thus be interpreted.

ADSORPTION CONFIGURATION

A main objective of the adsorption experiments is the determination of the configuration of the adsorbed polymer molecule in the equilibrium state. This configuration is a controlling factor in determining the flocculation mechanism. The most important configuration parameter is $\Delta\overline{G}$, the total adsorption energy per segment. The stronger the adsorption energy, the flatter the equilibrium configuration. While $\Delta\overline{G}$ is not measured in this experiment, it is safe to infer that the interaction energies between polymer and particle in this experiment are strong (15).

NONEQUILIBRIUM ADSORPTION CONFIGURATION

It is necessary to briefly describe the nonequilibrium state of an adsorbed polymer in order to distinguish it from the equilibrium state. It may be assumed that for a single polymer molecule and an isolated colloidal

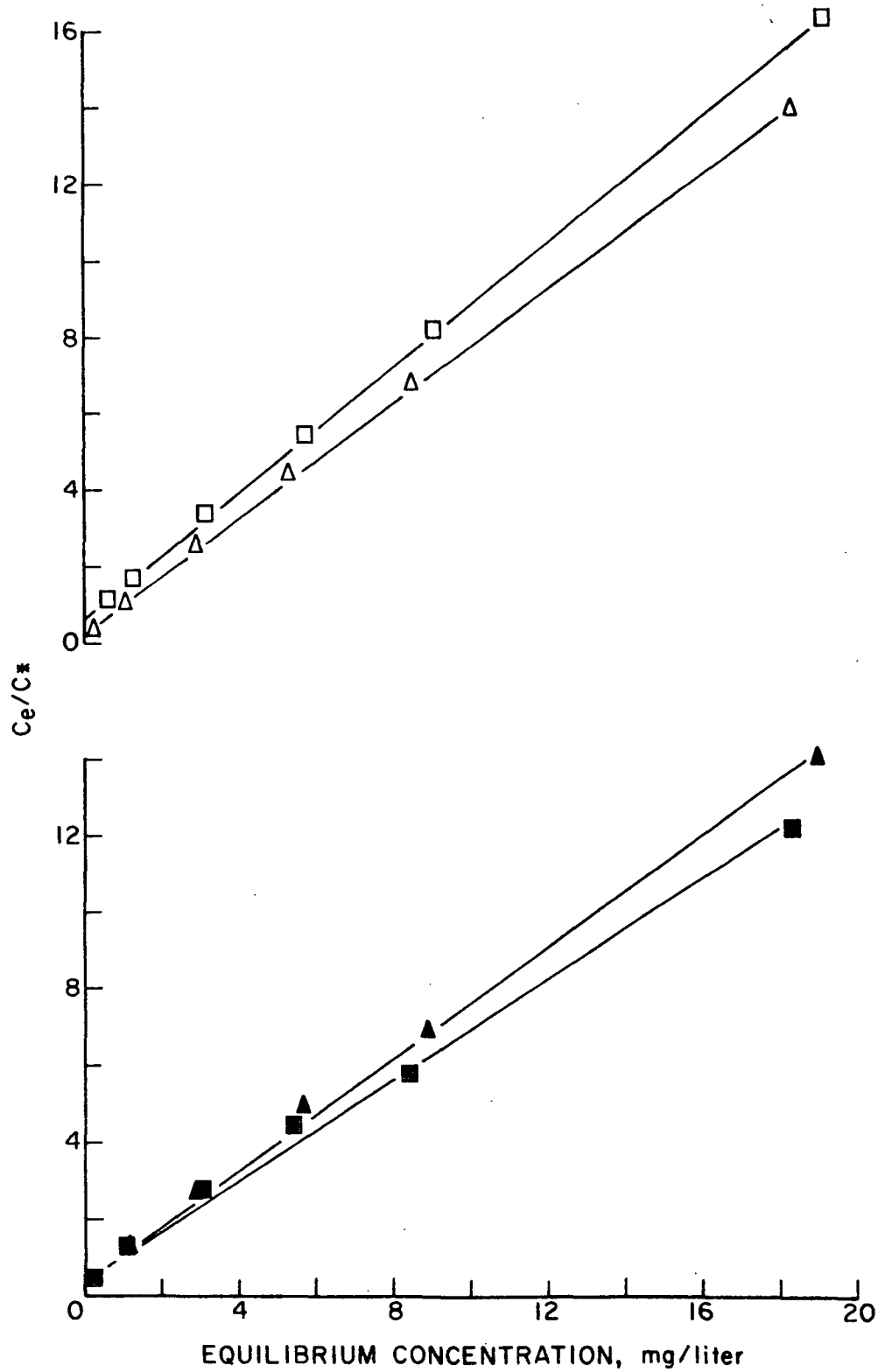

Figure 8. Equilibrium Adsorption Isotherms. Fractions F_1-6 and F_2-7 in 5×10^{-4}M NaCl (Upper) and 10^{-2}M NaCl (Lower). Particle Size 0.234, 73 mg/Liter

particle, adsorption takes place by a series of individual attachments at various points along the molecule over a finite period of time. As more contacts are made, the polymer configuration becomes flatter until some equilibrium state is reached. From the initial attachment of the polymer until the equilibrium state is attained, there is an interval during which loops may extend quite far into the solution.

POLYMER CONFIGURATION AT SATURATION ADSORPTION

The configuration of adsorbed polymers at the solid-solution interface is related to the molecular weight dependence of the maximum amount of polymer adsorbed. This dependence may be empirically expressed as:

$$C_M = KM_w^n, \tag{6}$$

where K and n are constants. The values of n fall into the range of $0 \leq n \leq 1$ if C_M is expressed as weight per unit area. When $n = 1$, only one segment of each polymer molecule is attached to the surface. On the other hand, when $n = 0$, either all segments are attached to the surface or loops exist in which the number of segments per loop is independent of molcular weight. That is, the number of segments per loop is a constant fraction of the total number of segments adsorbed. The models of Perkel and Ullman (42) provide a clear picture of the configuration of adsorbed molecules related to the value of n (see Fig. 9). Table II gives the values of n found under both salt conditions. It should be noted that the PSL particle diameters vary from 0.1-1.1 μm and the hydrodynamic molecular diameters of fractions F_1-6 and F_2-7 vary from 0.2-0.5 and 0.02-0.04 μm, respectively (see p. 148). Therefore, in some cases the polymer size is greater than the particle size.

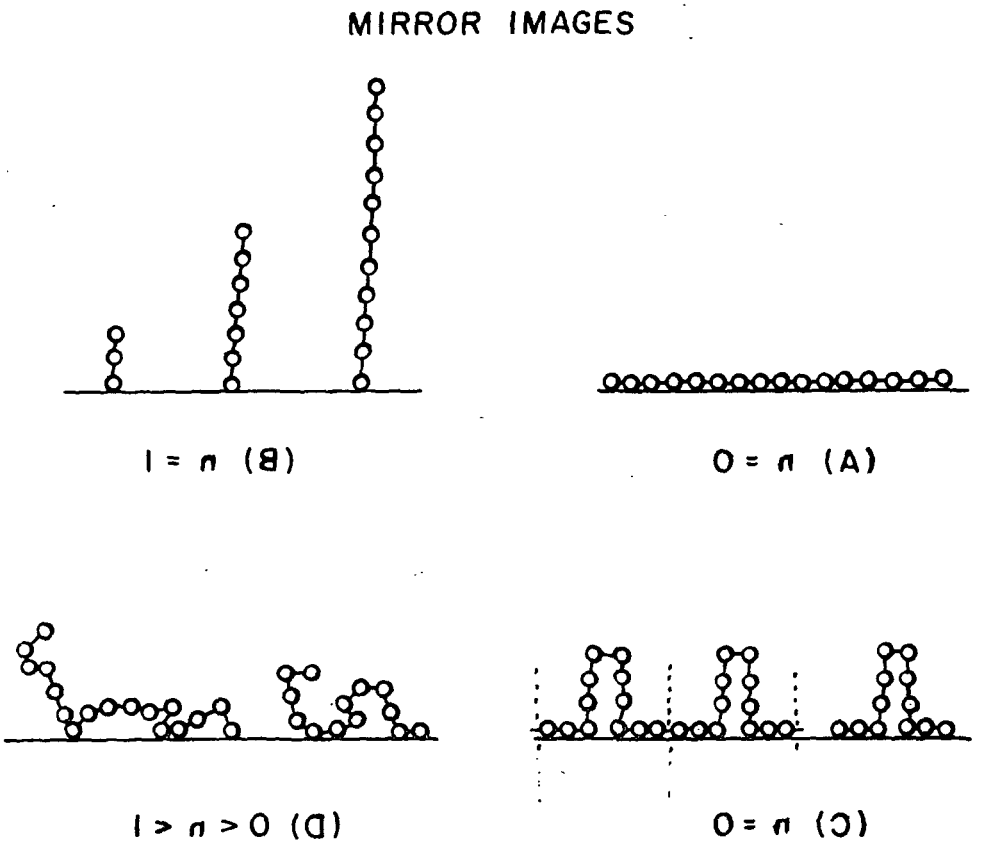

Figure 9. Two-Dimensional Models of Adsorbed Polymer Configurations for Various n Values. Perkel and Ullman (42)

TABLE II

VALUES OF $\underline{n}$ IN $10^{-2}\underline{M}$ NaCl AND $5 \times 10^{-4}\underline{M}$ NaCl
AFTER 16 HOURS CONTACT TIME

Particle Size	Solvent	$\underline{n}$	Particle Size	Solvent	$\underline{n}$
1.101	$10^{-2}\underline{M}$ NaCl	0.03	1.101	$5 \times 10^{-4}\underline{M}$ NaCl	-0.03
0.794		0.03	0.794		0.00
0.481		0.03	0.481		0.00
0.234		0.05	0.234		0.00
0.109		0.06	0.109		-0.04

The values of $\underline{n}$ are zero or very close to zero. This is in agreement with numerous experimental and theoretical works in the literature where the polymer-particle interactions are strong (15,17,18). There are several examples of negative $\underline{n}$ values reported in the literature (41,47); however, it is generally accepted that true $\underline{n}$ values cannot be negative. In the present case, the negative values can be attributed to lack of equilibrium or the fact that only two polymer molecular weights were used.

The zero and near zero values of $\underline{n}$ suggest that poly(DMVPB) lies in a flat configuration or with small loops whose size is independent of molecular weight. This approach should be treated with caution; however, Silberberg (39) has suggested that $\underline{n}$ decreases with $\underline{M}_w$ anyway. The amount adsorbed normally reaches a limiting value at very high molecular weights (48), and the actual dependence on $\underline{M}$ seems to be related strongly to solvency, in good solvent the dependence being less strong (49). Motomura and Matuura (30) have provided a theoretical treatment of an isolated polymeric chain at an interface, based on a three-dimensional random walk on a simple cubic lattice. One of their objectives was to evaluate the average number of

polymer segments attached directly to the surface versus the adsorption energy. At interaction energies 1 kT and greater, they predict that 90% of the polymer segments are attached directly to the surface. Roe (36), also using a model system, evaluated the parameter of polymer stiffness. He concluded that if a stiff molecule does adsorb, the majority of its segments attach directly to the surface. Higuchi (31) theoretically predicts that polymer molecular weight affects the bound fraction only when adsorption energies are intermediate. Molecules which have strong adsorption energies attach almost every segment to the surface regardless of molecular weight.

In contrast to the above theories, a molecular model of poly(DMVPB) indicates the impossibility of a completely flat configuration. Steric hindrance from the pyridinium ring does not allow consecutive monomer units to lie flat. Experimentally, Fontana and Thomas (28) found that at 70-90% surface coverage in a high interaction system (>5 kT), approximately 36% of the polymer segments are attached. Also the thickness of the adsorbed layer remained constant regardless of polymer molecular weight.

In summary, a low value of n is normally found both experimentally and theoretically for systems of high interaction between the polymer and the surface. This value of n is indicative of a relatively flat adsorbed layer with small loops but no loops or dangling ends extending far out into the solution.

FLOCCULATION RESULTS

DESCRIPTION OF FLOCCULATION CURVE

Figure 10 illustrates the dependence of zeta potential and relative turbidity on the poly(DMVPB) concentration. These parameters were determined for each flocculation study. The flocculation curve in Fig. 10 is representative of those flocculation curves determined in this work. This curve can be divided into three zones: a stable, dispersed colloidal zone (I), an unstable flocculated zone (II), and a stable, redispersed zone (III). In zone I the amount of polymer adsorbed on the colloidal particles has not affected their stability and the particles remain separate and discrete. As the polymer concentration increases, the sol becomes unstable and flocculation occurs (zone II). Additional polymer adsorption causes a charge reversal on the particles. The particles are redispersed and stabilized by the polymer charges.

Along the flocculation curve, there are three points of interest to this work: the critical flocculation concentration (CFC), the optimum flocculation concentration (OFC), and the restabilization concentration (RSC). The CFC is defined as the minimum concentration of polymer necessary to initiate flocculation. This point is determined by extrapolation of the turbidity of the sol to the turbidity prior to flocculation. The OFC is defined as the concentration of polymer necessary to produce the minimum relative turbidity. Not always an obvious visual point, the OFC is arbitrarily that point in the middle of the U-shaped flocculation zone. The RSC is defined as the concentration of polymer necessary to redisperse the sol by virtue of polymer charge. This point is arbitrarily determined to be 90% of the turbidity in zone I.

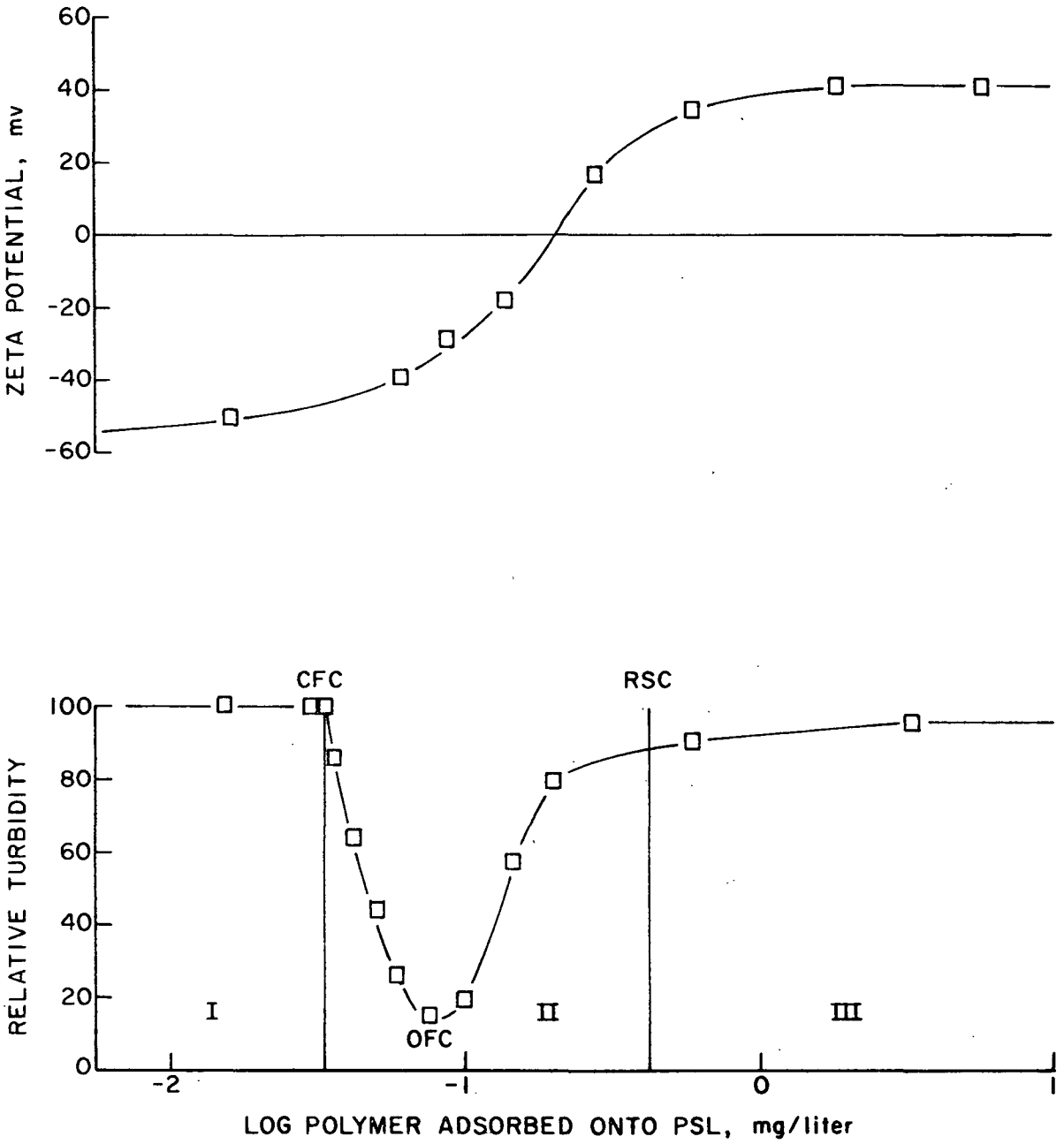

Figure 10. Dependence of Zeta Potential and Residual Turbidity on the Poly(DMVPB) Concentration. Particle Size 0.481 μm, 150 mg/Liter

Other parameters of interest are the point of charge neutralization and the zeta potentials at CFC, OFC, and RSC. All of these values are picked off a smooth curve of zeta potential versus polymer concentration.

RESULTS

In this section the results of the parameters CFC, OFC, point of charge neutralization, and RSC are discussed in terms of polymer molecular weight, salt concentration, surface charge density, and particle size effects. The data in this section are from the constant surface area experiment where the particle surface area was 1.78 m^2/liter. A flocculation mechanism is discussed in detail in a later section.

EFFECT OF PSL CONCENTRATION

All of the abovementioned parameters were measured in the constant surface area and constant number of particles experiments. Results obtained for all parameters in all cases clearly established a particle weight concentration, polymer concentration relationship. Specifically, a threefold increase of a particular particle weight concentration requires a threefold increase in polymer concentration to reach CFC, OFC, etc., parameters. This relationship is true for a specific particle size. Black and Vilaret (22) found the same relationship while studying the effect of particle size on turbidity removal. Therefore, all parameters from the constant charge experiment were determined empirically using the results and PSL particle weight concentration from the constant surface area experiment.

CRITICAL FLOCCULATION CONCENTRATION

Figure 11 is a plot of relative turbidity versus log poly(DMVPB) concentration. CFC values are determined by extrapolation to the initial turbidity

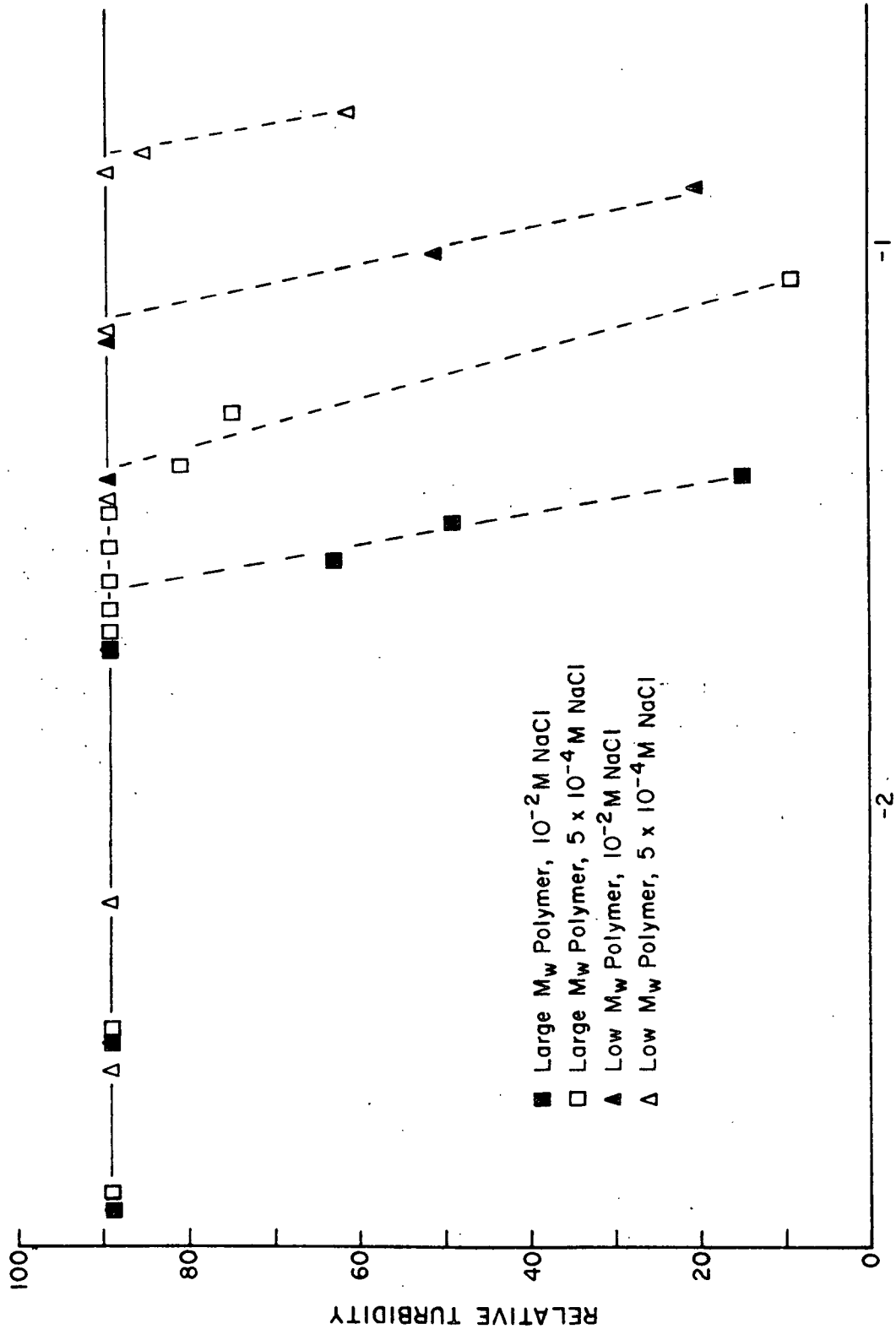

Figure 11. Relative Turbidity Versus Log Initial Poly(DMVPB) Concentration. Particle Size 1.101 μm, 341 mg/Liter

base line. Comparison of three duplicated experimental runs with the three original runs revealed a 12.5% uncertainty in determining their CFC values by this method (see Appendix V). The CFC values for all particle sizes are determined in this manner. Models of the number of poly(DMVPB) molecules per PSL particle at CFC and OFC are seen in Fig. 12 (also see Table XII). Table III presents the complete CFC data for the constant surface area experiment and the respective zeta potentials.

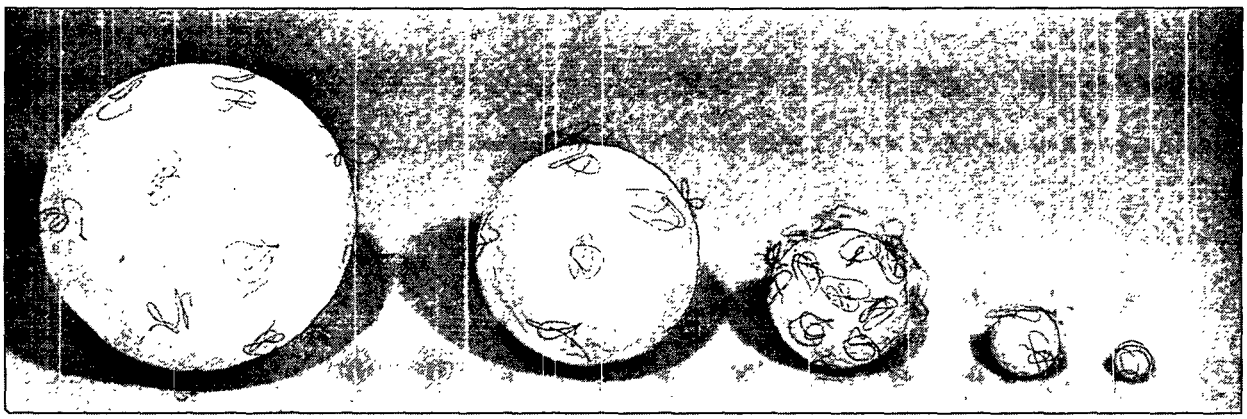

Figure 12. Models of Polymer Molecules per PSL Particle. Large Molecular Weight Polymer in 10^{-2}M NaCl at CFC for Particle Sizes 1.101 and 0.794 μm and at OFC for Particle Sizes 0.481, 0.234 and 0.109 μm. Models are Drawn to Scale Except for Thickness of Polymer Molecules Which is Approximately Five Times Too Large. Polymer Configuration is Based on Hydrodynamic Molecular Diameters in Solution. Adsorption Configuration is Not Correct. Low Molecular Weight Polymer Molecule Shown by Arrow

From Table III it is apparent that there is no correlation between zeta potential and the stability of this colloidal system. Trends are established, however, for polymer molecular weight, salt concentration, surface charge density, and particle size.

TABLE III

ZETA POTENTIALS OF CFC VALUES DETERMINED IN CONSTANT SURFACE AREA EXPERIMENT (0.0445 m^2)

Particle Size	Fraction	CFC, mg/liter	Zeta Potential, mv	Ads./Sat. Ad., %
		(A) In 10^{-2}M NaCl		
1.101	F_1-6	0.0235	-50	1.60
	F_2-7	0.0708	-38	4.7
0.794	F_1-6	0.0245	-48	1.8
	F_2-7	0.0610	-39	4.0
0.481	F_1-6	0.0234	-37	1.6
	F_2-7	0.0501	-37	3.4
0.234	F_1-6	0.0240	-39	1.5
	F_2-7	0.0426	-38	3.1
0.109	F_1-6	0.0206	-32	1.4
	F_2-7	0.0324	-24	2.3
		(B) In 5×10^{-4}M NaCl		
1.101	F_1-6	0.0380	-48	3.0
	F_2-7	0.1410	-36	10.0
0.794	F_1-6	0.0347	-45	2.9
	F_2-7	0.1380	-34	10.0
0.481	F_1-6	0.0347	-47	2.8
	F_2-7	0.1351	-30	9.5
0.234	F_1-6	0.0347	-43	2.8
	F_2-7	0.1000	-24	7.5
0.109	F_1-6	0.0370	-28	2.6
	F_2-7	0.0891	-25	6.6

EFFECT OF MOLECULAR WEIGHT

The data in Table III reveal that the CFC value is dependent on molecular weight. Under both salt conditions and with all particle sizes, the high molecular weight fraction is more effective initiating flocculation than the low molecular weight fraction. While the CFC parameter has been seldom studied by other workers, enough data are frequently presented by them to determine CFC trends. Data from Gregory and Sheiham (21), Kasper (15), and Gregory (13) all

suggest that the higher molecular weight polyelectrolyte is more effective than the lower weight polyelectrolyte in reaching CFC. Each used a linear cationic polymer and PSL particles. In each case, it can be assumed that the polymer size is the most important parameter. Polymer size appears the important parameter here. This trend is in agreement with the bridging and patch model mechanisms of flocculation.

EFFECT OF SALT CONCENTRATION

Table III indicates that the CFC is dependent on salt concentration. With both molecular weights, the CFC decreases within increasing salt concentration.

When the ionic strength of a suspension is low, the range of electrical interaction between particles is great and quite low values of surface potential are sufficient for stability. For this reason only a slight excess positive or negative charge would be necessary to stabilize PSL particles in distilled water. As the salt concentration increases, a greater charge is necessary to prevent flocculation.

EFFECT OF SURFACE CHARGE DENSITY AND PARTICLE SIZE

Figures 13 and 14 contain plots of CFC *versus* surface charge density and CFC *versus* particle size in 10^{-2}M NaCl, respectively. Similar plots are found for data obtained in a salt concentration of 5×10^{-4}M NaCl. Two trends are apparent: 1) with fraction F_1-6, the CFC is nearly independent of particle size and surface charge density, and 2) with fraction F_2-7, the CFC is dependent on particle size and surface charge density.

It is impossible to use the information in Fig. 13 and 14 to distinguish between the effects of surface charge density and particle size. In the

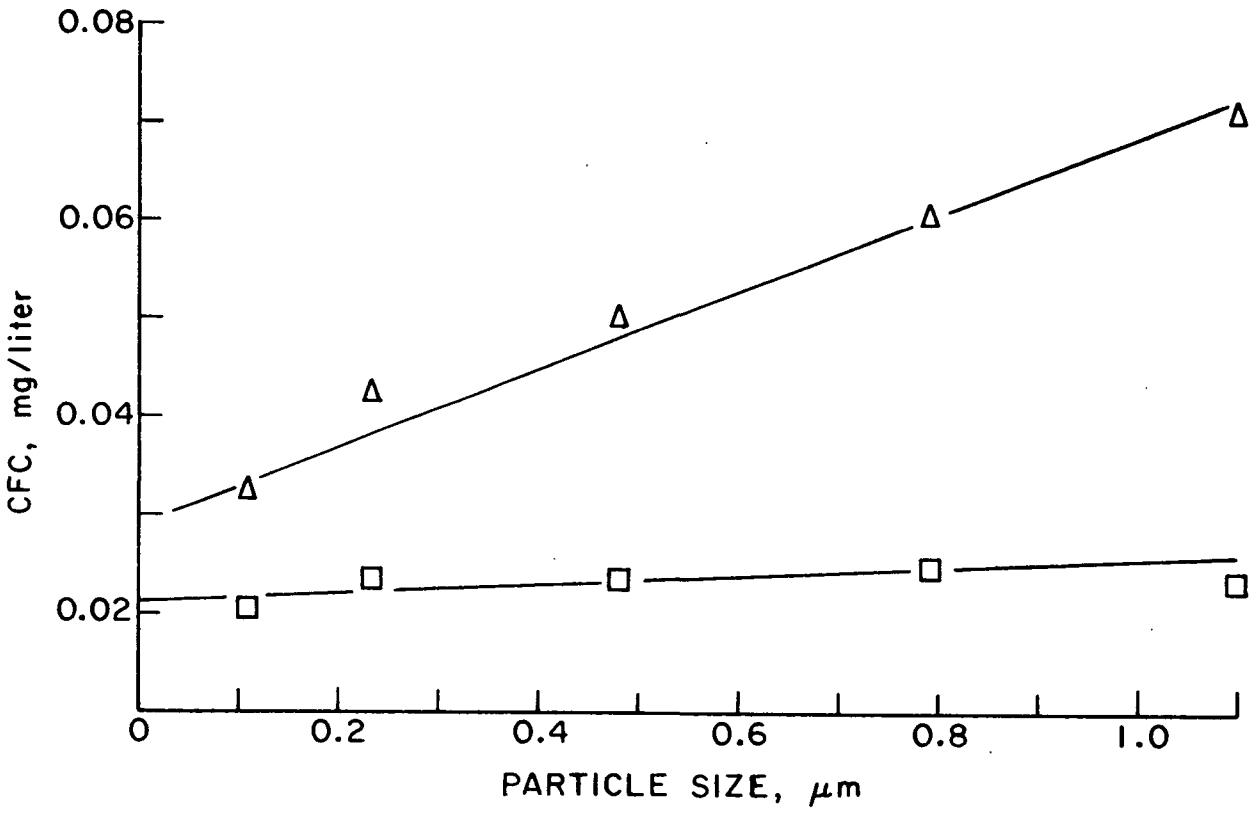

Figure 13. CFC Versus Particle Size with Fractions F_1-6 (□) and F_2-7 (Δ) in 10^{-2}M NaCl

flocculation of colloidal particles by electrolyte, the DLVO theory predicts that the main parameters in the flocculation concentration are the potential of the Stern layer and the valence of the counterion (50). The flocculation concentration is independent of particle radius. However, the behavior of an adsorbed polyelectrolyte is much more complex than an equal weight of adsorbed electrolyte and the applicability of the DLVO theory concerning particle size is uncertain.

Additional flocculation work was performed with a PSL particle supplied by Professor I. M. Krieger (see Appendix I). The PSL particle has a lower surface charge density to particle size ratio than the Dow PSL particles. Pertinent characteristics of the particle and CFC values are listed in Table IV.

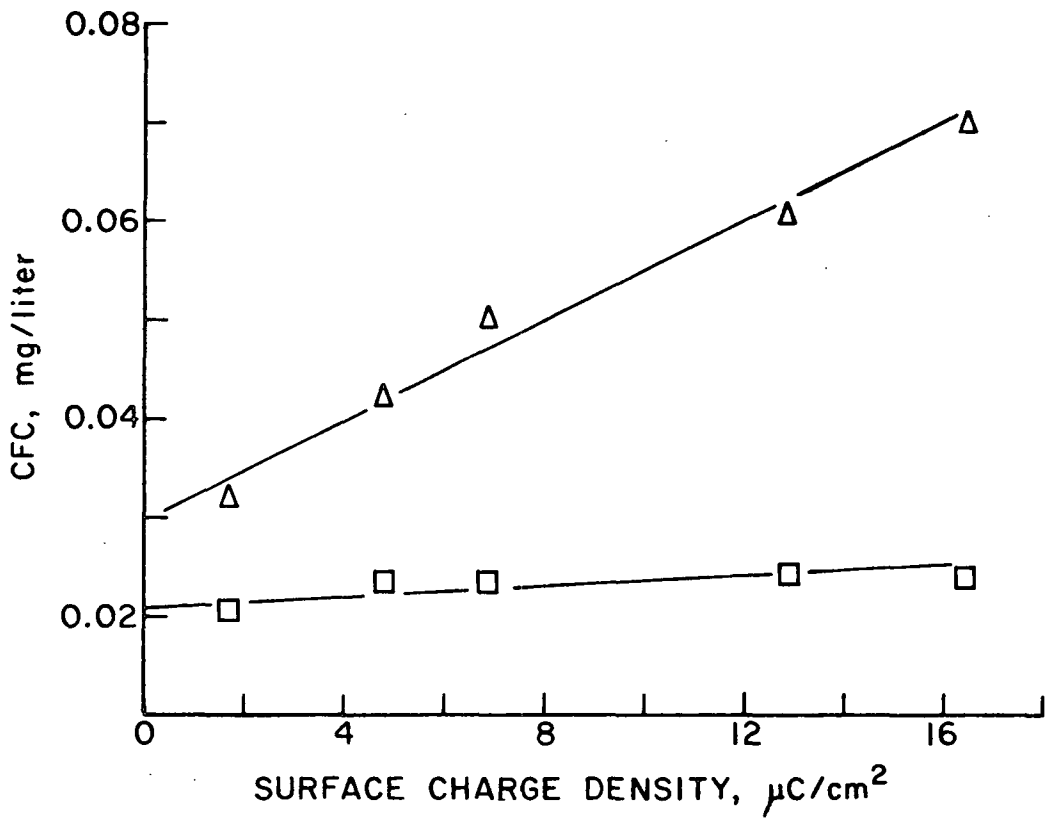

Figure 14. CFC Versus Surface Charge Density with Fractions F_1-6 (□) and F_2-7 (Δ) in 10^{-2}M NaCl

Also listed are CFC values picked off the curves in Fig. 13 and 14 which empirically correspond to a particle size 0.330 μm and surface charge density of 3.45 μC/cm², respectively.

Comparison of the experimentally determined CFC values with those empirically derived establishes a definite trend; the particle size data are closer in value to the experimentally determined CFC value than the surface charge density data. From Table IV it appears that this trend is more evident for fraction F_2-7 than F_1-6. This trend suggests that CFC values are influenced to a greater extent by the parameter of particle size than by surface charge density.

TABLE IV

CFC VALUES OF 0.330 μm PSL, 3.45 μC/cm^2
AT CONSTANT SURFACE AREA CONCENTRATION

Method	NaCl Concentration, M	Fraction	CFC, mg/liter
Experimental	10^{-2}	F_1-6	0.0270
CFC vs. particle size			0.0232
CFC vs. surface charge density			0.0220
Experimental	10^{-2}	F_2-7	0.0540
CFC vs. particle size			0.0450
CFC vs. surface charge density			0.0380
Experimental	5×10^{-4}	F_1-6	0.0370
CFC vs. particle size			0.0355
CFC vs. surface charge density			0.0355
Experimental	5×10^{-4}	F_2-7	0.1210
CFC vs. particle size			0.1143
CFC vs. surface charge density			0.0953

Figure 15 presents another means of evaluating the effect of PSL surface charge density. Figure 15 is a plot of the ratio negative charges/positive charges per particle at CFC versus surface charge density. The negative charges per particle were calculated from the surface charge densities and geometric surface areas of the PSL particle. The number of polymer molecules per particle was calculated from the polymer concentration, based on narrow molecular weight fractions (see p. 125). A zero or near zero slope would indicate that a specific negative/positive charge ratio was necessary to reach CFC, thus implying the significance of surface charge density in reaching CFC. The more positive the slope becomes, the less dependent CFC values are on surface charge density.

From the data it can be concluded that both particle size and surface charge density have an effect on the CFC value. While the exact percentage each parameter contributes to CFC cannot be determined, particle size seems to play the dominant role.

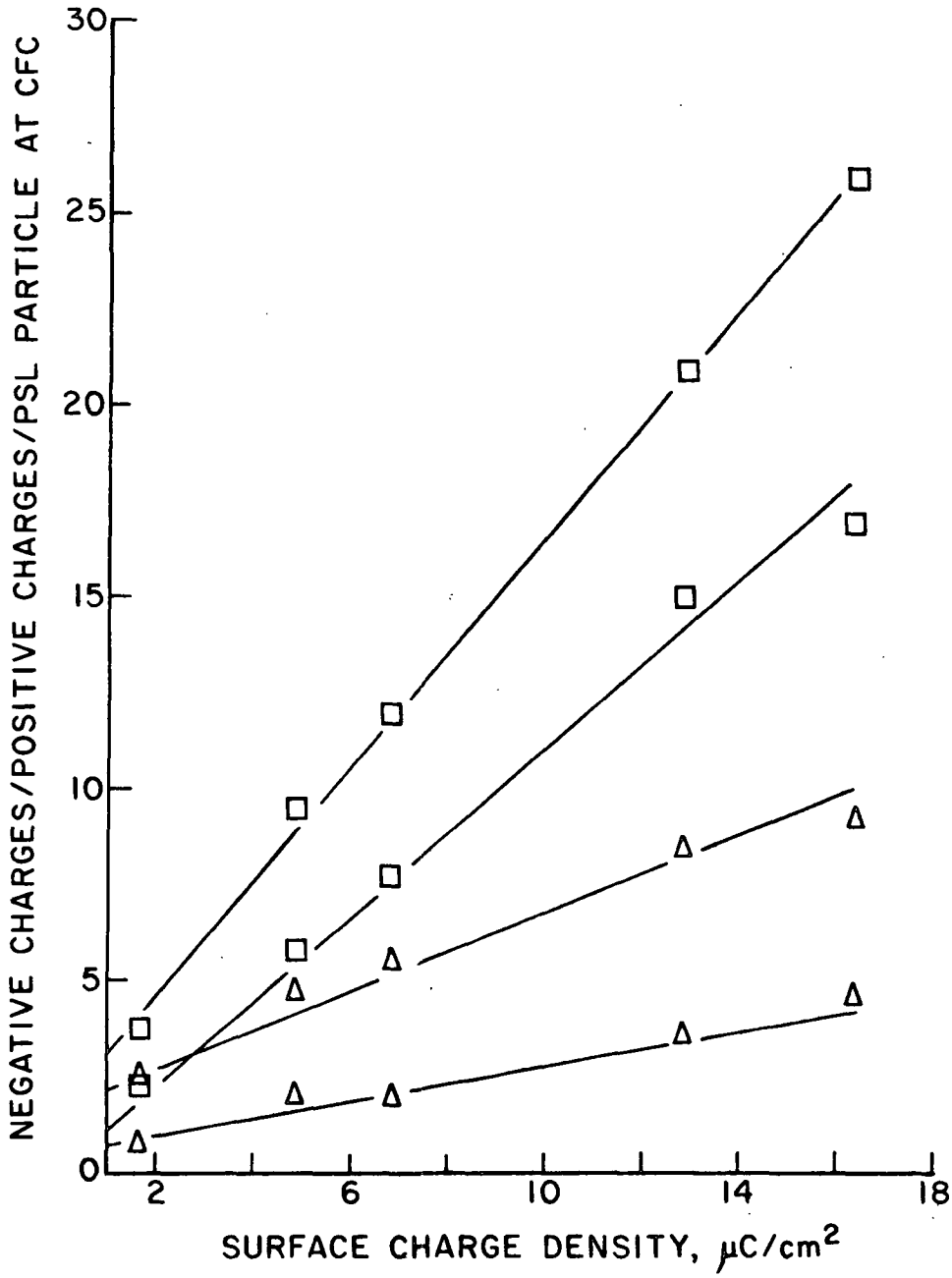

Figure 15. Negative Charges/Positive Charges Per PSL Particle Versus Surface Charge Density at CFC

OPTIMUM FLOCCULATION CONCENTRATION

Figure 16 is a plot of relative turbidity versus poly(DMVPB) concentration. The OFC point bisects the flocculation curve. Comparison of three duplicated experimental runs with the three originals revealed an 18% uncertainty in determining their OFC values by this method. Table V presents the complete OFC data for the constant surface area experiment and the respective zeta potentials.

The data indicate optimum flocculation occurs before the charge neutralization point is reached. There is one case, however, where the OFC does not occur until the net particle charge is positive. There is no explanation for this result at this time except that this is the only case and the zeta potential is very close to zero where the experimental precision is poor.

EFFECT OF MOLECULAR WEIGHT

The data in Table V show that at a salt concentration of 10^{-2}M NaCl, there is little dependence of the OFC value on polymer molecular weight. In a salt concentration of 5×10^{-4}M NaCl the conclusion is not clear. The values for particle sizes 1.101 and 0.109 μm tend to be only slightly dependent on polymer molecular weight while those for particle sizes 0.794, 0.481, and 0.234 μm tend to be more so. This inconsistency is not explainable at this time. However, the OFC values determined from the constant particle experiment had little dependence on polymer molecular weight under both salt conditions (Appendix VI). From these findings it can be assumed that the significant difference which is found at the OFC with particle sizes 0.794, 0.481, and 0.234 μm is a maximum.

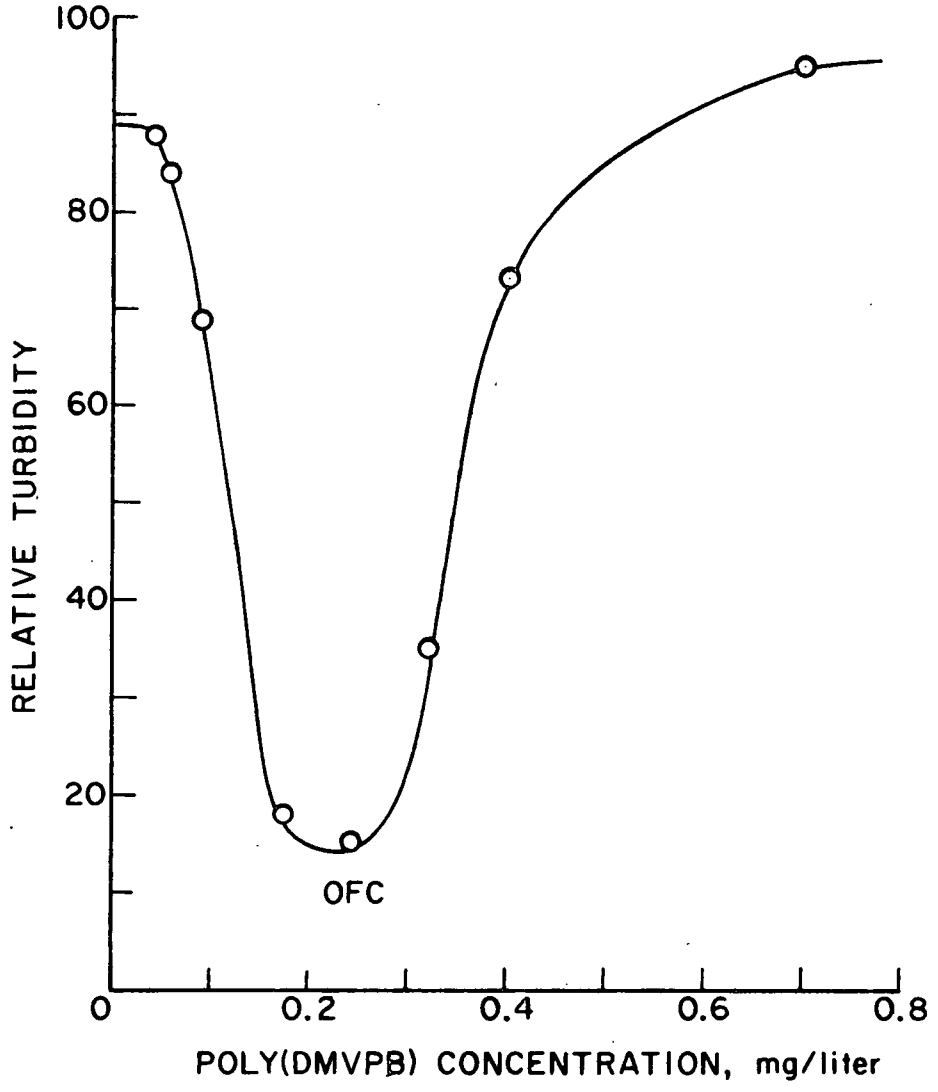

Figure 16. Relative Turbidity Versus Poly(DMVPB) Concentration; Particle Size 1.101 μm, 341 mg/Liter

TABLE V

ZETA POTENTIALS FOR OFC VALUES DETERMINED IN CONSTANT SURFACE AREA EXPERIMENT

Particle Size	Fraction	OFC, mg/liter	Zeta Potential, mv	Ads./Sat. Ad., %
		(A) In 10^{-2}M NaCl		
1.101	F_1-6	0.200	-23	13.1
	F_2-7	0.245	-16	16.3
0.794	F_1-6	0.185	-21	13.4
	F_2-7	0.225	-10	15.3
0.481	F_1-6	0.165	-6	11.5
	F_2-7	0.170	-8	11.6
0.234	F_1-6	0.120	-20	7.6
	F_2-7	0.105	-20	7.6
0.109	F_1-6	0.100	-8	6.8
	F_2-7	0.105	-4	7.4
		(B) In 5×10^{-4}M NaCl		
1.101	F_1-6	0.180	-24	14.1
	F_2-7	0.230	-17	16.3
0.794	F_1-6	0.155	-28	13.1
	F_2-7	0.260	+4	17.7
0.481	F_1-6	0.110	-30	8.5
	F_2-7	0.200	-18	14.1
0.234	F_1-6	0.080	-29	6.6
	F_2-7	0.160	-12	11.9
0.109	F_1-6	0.090	-18	6.9
	F_2-7	0.125	-4	9.3

The OFC is one of the most extensively studied parameters in flocculation experiments. Brown, et al. (51) who investigated the flocculation of a negatively charged aqueous polymer latex by poly(dimethyl-aminoethylmethacrylate) found that the OFC decreased with increasing polymer molecular weight. In fact, Williams and Ottewill (52) showed that the OFC, C_2^*, in the case of positive silver iodide sols flocculated by poly(acrylic acid), can be represented by a relationship of the following kind:

$$C_{\frac{1}{2}}^{*} = aM_v^{-b}, \qquad (7)$$

where a and b are constants and M_v is the viscosity average molecular weight of the polymer.

On the other hand, Gregory (13), flocculating a polystyrene latex, found that there was little dependence of either the OFC or the rate of flocculation at the OFC on the molecular weight of the added polymethacrylate over the range of 5×10^4-10^5. Gregory and Sheiham (21) flocculated PSL (particle size 0.091 μm) with poly(1-ethyl 5-methyl 2-vinyl pyridinium bromide) having molecular weights of 9×10^3 and 10^6 and found no dependence on molecular weight in reaching OFC.

From the data it can be concluded that polymer size is not the most important parameter at the OFC and that polymer charge plays a dominant role. This trend is in agreement with the charge neutralization and electrostatic patch model mechanisms of flocculation.

EFFECT OF SALT CONCENTRATION

Increasing salt concentration has a greater effect on the PSL particles than on the poly(DMVPB) molecules. Nagasawa (53), reviewing the thermodynamic and hydrodynamic properties of polyelectrolytes, states that studies have shown the degree of ion binding is nearly independent of concentration of added neutral salt. With increasing salt concentration the diffuse layer of the PSL particles is compressed, thus reducing the stability of the PSL particle. Therefore one would predict that the OFC would decrease with increasing salt concentration because of the decreased stability of the PSL particles. However, Table V indicates there is very little, if any, dependence on salt concentration in determining the OFC value. The reason

for this result is not known. It may be speculated that the increased number of polymer molecules per PSL particle (see p. 82) at OFC influences the stability of the PSL particle. At CFC there is fairly low surface coverage and the electric double layer of the particle is probably intact. At OFC it is possible that the electric double layer is broken up and as a result the stability of the particle is influenced more by the number of adsorbed polymer charges rather than the salt concentration.

EFFECT OF SURFACE CHARGE DENSITY AND PARTICLE SIZE

Figure 17 plots OFC versus surface charge density and OFC versus particle size for fraction F_1-6 in 10^{-2}M NaCl. The similarity of the plots makes it impossible to distinguish between the effect of surface charge density and particle size on OFC. Figure 16 is representative of similar plots with fraction F_2-7 in 10^{-2}M NaCl and both fractions in 5×10^{-4}M NaCl.

Table VI consists of experimentally determined OFC values for particle size 0.330 μm and empirically determined OFC values by picking points off the smooth curves of OFC versus surface charge density and OFC versus particle size.

Comparison of the experimentally determined OFC values with those empirically derived establishes the trend which was previously seen from the CFC data; i.e., particle size influences the OFC value to a greater extent than surface charge density does for this system.

Figure 18 is a plot of the ratio of negative charges/positive charges per particle at OFC versus surface charge density in a salt concentration of 10^{-2}M NaCl for both fractions. Similar results are found in 5×10^{-4}M NaCl.

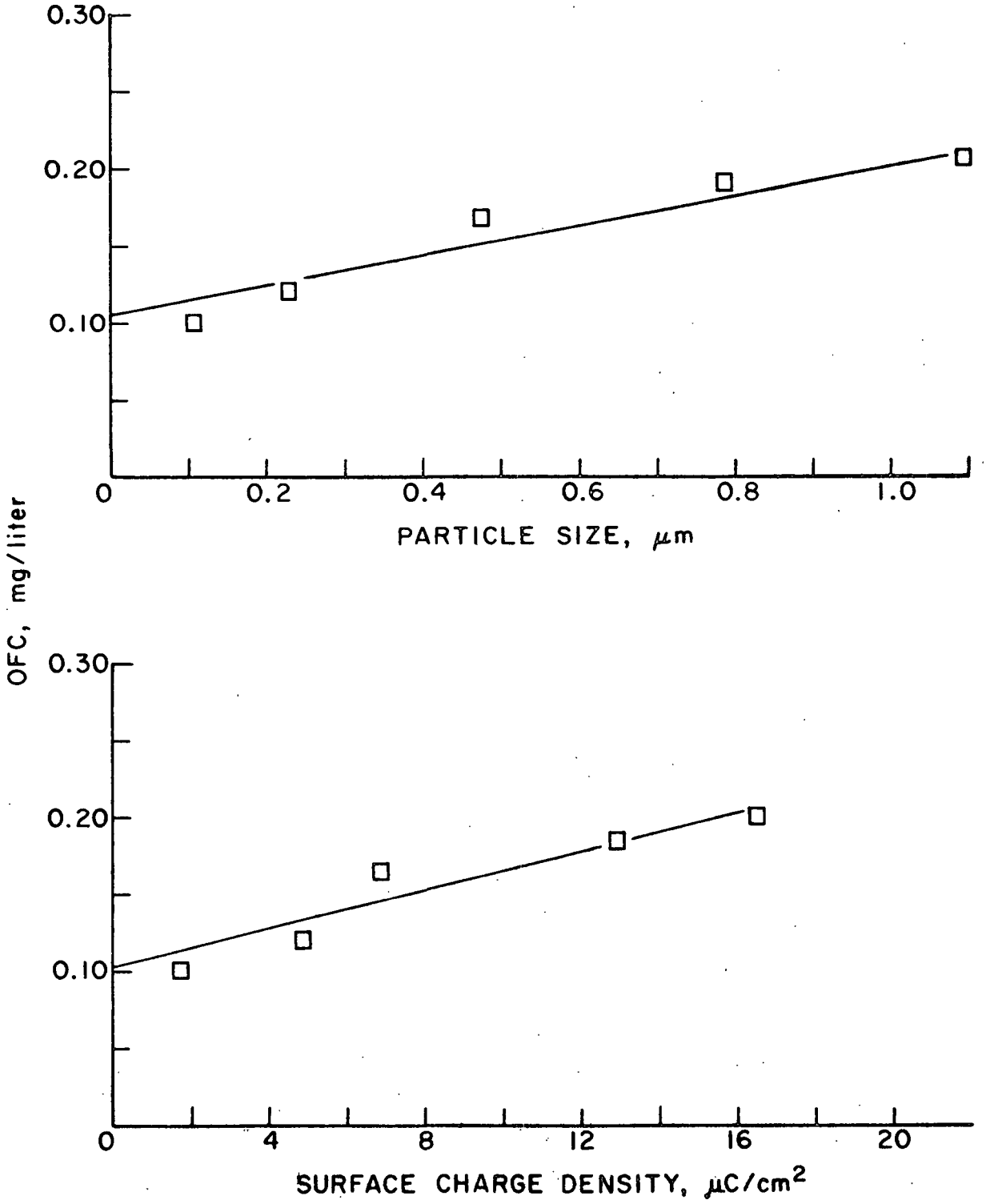

Figure 17. OFC Versus Particle Size and OFC Versus Surface Charge Density with Fraction F_1-6 in 10^{-2}M NaCl

TABLE VI

THE EFFECT OF PARTICLE SIZE IN DETERMINING OFC

Method	Fraction	NaCl Concentration, M	OFC
Experimental	F_1-6	10^{-2}	0.1650
CFC vs. particle size			0.1390
CFC vs. surface charge density			0.1110
Experimental	F_1-6	5×10^{-4}	0.1400
CFC vs. particle size			0.0990
CFC vs. surface charge density			0.0850
Experimental	F_2-7	10^{-2}	0.1700
CFC vs. particle size			0.1310
CFC vs. surface charge density			0.1050
Experimental	F_2-7	5×10^{-4}	0.1500
CFC vs. particle size			0.1720
CFC vs. surface charge density			0.1420

Again, the more positive the slope, the less dependent OFC values are on surface charge density. The slopes in Fig. 18 are smaller than those found at the CFC, implying either that the effect of particle surface charge density is greater in determining OFC than it is in determining CFC or that the effect of particle size is less at OFC than at CFC.

POINT OF CHARGE NEUTRALIZATION

Table VII presents the amount of polymer necessary to reach the point of charge neutralization. These points are picked off smooth curves of zeta potential versus polymer concentration. There are three trends that are apparent from the data: 1) the point of charge neutralization is independent of polymer molecular weight, 2) the point of charge neutralization is independent of salt concentration, and 3) a 1:1 negative/positive charge ratio is not necessary to achieve charge neutralization.

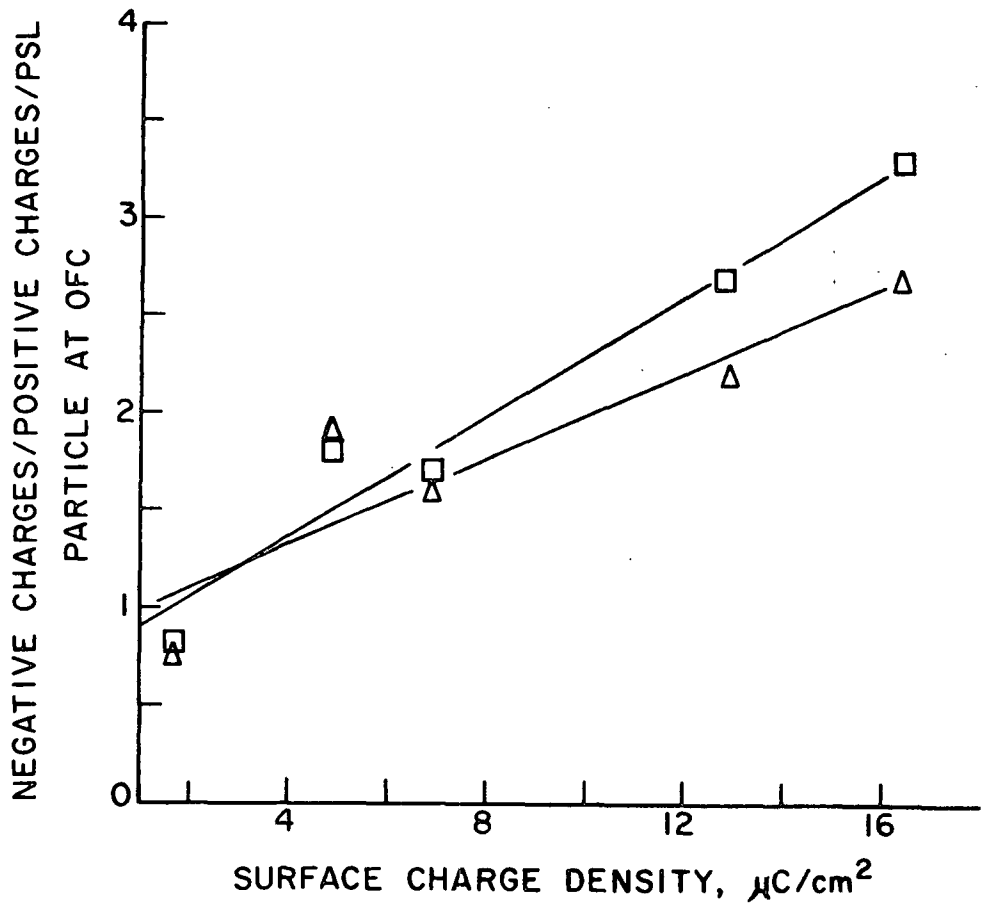

Figure 18. Negative Charges/Positive Charges per PSL Particle at OFC Versus Surface Charge Density. Fraction F_1-6 (□) and Fraction F_2-7 (Δ) in 10^{-2}M NaCl

TABLE VII

POLYMER ADSORPTION AND NEGATIVE/POSITIVE CHARGE RATIO AT POINT OF CHARGE NEUTRALIZATION

Particle Size	Fraction	NaCl Concentration, M	Amount Adsorbed, mg/liter	Ads./Sat. Ads., %	Negative Charges/ Positive Charges
1.101	F_1-6	10^{-2}	0.280	18.3	2.3
		5×10^{-4}	0.310	24.2	2.1
	F_2-7	10^{-2}	0.300	20.0	2.2
		5×10^{-4}	0.320	22.7	2.0
0.794	F_1-6	10^{-2}	0.250	18.1	2.0
		5×10^{-4}	0.240	20.3	2.1
	F_2-7	10^{-2}	0.240	16.3	2.1
		5×10^{-4}	0.250	17.0	2.2
0.481	F_1-6	10^{-2}	0.200	13.9	1.4
		5×10^{-4}	0.225	17.4	1.2
	F_2-7	10^{-2}	0.220	15.1	1.2
		5×10^{-4}	0.237	16.7	1.2
0.234	F_1-6	10^{-2}	0.170	10.9	1.3
		5×10^{-4}	0.150	12.3	1.3
	F_2-7	10^{-2}	0.160	11.5	1.2
		5×10^{-4}	0.185	13.8	1.1
0.109	F_1-6	10^{-2}	0.100	6.8	0.3
		5×10^{-4}	0.120	9.2	0.6
	F_2-7	10^{-2}	0.110	7.7	0.7
		5×10^{-4}	0.125	9.3	0.6

The first two points support the contention that polymer charge is important at charge neutralization. Polymer size plays a minor role and, as pointed out earlier, salt concentration does not significantly affect polymer charge. The reasons concerning the third point are not very clear even though this effect is found in the literature (15,22). The arrangement of the sulfate end-groups and the adsorbed polymer configuration could be the key factors; however, this is only speculation.

RESTABILIZATION CONCENTRATION

Table VIII presents the complete restabilization concentration data for the constant surface area experiment and the respective zeta potentials. The restabilization concentration is that polymer concentration necessary to reach 90% of the turbidity in zone I.

TABLE VIII

ZETA POTENTIALS FOR RSC VALUES DETERMINED IN CONSTANT SURFACE AREA EXPERIMENT

Particle Size	Fraction	NaCl Concentration, M	RSC, mg/liter	Ads./Sat. Ads., %	Zeta Potential
1.101	F_1-6	10^{-2}	0.560	37	+38
		5×10^{-4}	0.500	39	+24
	F_2-7	10^{-2}	0.600	40	+34
		5×10^{-4}	0.430	31	+24
0.794	F_1-6	10^{-2}	0.450	32	+26
		5×10^{-4}	0.460	39	+40
	F_2-7	10^{-2}	0.410	29	+28
		5×10^{-4}	0.490	33	+32
0.481	F_1-6	10^{-2}	0.410	28	+24
		5×10^{-4}	0.400	31	+30
	F_2-7	10^{-2}	0.500	39	+32
		5×10^{-4}	0.450	32	+30
0.234	F_1-6	10^{-2}	0.260	16	+26
		5×10^{-4}	0.300	25	+32
	F_2-7	10^{-2}	0.290	21	+32
		5×10^{-4}	0.380	29	+24
0.109	F_1-6	10^{-2}	0.230	16	+24
		5×10^{-4}	0.220	17	+24
	F_2-7	10^{-2}	0.190	14	+18
		5×10^{-4}	0.290	22	+19

From Table VIII, it is seen that RSC depends very little upon polymer molecular weight and salt concentration. Theoretically (50), one would predict that the weak salt solution would be restabilized at a lower polymer concentration. It is not clear why this did not occur.

FLOCCULATION CURVES

Figures 19 and 20 show representative flocculation curves of PSL 1.101 and 0.109 μm by fractions F_1-6 and F_2-7 in 10^{-2}M NaCl and 5×10^{-4}M NaCl. In all cases, as the particle size and surface charge density are decreased the flocculation curve becomes narrower. Table IX presents data on the width of the flocculation curve taken at a point midway between OFC and RSC. Two trends are apparent from Fig. 19 and 20: the turbidity at OFC is independent of polymer molecular weight in 10^{-2}M NaCl and dependent on polymer molecular weight in 5×10^{-4}M NaCl.

In 5×10^{-4}M NaCl the residual turbidity increases as the polymer molecular weight decreases. The observed difference in floc settling could be due to a difference in floc density and/or floc size. Assuming that poly(DMVPB) adsorbs in a relatively flat configuration with loop sizes independent of molecular weight, it seems unlikely that the structure or "compactness" of the flocs would vary with differences of polymer molecular weight. It is probable, however, that as the electrostatic patch size increases, the interaction between patch and nonpatch area increases, therefore increasing the strength of the floc. The strength of the floc would also be dependent on the repulsive patch-patch and nonpatch-nonpatch interaction of the two particles. The size of the flocs would be determined by the agitation in the system. As the salt concentration increases, the electric interaction range of the system decreases. Therefore, floc strength would be more dependent on patch size as the salt concentration decreases. The agitation of the system would break up more flocs created by low molecular weight polymer than the larger molecular weight polymer and hence the relative turbidity of the low molecular weight polymer-PSL solution with low salt concentration would be high.

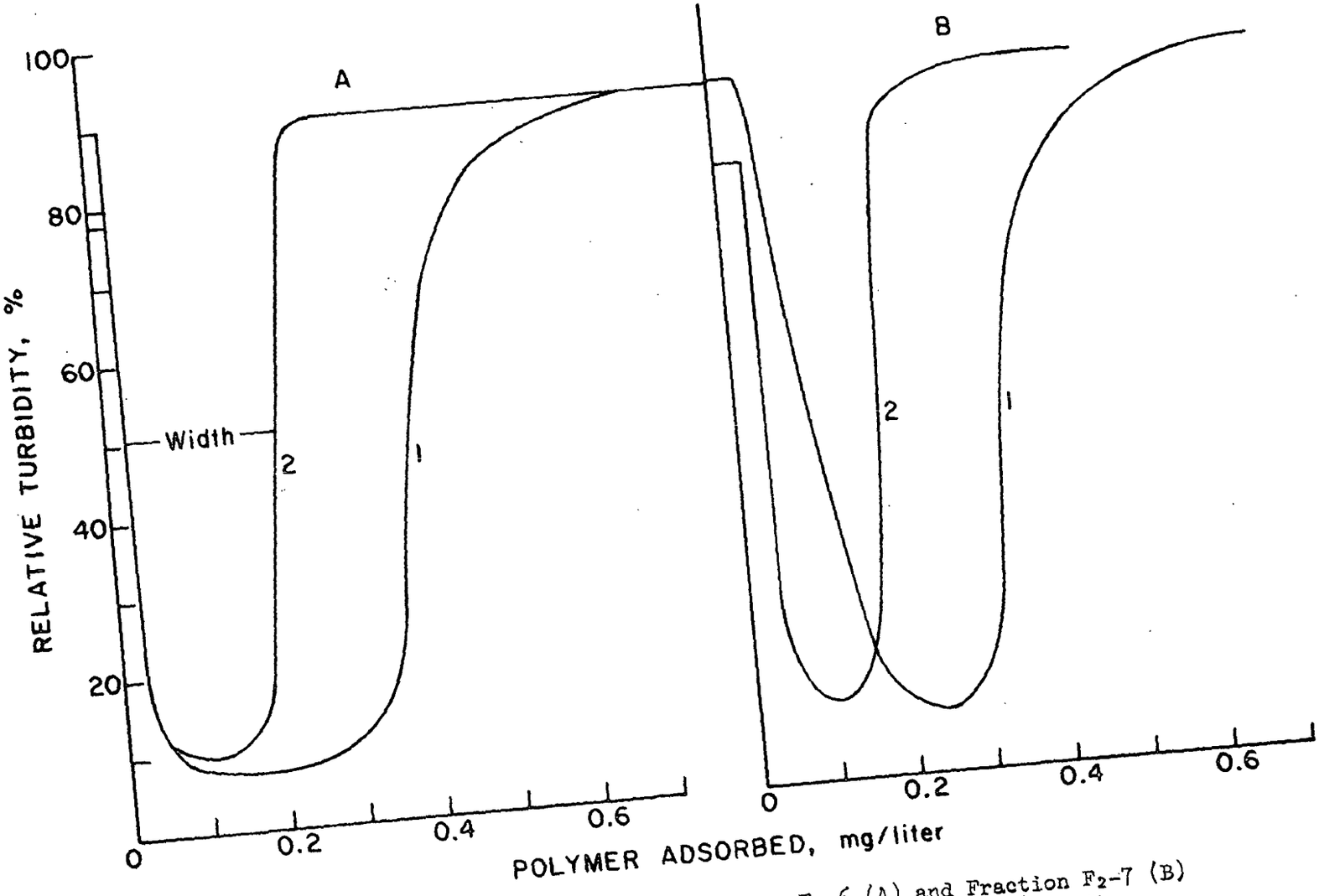

Figure 19. Flocculation Curves of Fraction F_1-6 (A) and Fraction F_2-7 (B) with Particle Size 1.101 μm (1) and 0.109 μm (2) in 10^{-2} M NaCl

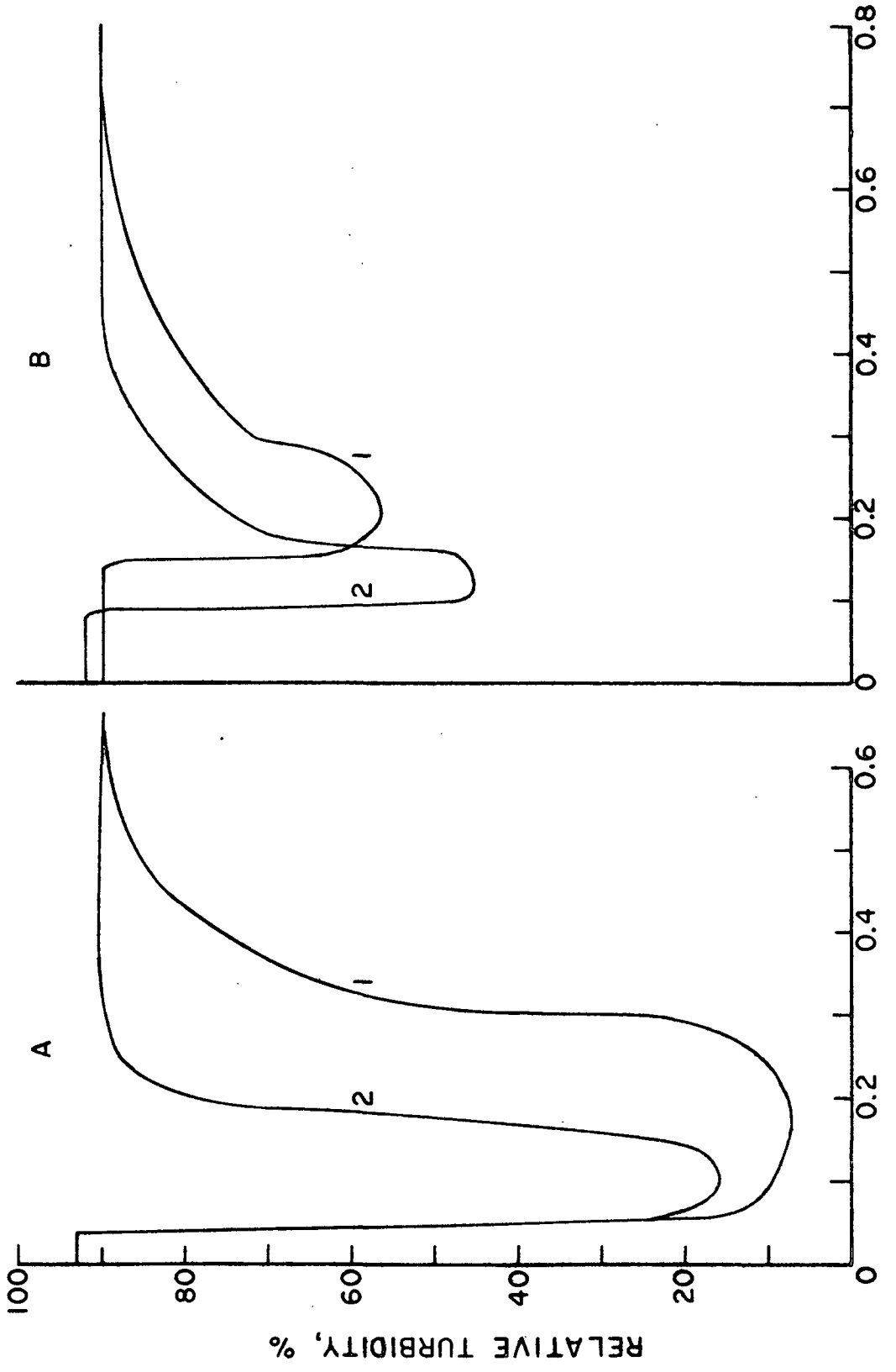

Figure 20. Flocculation Curves of Fraction F_1-6 (A) and Fraction F_2-7 (B) with PSL Particle Size 1.101 μm (1) and 0.109 μm (2) in 5×10^{-4} M NaCl

TABLE IX

WIDTH OF FLOCCULATION CURVES FOR CONSTANT SURFACE AREA EXPERIMENT

Particle Size, μm	Fraction	Width, mg/liter
	10^{-2}M NaCl	
1.101	F_1-6	0.38
	F_2-7	0.24
0.794	F_1-6	0.36
	F_2-7	0.23
0.481	F_1-6	0.30
	F_2-7	0.22
0.234	F_1-6	0.19
	F_2-7	0.14
0.109	F_1-6	0.18
	F_2-7	0.14
	5×10^{-4}M NaCl	
1.101	F_1-6	0.26
	F_2-7	0.20
0.794	F_1-6	0.24
	F_2-7	0.22
0.481	F_1-6	0.19
	F_2-7	0.10
0.234	F_1-6	0.14
	F_2-7	0.13
0.109	F_1-6	0.12
	F_2-7	0.07

In summary, it is speculated that the decrease in residual turbidity at OFC in 5×10^{-4}M NaCl as polymer molecular weight increases is due to a difference in floc size. As the electrostatic patch size increases, floc strength and subsequently floc size increases.

SUMMARY OF FLOCCULATION

Figure 21 presents a schematic summary of the flocculation results. The effects of polymer molecular weight, salt concentration, particle size, and surface charge density on the flocculation parameters of CFC, OFC, charge neutralization, and RSC are shown.

	Molecular Weight	Salt Concentration	Particle Size	Surface Charge Density
CFC	D	D	I	I
OFC	LC	LC	I	I
Charge Neutralization	LC	LC	I	I
RSC	LC	LC	I	I

Figure 21. General Trends of Flocculation Results Indicating the Effects of Increasing Polymer Molecular Weight, Salt Concentration, Particle Size and Surface Charge Density on CFC, OFC, Charge Neutralization and RSC Values. I = Increasing With; D = Decreasing With; LC = Little Change

DISCUSSION OF FLOCCULATION RESULTS

The bridging, charge neutralization and electrostatic patch models are discussed as possible mechanisms of flocculation. The best possible model is that defined as being consistent with the flocculation results, i.e., CFC and OFC data.

THE BRIDGING MODEL

The bridging theory is based on the physical interactions between colloidal particles and polymer, neglecting the electrostatic interactions. The requirements for flocculation by bridging are: 1) that adsorption sites are available and 2) that the configuration of adsorbed polymer is such that sufficient polymer segments exist which extend greater than the interaction distances of the repulsive forces. From this it is safe to assume only a small fraction of the polymer attaches to the colloidal particle and the greater the polymer size, the more efficient it is as a flocculant.

The rate of polymer adsorption is fast in comparison to the flocculation rate (15,21). Therefore, once a polymer molecule attaches to a colloidal particle, flocculation can occur in either the polymer's non-equilibrium or equilibrium adsorption configuration state.

Even though an adsorbed polymer configuration in the equilibrium state is flat, until the equilibrium state is attained, the polymer loops may extend quite far into the solution (21). From the standpoint of flocculation, the crucial factor is the particle collision frequency (and hence the particle number concentration). In a concentrated sol, a particle may experience many collisions during the time in which the adsorbed polymer achieves its equilibrium configuration and bridging could then be a significant

flocculation mechanism. An example of nonequilibrium flocculation has been presented by Gregory and Sheiham (21). They studied the flocculation of PSL, particle diameter 0.091 μm, by poly(1-ethyl 5-methyl 2-vinylpyridinium bromide) having polymer molecular weights of 9×10^3 and 10^6. In PSL concentration of 20 mg/liter, both polymer molecular weights behave identically. At a higher latex concentration of 100 mg/liter, the lower molecular weight polymer showed essentially the same behavior as in the lower PSL sol; however, the high molecular weight polymer gave flocculation over a broader range of concentration. A visual picture of this phenomena is seen in Fig. 22 (21). When excess high $\underline{M_w}$ polymer is adsorbed, the reconformation of the absorbed chains is considerably slower due to steric hindrance of neighboring adsorbed polymer molecules. For a few seconds bridge formation is possible and flocculation occurs even though the PSL is now positively charged. This "nonequilibrium flocculation" becomes important with particle concentrations of about 10^{11} cm^{-3} or greater.

The critical particle collision frequency of Gregory and Sheiham (21), which determined when nonequilibrium bridging became an important flocculation mechanism, cannot be used as a means of comparison for this system. Agitation was present in this work after mixing particles and polymer, and it was absent in Gregory and Sheiham's work. As a result, the particle collision frequencies are calculated in different manners.

By describing the present system as one where the particles are subjected to simple laminar flow, the particle collision frequency of this system can be described by the following equation (7):

$$F_o = 4/3(R^*)^3(\frac{du}{dz})\ Ni^2 \qquad (8)$$

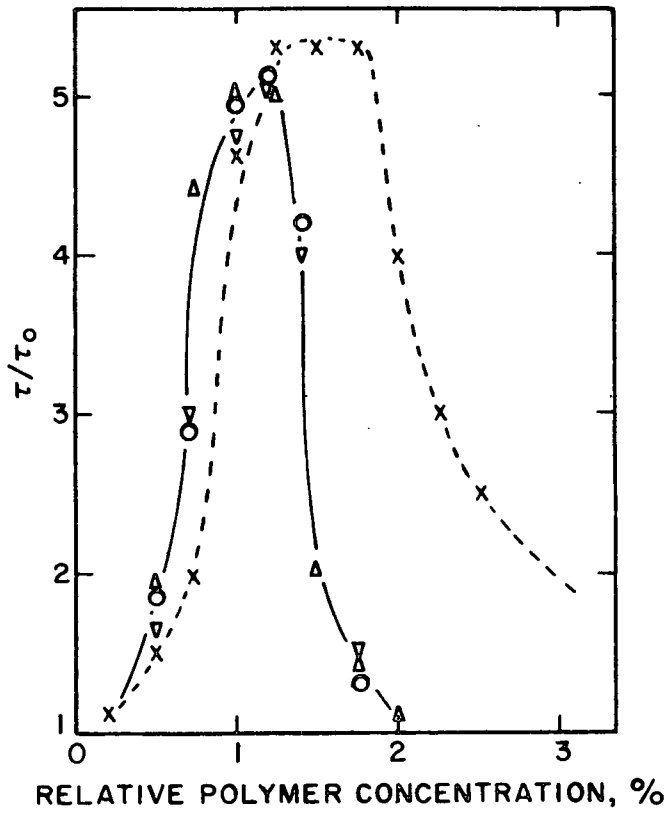

Figure 22. Flocculation of Latex at Two Concentrations: 20 mg/Liter With Large $\underline{M}_w$ Polymer (Δ) and Low $\underline{M}_w$ Polymer (∇); 100 mg/Liter With Large $\underline{M}_w$ Polymer (x) and Low $\underline{M}_w$ Polymer (o). Results Plotted as Relative Turbidity Versus Relative Polymer Concentration (21)

where $\underline{F}_o$ = particle collision frequency

$\underline{R}^*$ = the collision diameter (taken here as the particle diameter)

$(\underline{du}/\underline{dz})$ = the velocity gradient (assumed the same for all cases in this work)

$\underline{Ni}$ = the number of particles/cm^3

Table X indicates the reduced particle collision frequencies for this system. From Gregory and Sheiham's results (21) one would predict that as $\underline{F}_o$ increases, the probability of nonequilibrium flocculation also increases. Figures 23 and 24 show relative turbidity plotted against polymer concentration for fraction F_1-6 in 5×10^{-4}M NaCl and particle sizes 0.794 and 1.101 μm, respectively, at the latex concentrations which correspond to the constant surface area and constant particle experiments. Two trends are apparent: 1) in Fig. 23, fraction

F_1-6 behaves approximately the same for both latex concentrations and 2) in Fig. 24 the constant particle flocculation curve is extended beyond the constant surface area flocculation curve. This effect is similar to that observed by Gregory and Sheiham (21) which was concluded to indicate non-equilibrium bridging. It should be noted that this effect took place in that experiment where the particle collision frequency was the greatest. This effect was not observed with particle sizes 0.481 and 0.234 μm. With the available data, the critical particle collision frequency of this system lies between 429×10^4 (du/dz) and 1116×10^4 (du/dz).

TABLE X

REDUCED PARTICLE COLLISION FREQUENCY FOR CONSTANT SURFACE AREA (A) AND CONSTANT PARTICLE (B) EXPERIMENT

Particle Size, μm	R*, cm	Ni	$F_o/(du/dz)$
	(A)		
1.101	1.10×10^{-4}	4.7×10^8	3.9×10^5
0.794	0.79×10^{-4}	8.9×10^8	5.4×10^5
0.481	0.48×10^{-4}	2.5×10^9	9.3×10^5
0.234	0.23×10^{-4}	1.0×10^{10}	1.6×10^6
0.109	0.11×10^{-4}	4.7×10^{10}	3.9×10^6
	(B)		
1.101	1.10×10^{-4}	2.5×10^9	1.1×10^7
0.794	0.79×10^{-4}	2.5×10^9	4.3×10^6
0.481	0.48×10^{-4}	2.5×10^9	9.3×10^5
0.234	0.23×10^{-4}	2.5×10^9	1.0×10^5

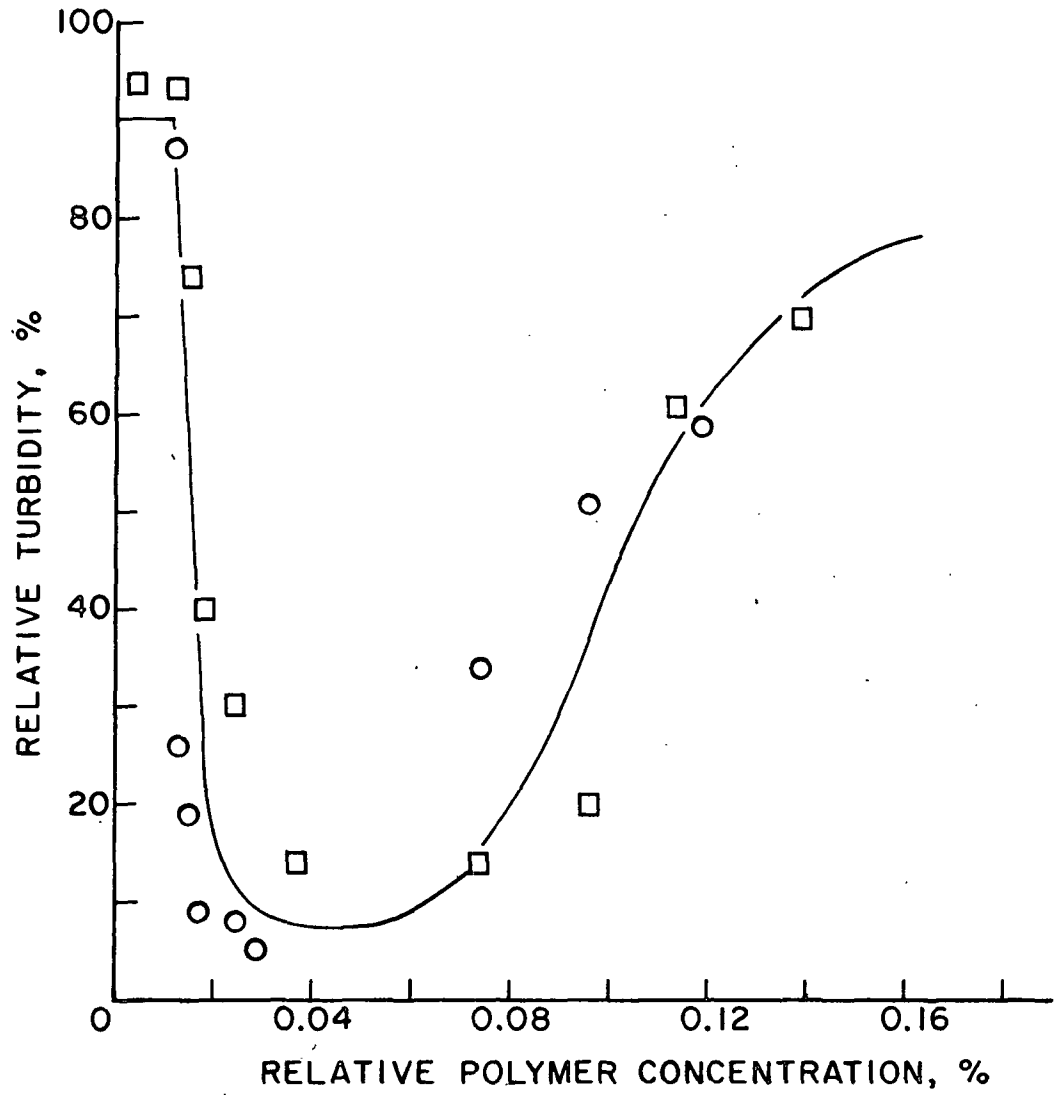

Figure 23. Relative Turbidity Versus Polymer Concentration for Fraction F_1-6 in 5×10^{-4} M NaCl and Particle Size 0.794 μm. Constant Surface Area Data (□) and Constant Particle Data (o). Polymer Concentration Expressed as % of PSL Weight

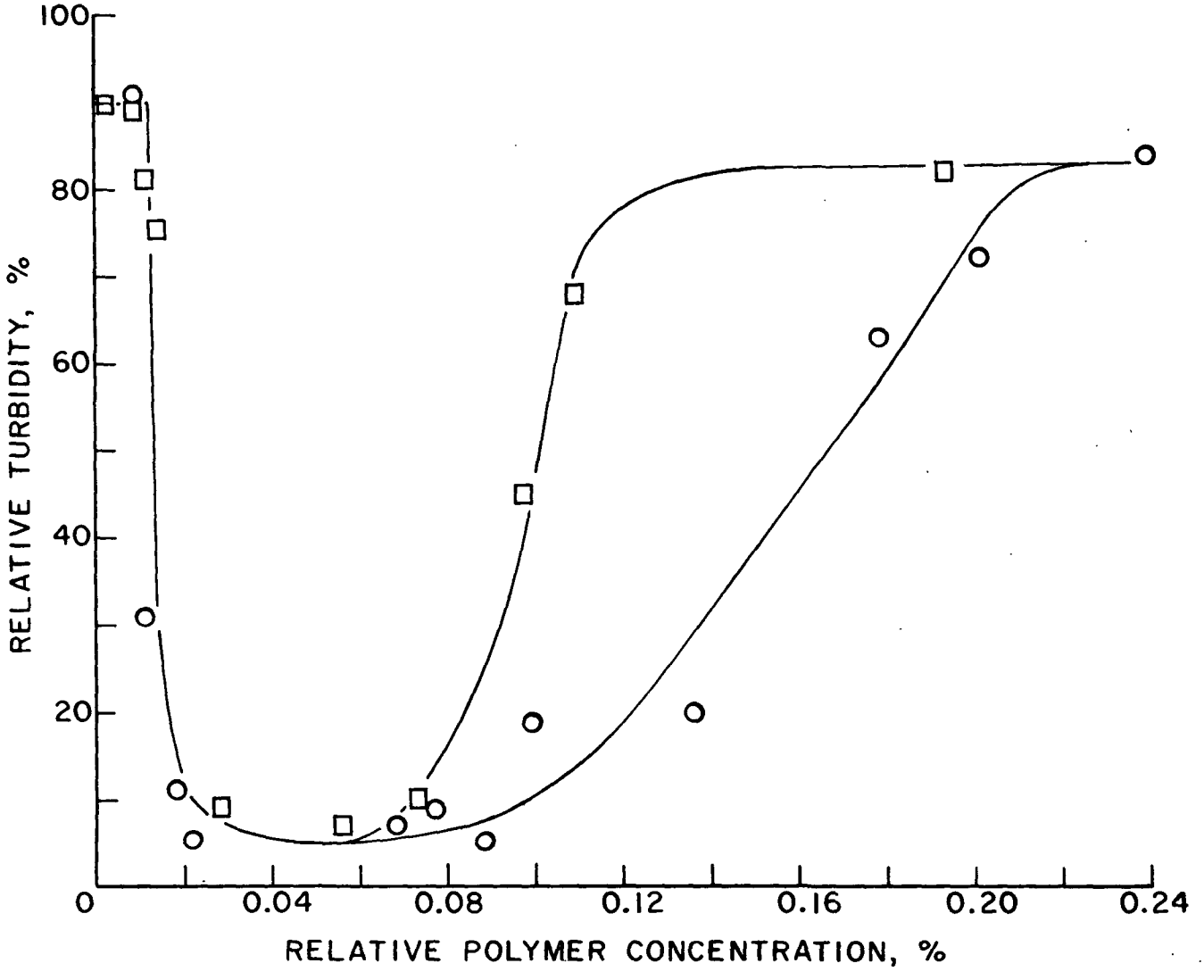

Figure 24. Relative Turbidity Versus Polymer Concentration for Fraction F_1-6 in 5×10^{-4} M NaCl and Particle Size 1.101 μm. Constant Surface Area Data (□) and Constant Particle Data (o). Polymer Concentration Expressed as % of PSL Weight

The conformation of poly(DMVPB) in the equilibrium state was predicted in an earlier section (Polymer Adsorption — Results and Discussion) to be in a relatively flat layer with small loops but with no loops or dangling ends extending far out into the solution. In a system of cationic polymer and anionic colloidal particles, the smaller the loops of the adsorbed polymer, the lower the probability of bridging being a significant flocculation mechanism. It must be emphasized that poly(DMVPB)'s adsorbed configuration is based only on theoretical predictions and an empirical formula. The thickness of the adsorbed layer has not been experimentally measured.

Surprisingly the CFC results are consistent with a bridging mechanism; in all cases, the larger the polymer molecular weight, the more efficiently the polymer initiates flocculation. However, the OFC results indicate that optimum flocculation is independent of polymer molecular weight. This inconsistency raises the question of the validity of a bridging mechanism at CFC. It can be assumed that the adsorbed polymer configuration at OFC is not drastically different than that at CFC; if anything, the adsorbed polymer layer is theoretically predicted to increase as more adsorption sites become occupied (54). Since the results at OFC imply bridging is not a significant flocculation mechanism and assuming no significant difference of adsorbed polymer configuration at CFC and OFC, then deductively bridging cannot be a significant flocculation mechanism at CFC.

In conclusion, the flat polymer configuration predicted from adsorption results and the flocculation results at CFC and OFC suggest that bridging is not a significant flocculation mechanism when the adsorbed polymer is in its equilibrium state.

THE CHARGE NEUTRALIZATION MODEL

The charge neutralization theory is based on the reduction of the height of the repulsive energy barriers of the colloidal particles such that the attractive Van der Waals forces cause flocculation. The most important parameter of this theory is polymer charge. There is no dependence on polymer molecular weight. Generally speaking the system under study implies that charge neutralization would take place and the data support the contention that charge neutralization plays a role in the destabilization and restabilization of PSL particles. However, because of the following observed trends which are inconsistent with the predictions of the charge neutralization model, it is obviously inadequate for describing the flocculation phenomena. These trends are: 1) the dependence of CFC on polymer molecular weight, 2) the dependence of breadth of the flocculation curve on polymer molecular weight, and 3) OFC values that occur at highly negative zeta potential values. Furthermore, several workers (13,36,55) have shown that the flocculation rate achieved by polyelectrolytes is greater than the flocculation rate achieved by simple electrolyte (i.e., attributable to Van der Waals forces). Evidently additional interactions are occurring in the case of polyelectrolytes which must account for the latter's enhanced effectiveness.

THE ELECTROSTATIC PATCH MODEL

The electrostatic patch theory is based on the electrostatic attraction forces that exist between positive and negative patches. This effect arises when highly charged cationic polymers are adsorbed on particles of fairly low negative surface charge density. The particle surface is then composed of an array of positive and negative patches. For flocculation to occur, the total net charge of the particle need not be zero because the net interaction force is weighted heavily by localized charges.

EXISTENCE OF ELECTROSTATIC PATCH

Table XI presents the surface charge density of the PSL particles as negative charges per 100 A^2. In comparison, molecular models indicate that the separation distance between the ionized groups attached to the polymer backbone is between three and eight angstroms depending on the backbone conformation.

TABLE XI

NEGATIVE CHARGES/100 A^2 FOR PSL

Particle Size	Negative Charge/100 A^2	Average Distance Between Negative Charges, A
1.101	1.03	10
0.794	0.80	13
0.481	0.43	25
0.234	0.31	33
0.109	0.12	100

As poly(DMVPB) adsorbs onto a PSL particle, the particle charge cannot be neutralized uniformly. As a result, that area on the PSL particle surface covered by poly(DMVPB) has a net positive charge. The particle surface then resembles a "mosaic" pattern of positively and negatively charged areas. This contention is based on the assumption of immobile charges on the PSL surface. It must be noted that the role of the polyelectrolyte counterion must also be considered. Those counterions "bound" to the polyelectrolyte would result in a cancellation of cationic charges and would reduce the overall positive charge of the polyelectrolyte. While the effect of the counterion has not been quantitatively evaluated in this work, the polymer characterization work supports the contention that poly(DMVPB) is highly charged in solution. Molecular size determinations by standard light scattering,

viscosity and diffusion techniques all indicate that poly(DMVPB) acts more like a rigid rod than a random coil in solution (p. 148), thus indicating that poly(DMVPB) is strongly cationic. In addition, the adsorption data indicate that only a small fraction of the PSL particle surface needs to be covered by poly(DMVPB) to reach charge neutralization. If the adsorbed polymer patch were neutral or only slightly positive, a much greater area of the particle would have to be covered before charge neutralization is reached. It is therefore concluded that the adsorbed polymer patch has a net positive charge. The net positive charge is defined as the total positive charges per patch minus the total negative charges covered by the patch assuming negligible counterion binding.

EFFECT OF ELECTROSTATIC PATCHES ON DLVO THEORY

The basic premise of the DLVO theory is that the stability of lyophobic colloidal dispersions can be described in terms of the sum of repulsive and attractive contributions to the total interaction between particles. The presence of an adsorbed poly(DMVPB) layer not only results in the neutralization of a portion of the surface charges but also provides a net positive patch. The existence of a positive patch affects the structure of the electric double layer around PSL and hence modifies the electrical repulsion term. The main changes can be summarized as:

1) displacement of specifically adsorbed counterions;
2) displacement of oriented water dipoles; and
3) changes in the local dielectric constant.

The restructured double layer can be divided into three regions: the polymer-free surface has a negative potential, the polymer patch has a

positive potential, and a complex transition zone exists between the polymer-free surfaces and the polymer patch in which both double layers are disrupted.

It must be reiterated that changes that occur upon the adsorption of poly(DMVPB) onto PSL are complex and that the effects of these changes cannot be stated in anything but general terms. It may be assumed that poly(DMVPB) patches on a PSL particle not only decrease the overall repulsive term of the particle but also cause a directional attraction effect due to electrostatic interaction between positive and negative patches, respectively, on adjacent particles.

Figure 25 schematically depicts the elementary case of the adsorption of one poly(DMVPB) molecule onto a PSL particle. An adsorbed electrostatic patch results in two changes that are directly responsible for the flocculation between two such particles. First, some negative charges on the PSL surface are neutralized. Second, net positive charges are present in the polymer patch. Since the cationic strength of the patch cannot be quantitatively determined, two mechanisms of flocculation can be envisioned. In the first case the patch is only slightly positive, such that the function of the patch is the disruption of the PSL double layer, allowing Van der Waals forces to initiate flocculation. In this case patch-patch interaction of different particles would determine the rate of flocculation. The rate of flocculation would be determined by the Van der Waals interaction minus the repulsive interaction of the positive patches. In the second case, the cationic strength of the patch is such that patch-nonpatch interaction initiates flocculation, and this attractive electrostatic interaction dominates. The rate of flocculation, however, consists of the contribution of the electrostatic interaction plus Van der Waals' force. Flocculation rate

studies (13,36,55) have shown that oppositely charged polyelectrolytes always provide a greater rate of flocculation than do simple electrolytes whose net effect leads to interaction by Van der Waals forces only. From these studies, it can be assumed that the electrostatic interaction dominates in this work.

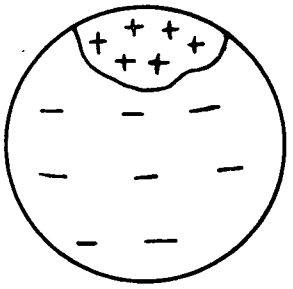

Figure 25. Adsorption of One Poly(DMVPB) Molecule Onto a PSL Particle

It may also be speculated that another orientation effect is taking place in this system. When the polymer molecule and PSL particle in Fig. 25 are considered to be one (entity), the center of the negative charges then do not coincide with the center of the positive charges. The center of the negative charges would be located near the center of the PSL particle and the center of the positive charges would be located near the center of the polymer patch. This separation of positive and negative charge centers would result in this particle having a dipole effect. An approaching PSL particle with a similar dipole will be oriented such that there is a net attractive force between them. The strength of such a dipole could be much greater than Van der Waals interaction. Assuming 100 net positive charges on the patch and a separation distance between positive and negative centers of 0.05 μm, the dipole moment for this particle would be approximately 2×10^5 Debeyes compared to Van der Waals in interactions which have dipole moments in the order of one Debeye. The example just illustrated is not typical for the system. Instead of a dipole force, it is necessary to talk in terms of multipole forces which are

smaller. The number of poly(DMVPB) molecules per particle are listed in Table XII, and some examples are illustrated in Fig. 12. A quantitative approach to calculate these forces would prove too difficult. At most, it is felt that only a minor contribution would be made in this system from these dipole and multipole orientations.

TABLE XII

POLYMER MOLECULES/PSL PARTICLE-CONSTANT AREA EXPERIMENT

Particle Size	Fraction	CFC	OFC	Zeta Potential	RSC
		(A) In 10^{-2}M NaCl			
1.101	F_1-6	32.0	257	362	723
	F_2-7	2,800	9,600	11,700	23,400
0.794	F_1-6	16.0	124	167	354
	F_2-7	1,200	4,600	4,900	11,400
0.481	F_1-6	6.0	40.0	49.0	110.0
	F_2-7	370	1,300	1,600	4,200
0.234	F_1-6	1.2	6.4	8.8	18.0
	F_2-7	74.0	180	280	580
0.109	F_1-6	0.3	1.2	1.2	3.0
	F_2-7	12.0	40.0	42.0	84.0
		(B) In 5×10^{-4}M NaCl			
1.101	F_1-6	49.0	231	400	670
	F_2-7	5,500	9,000	12,500	23,400
0.794	F_1-6	23.0	100	160	330
	F_2-7	2,800	4,900	4,700	11,200
0.481	F_1-6	9.0	27.0	55.0	97.0
	F_2-7	1,000	1,500	1,750	3,550
0.234	F_1-6	2.0	4.8	9.0	17.0
	F_2-7	175	280	324	660
0.109	F_1-6	0.4	1.2	2.0	3.0
	F_2-7	34.0	48.0	48.0	111.0

In conclusion, electrostatic and Van der Waals forces act together in the flocculation of this system, the electrostatic interaction being the dominant one. An additional orientation effect may be speculated to occur due to a dipole or multipole effect.

EFFECT OF PATCH SIZE

Light scattering, viscosity, and diffusion data have shown that poly-(DMVPB) behaves as a stiff molecule in solution and as such its configuration is more like a rod than a random-coil. Studies of nonionic polymers adsorbing onto PSL have determined that the adsorbed configuration occupied approximately the same volume as that occupied by the effective hydrodynamic sphere in bulk solution (54). However, in this case, the electrostatic interaction between particle and polymer greatly affects the adsorbed polymer equilibrium configuration and makes it impossible to predict an adsorbed polymer configuration valid for each polymer molecule or for each particle size except that it will be relatively flat. It can be assumed that the adsorbed polymer configurations in 10^{-2}M NaCl are generally more compact in area, resulting in a higher patch charge density than those in 5×10^{-4}M NaCl. The distribution of adsorbed polymer molecules on a PSL particle is assumed to be uniform; the repulsion between adsorbed polymer molecules and those to be adsorbed would cause a degree of symmetry.

The effect of molecular weight in determining CFC is now more apparent. The use of narrow molecular weight fractions permits the calculation of the number of poly(DMVPB) molecules per PSL particle. Table XII contains the results of the calculations at CFC and those at OFC, charge neutralization, and RSC. From Table XII it is indicated that the number of high molecular weight molecules is small in comparison to the low molecular weight molecules.

Assuming a random distribution for both molecules, the polymer charges of the high molecular weight polymer are much more unevenly distributed on the particle's surface than the low molecular weight polymer.

Figure 26 schematically depicts the adsorption of poly(DMVPB) onto a PSL particle. Equal weights of fractions F_1-6 and F_2-7 are adsorbed in (A) and (B), respectively. The overall charge of the PSL particles depicted is negative even with the presence of cationic poly(DMVPB). As a result of this uneven distribution of polymer charge in (A), the patch size of (A) is greater than any patch size in (B). Since the electrostatic interaction is directly correlated to the number of positive and negative charges, the electrostatic interaction in the vicinity of the large molecular weight patch will be greater than the electrostatic interaction in the vicinity of any of the low molecular weight patches. Therefore since the electrostatic interaction (including orientation) increases with patch size then the probability of flocculation also increases with patch size. As stated previously, a dipole or multipole effect could exist to some extent in this system and this effect would also increase the flocculation probability as patch size increases.

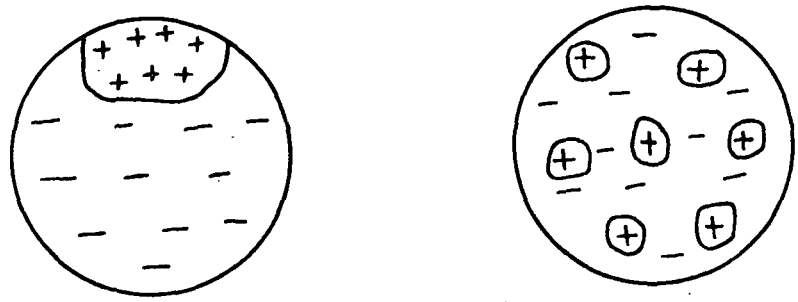

Figure 26. Adsorption of Equal Weights of Fraction F_1-6 (A) and Fraction F_2-7 (B) on PSL

The above contention can be supported qualitatively by establishing an interrelationship between polymer size and particle size. Figures 27 and 28 plot CFC versus the ratio of polymer hydrodynamic molecular diameter/PSL diameter. From Fig. 27 and 28 it is apparent that as patch size increases the CFC decreases until the CFC becomes independent of patch size. It can be argued that as the patch size increases, the number of patches per particle would decrease. These two effects would counter each other and would result in an optimum patch size above which the total force of attraction due to electrostatic patches remains constant.

Extrapolation of the low molecular weight CFC data to the high molecular weight CFC data curve results in optimum patch/particle diameters of approximately 17% in 10^{-2}M NaCl and 35% in 5×10^{-4}M NaCl. A patch ratio higher than those mentioned would not result in a lower CFC. The dependence of patch size on salt concentration could result from one of two points: 1) PSL particle stability decreases with increasing salt concentration, and 2) the patch charge density increases with increasing salt concentration.

At OFC, the number of polymer molecules adsorbed per PSL particle is significantly greater than that amount adsorbed at CFC (see Table XII). It can be assumed that as a greater number of polymer molecules are adsorbed onto a PSL particle, the positive charge distribution becomes more uniform. As a result, the difference in attractive force between equal weights of the high and low molecular weight patches at low surface coverage becomes less with increased adsorption. The OFC values are harmonious with such an explanation since there is little if any dependence on polymer molecular weight at this point. At this adsorption level, the large molecular weight polymer patch may influence the rate of flocculation to a greater extent than the smaller patches. There are numerous examples of this increased

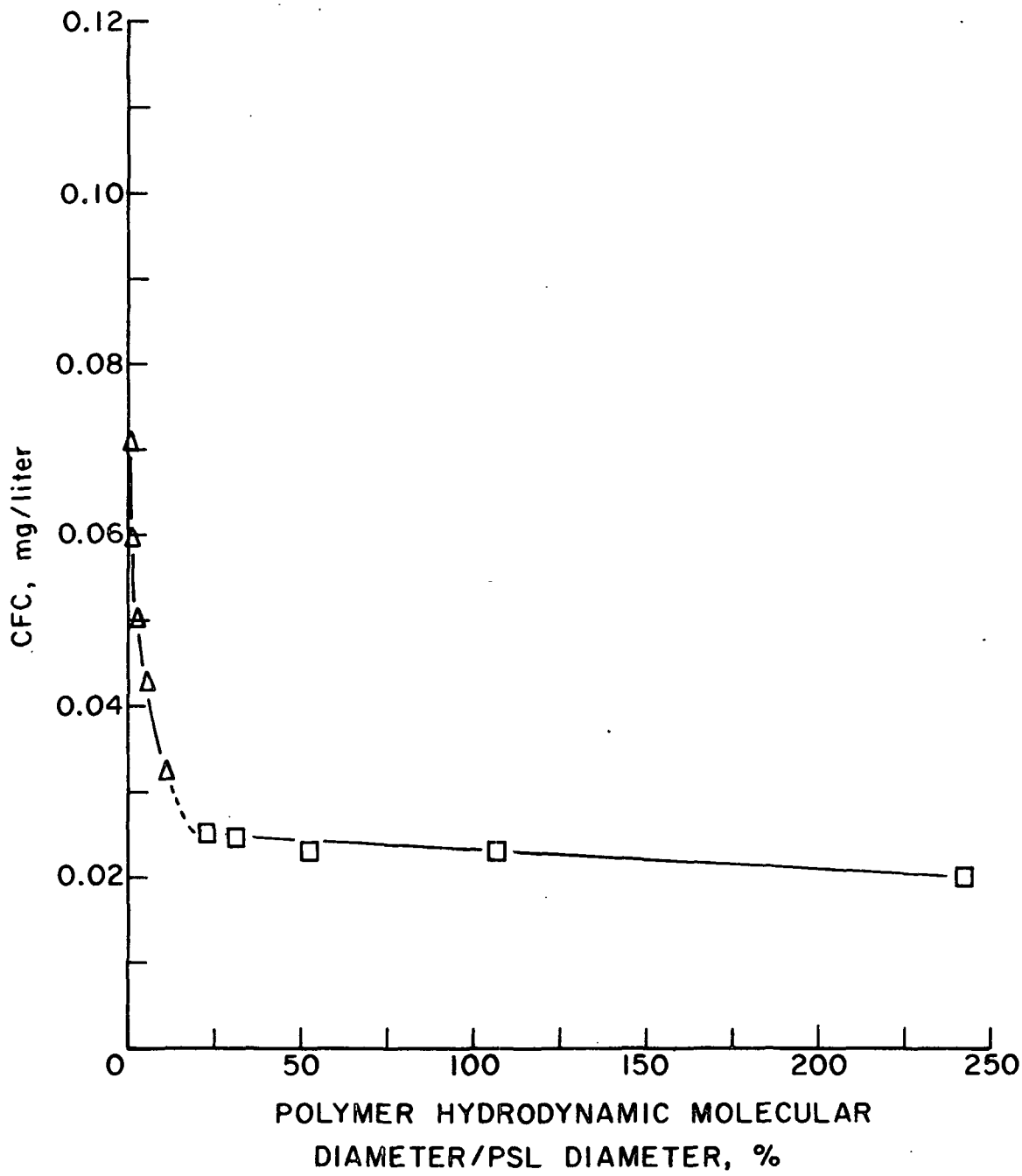

Figure 27. CFC Versus Polymer Hydrodynamic Molecular Diameter/PSL Diameter. Fractions F_1-6 (□) and F_2-7 (Δ) in 10^{-2}M NaCl

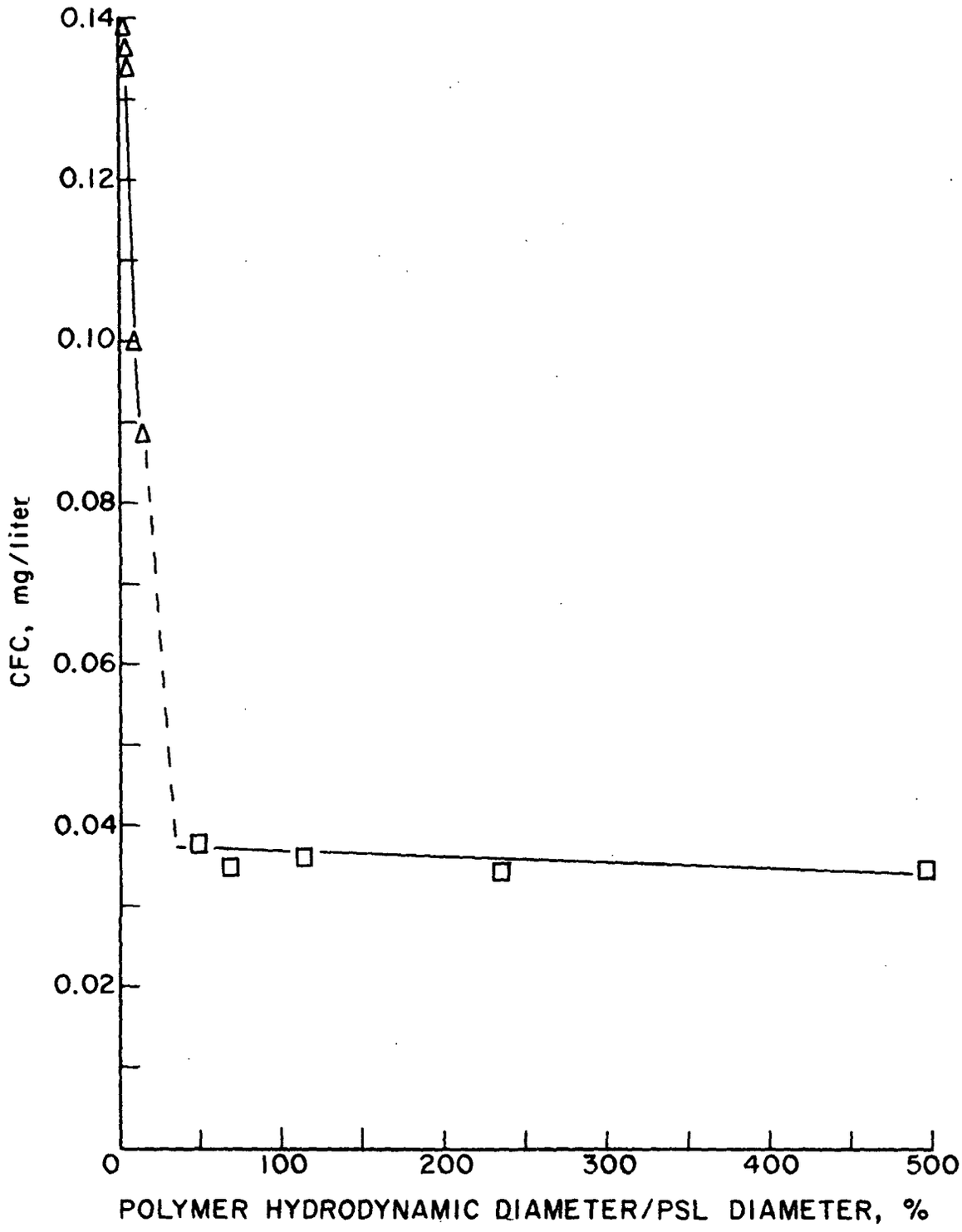

Figure 28. CFC Versus Polymer Hydrodynamic Diameter/PSL Diameter. Fractions F_1-6 (□) and F_2-7 (Δ) in 5×10^{-4} M NaCl

rate of OFC due to polymer molecular weight even though the OFC is independent of polymer molecular weight (13,36,55). These findings can be summarized: 1) the rate of flocculation with polymer is always faster than that of electrolyte alone, 2) there exists a limiting polymer molecular weight after which the flocculation rate does not increase significantly, and 3) as the salt concentration increases, the rate of flocculation becomes independent of polymer molecular weight. It can be assumed that the increasing ionic strength decreases the range over which the extra attractive forces operate until there is no effect on the flocculation rate.

RECAPITULATION

The destabilization of PSL particles by poly(DMVPB) is primarily by electrostatic interactions between polymer patch and nonpatch areas of different particles. The critical flocculation concentration is dependent on patch size and salt concentration. The optimum patch size to initiate flocculation was determined by the interrelationship between polymer molecular weight and particle size. Optimum flocculation occurred while the potentials of the colloidal particles were negative. The optimum flocculation concentration has little dependence on patch size and salt concentration.

At high particle concentrations, bridging flocculation may occur with high molecular weight polymers.

ACKNOWLEDGMENTS

Many people have contributed greatly to the successful completion of this thesis. Recognition of the Board of Directors and member companies is given for the creation and continued support to The Institute of Paper Chemistry. The staff and faculty members are recognized for their service which continues to provide the opportunity for a graduate studies doctoral program.

Recognition of the invaluable help of the Thesis Advisory Committee is gratefully acknowledged. Bob Stratton served as chairman of the Advisory Committee. His willingness to undertake many stimulating discussions from day to day is appreciated. Dale Williams, Gary Baum and John Swanson who also served on the Advisory Committee deserve special mention in contributing time and knowledge to the completion of this thesis.

Special gratitude is extended to John Carlson who provided invaluable assistence in operating the instruments for diffusion coefficient and molecular weight determinations.

My fellow students and their wives are wholeheartedly thanked for making these past few years pass quickly.

And last but not least, a very special thanks to my loving wife, Sara, who did an outstanding job of providing understanding and encouragement.

NOMENCLATURE

A_2 = second virial coefficient

C = concentration, mg/liter

Ce = equilibrium concentration, mg/liter

C_0 = initial concentration, mg/liter

C_M = maximum adsorbed concentration, mg/liter

C_* = $C_o - Ce$

CFC = critical flocculation concentration of poly(DMVPB)

D = apparent diffusion coefficient at infinite time

D_o = diffusion coefficient at infinite time and dilution

F_1-6 = fraction number six of large molecular weight polymer fractionation

F_2-7 = fraction number seven of low molecular weight polymer fractionation

G = adsorption energy

K = Langmuir constant, liters/mg

k = Boltzmann constant

M_n = number average molecular weight

M_w = weight average molecular weight

N = Avogadro's number

OFC = optimum flocculation concentration of poly(DMVPB)

PSL = polystyrene latex

R_e = hydrodynamic equivalent sphere

R_G = radius of gyration

RSC = restabilization concentration of poly(DMVPB)

R = gas constant

T = absolute temperature

Γ_s = specific adsorption, mg poly(DMVPB)/M^2 PSL

ε = R_e/R_G

η = viscosity coefficient, poise

π = 3.1416

θ conditions = an ideal solution when the heat of mixing $\underline{H}$ = 0

ρ = solution density

ω = angular velocity, sec^{-1}

LITERATURE CITED

1. LaMer, V., and Healy, T. W., Rev. Pure Appl. Chem., 13:112-33(1963).

2. Black, A. F., Birkner, F. B., and Morgan, J. J., J. Colloid Interface Sci., 21:626-48(1966).

3. Helmholtz, H., Wied. Ann., 7:337(1879).

4. Gouy, G., J. Phys. Rad., 9:457(1910).

5. Chapman, D. L., Phil. Mag., 25:475(1913).

6. Stern, O., Z. Elektrochem., 30:508(1924).

7. Von Smoluchowski, M., Physik. Z., 557:585(1966).

8. Overbeek, J. Th. G. The interaction between colloidal particles. In Kruyt's Colloid science. Vol. 1. p. 245-77. Elsevier Publ. Co., N.Y., 1949.

9. Verwey, E. J. W., and Overbeek. J. Th. G. Theory of the stability of lyophobic colloids. p. 205. New York, Elsevier, 1948.

10. Webb, J. T. An investigation of electric-double-layer concepts and colloidal stability of titanium dioxide dispersions. Doctoral Dissertation. Appleton, Wisconsin, The Institute of Paper Chemistry, 1973. 179 p.

11. Audsley, A. Mineral Processing Note No. 5. England, Warren Spring Lab., Ministry of Tech., 1965.

12. Kitchener, J. A., British Polym. J., 4:217(1972).

13. Gregory, J., Trans. Faraday Soc., 65:2260(1969).

14. Teot, A. S., Ann. N.Y. Acad. Sci., 155:593(1969).

15. Kasper, D. R. Theoretical and experimental investigations of the flocculation of charged particles in aqueous solutions by polyelectrolytes of opposite charge. Doctoral Dissertation. Pasadena, California, California Institute of Technology, 1971. 201 p.

16. Gregory, J., J. Colloid Interface Sci., 42:454(1973).

17. Lindquist, G. M. The role of charge density and molecular weight on the adsorption and flocculation of colloidal silica with polyethylenimine. Doctoral Dissertation. Appleton, Wisconsin, The Institute of Paper Chemistry, 1975. 239 p.

18. Dixon, J. K., and Zielyk, M. W., Environ. Sci. Tech., 3:551(1969).

19. LaMer, V. K., Dixon, J. K., Li, C., Messinger, S., and Linford, H. B., J. Colloid. Interface Sci., 23:465(1967).

20. Brown, D., Livesey, P. J., and Tuckley, E. S. G., I. C. I. Internal Report, I. C. I. Corp. Lab., Runcorn and I. C. I. Organics Division, Manchester, England, 1970.

21. Gregory, J., and Sheiham, I., British Polym. J., 6:47-59(1974).

22. Black, A. P., and Vilaret, M. R., J. Am. Water Works Assocn., 61:209(1969).

23. Iler, R. K., J. Colloid Interface Sci., 37:364(1971).

24. Patat, F., Killmann, E., and Schliebener, C., Fortschr. Hochpoly-Forsch., 3S:332(1964).

25. Rosoff, M. "Physical methods in macromolecular chemistry," 1:1. New York, Marcel Dekker, 1969.

26. Vincent, B., Advan. Colloid Interface Sci., 4:193(1974).

27. Fleer, G. J. Polymer adsorption and its effect on colloidal stability. Doctoral Dissertation. Wageningen, The Netherlands, Agriculture University, 1971. 144 p.

28. Fontana, B. J., and Thomas, J. R., J. Phys. Chem., 65:480(1961).

29. Garvey, M. J., Tadros, Th. F., and Vincent, B. Forty-ninth ACS National Colloid Symp., Potsdam, New York, 1975.

30. Motomura, K., and Matuura, R., J. Chem. Phys., 50:1281(1969).

31. Higuchi, W. I., J. Phys. Chem., 65:488(1961).

32. Roe, R. J., J. Phys. Chem., 43:1591(1965).

33. Hawk, G. L., Cameron, J. A., and Dufault, L. B., Preparative Biochemistry, 2(2):193-203(1972).

34. Ottewill, R. H., and Vincent, B., J. Chem. Soc., Faraday Trans. I, 68: 1533-43(1972).

35. Van den Hul, H. J., and Vanderhoff, J. W. p. 3. New York-Lond, Polymer Colloids, Plenum Press, 1971.

36. Birkner, F. B., and Morgan, J. J., J. Am. Water Works Assocn., 60:175(1968).

37. Connor, P. p. 469. Proc. Fifth Intern. Congr., Surface Active Substances, Barcelona, II, 1969.

38. Ottewill, R. H., and Connor, P., J. Colloid Interface Sci., 37:642(1971).

39. Silberberg, A., J. Chem. Phys., 48:2835(1968).

40. Hoeve, C. A. J., J. Polymer Sci. C, 30:361(1970).

41. Shyluk, W. P., J. Polymer Sci. A, 6:2009(1968).

42. Perkel, R., and Ullman, R., J. Polymer Sci., 54:127(1961).

43. Ellerstein, S., and Ullman, R., J. Polymer Sci., 55:123(1961).

44. Koopal, L., and Lyklema, J., Disc. Faraday Soc., 59. In press.

45. Tadros, Th. F. Forty-ninth ACS Colloid Symp., Potsdam, New York, 1975. In press.

46. Adamson, A. W. Physical chemistry of surfaces. 2nd ed. p. 747. New York, Interscience Publ., 1967.

47. Patat, F., Killmann, E., and Schliebener, C., Rubber Chem. Tech., 39:36 (1966).

48. Passaglia, E., and Stromberg, R. R., Poly. Prep. Am. Chem. Soc., Div. Polymer Chem., 5:508(1964).

49. Gilliland, E. R., and Gutoff, E. B., J. Appl. Polymer Sci., 3:26(1960).

50. Verwey, E. J. W., and Overbeek, J. Th. G. Theory of the stability of lyophobic colloids. Amsterdam, Elsevier, 1948.

51. Brown, D., Livesey, P. J., and Tuckley, E. S. G. Internal Report, Manchester, England, I. C. I. Corp. Lab., 1970.

52. Williams, D. J. A., and Ottewill, R. H., Kolloid. Z. Z. Poly., 243:141(1971).

53. Nagasawa, M., J. Polymer Sci. Symp., 49:1(1975).

54. Tadros, Th. F., Garvey, M. J., and Vincent, B., J. Colloid Interface Sci., 49:57(1974).

55. Gregory, J. Forty-ninth ACS Colloid Symp., Potsdam, New York, 1975. In press.

56. Bovey, F. A., Kolthoff, I. M., Medalia, A. I., and Meehan, E. J. Emulsion polymerization. New York, Interscience, 1955.

57. Van der Hoff, B. M. E. Kinetics of emulsion polymerization. In Advances in chemistry Series No. 34: Polymerization and polycondensation processes. Washington, D.C., American Chem. Soc., 1962.

58. Woods, M. E., Dodge, J. S., Krieger, I. M., and Pierce, P. E., J. Paint Technol., 40:541(1968).

59. Sikora, M. D. Unpublished work, 1975.

60. Kenchington, A. W. Analytical information from titration curves. In Alexander and Block's A laboratory manual of analytical methods of protein chemistry. Vol. 2. p. 353-88. New York, Pergamon Press, 1960.

61. Tanford, C. Hydrogen ion titration curves of proteins. In Shedlovsky's Electrochemistry in biology and medicine. p. 218-65. New York, Wiley and Sons, 1955.

62. Clapp, R. R. An investigation of the relations between carboxyl content and zeta potential. Doctoral Dissertation. Appleton, Wisconsin, The Institute of Paper Chemistry, 1972. 138 p.

63. Ottewill, R. H., and Shaw, J. N., J. Electroanal. Chem., 37:133(1972).

64. Zeter-Meter Inc. Operation Manual. 2nd ed. New York, New York, 1968.

65. Wiersema, P. H., Loeb, A. L., and Overbeek, J. Th. G., J. Colloid Interface Sci., 22:78(1966).

66. Shyluk, W. P., J. Polymer Sci., Part A, 2:2191-206(1964).

67. Analytical Group Method 52. Appleton, Wisconsin, The Institute of Paper Chemistry, June 2, 1964.

68. Wales, M., Adler, F. T., and Van Holde, K. E., J. Phys. Colloid Chem., 64:1830(1960).

69. Yphantis, D., Biochemistry, 3:297(1964).

70. Gosting, L. J. In Advances in protein chemistry. Vol. XI. p. 429. New York, Academic Press, 1956.

71. Zimm, B. H., J. Chem. Phys., 16:1093-9(1948).

72. Phoenix Precision Instrument Co. Operation Manual OM-1000, Philadelphia, PA, 1955.

73. Cabannes, J., and Rocard, Y. La diffusion moleculaire de la lumiere. Paris, Les Presses Universitaires, 1929.

74. Timell, T. E., Svensk Papperstid., 57:777-88(1954).

75. Utiyama, H., Tagata, N., and Kurata, M., J. Phys. Chem., 73:1448(1969).

76. Creeth, J. M., J. Am. Chem. Soc., 77:6428(1955).

77. Daniel, E., and Alexandrowicz, Z., Biopolymers, 1:473-95(1963).

78. Kindler, W. A. Jr. Adsorption kinetics in the polyethylenimine-cellulose fiber system. Doctoral Dissertation. Appleton, Wisconsin, The Institute of Paper Chemistry, 1971. 136 p.

79. Laity, J., J. Phys. Chem., 63:80(1959).

80. Spiegler, K. S., Trans. Faraday Soc., 54:1408(1958).

81. Stokes, G., Trans. Cambridge Phil. Soc., 8:278(1847).

82. Tanford, C. Physical chemistry of macromolecules. New York, Interscience Publishers, 1965.

83. Mandelkorn, L., Krigbaum, W. R., Scheraga, H. A., and Flory, P. J., J. Chem. Phys., 20:1392(1952).

84. Schneider, N. S., and Doty, P. M., J. Phys. Chem., 58:762(1954).

85. Trap, H. J. L., and Hermans, J. J., J. Phys. Chem., 58:757(1954).

86. Takahashi, A., Kato, T., and Nagasawa, M., J. Phys. Chem., 74:944-6(1970).

87. Fuoss, R. M., and Strauss, U. P., J. Polymer Sci., (8):1993-2005(1967).

88. Einstein, A., Ann. Physik 4, 19:289(1906); 34:591(1911).

89. Kirkwood, J. G., and Riseman, J., J. Chem. Phys., 16:565(1948).

90. Morawetz, H. Macromolecules in solution. p. 495. New York, Interscience Publishers, 1965.

91. Arnold, R., and Overbeek, J. Th. G., Recueil, 69:192-205(1950).

92. Koleske, J. V. The configuration and hydrodynamic properties of fully acetylated garan. Doctoral Dissertation. Appleton, Wisconsin, The Institute of Paper Chemistry, 1963. 175 p.

93. Huque, M. M., Goring, D. A. I., and Mason, S. G., Can. J. Chem., 36:952 (1958).

94. Brown, W., Arkiv. Kemi., 18:227(1961).

APPENDIX I

THE CHARACTERIZATION OF POLYSTYRENE LATEX PARTICLES

SELECTION AND DESCRIPTION OF PARTICLES

Dow Uniform Latex Particles were manufactured by and obtained from the Dow Chemical Company. The latex preparation has been reviewed by others (52,57,58) and will not be discussed here. The sizes quoted by the manufacturer for the latex particles used in this program are given in Table XIII. PSL particles have a density of 1.05 g/cu cm.

TABLE XIII

THE CHARACTERIZATION OF POLYSTYRENE LATEX PARTICLES

Average Diameter in Micrometers	One Standard Deviation in Micrometers
0.109	0.0027
0.234	0.0026
0.481	0.0018
0.794	0.0044
1.101	0.0054

An additional PSL sample, generously supplied by Professor I. M. Krieger of Case Western Reserve University was used in this work. This monodisperse PSL was prepared with an ionic comonomer and without conventional emulsifiers. The average diameter of the particles was 0.331 μm ± 0.0011 μm, determined by measuring electron micrographs (59). This latex was characterized in the same manner as those particles previously mentioned. The absence of adsorbed emulsifier on this particle's surface made it unnecessary to go through the latex clean-up process prior to potentiometric titration.

LATEX CLEAN-UP

The polystyrene latex particles as received are negatively charged. Both the adsorbed emulsifier molecules and the sulfate end groups of the polymer molecules contribute to the negative charge. The sulfate end groups are chemically bound to the particle surface whereas the emulsifier is not. Desorption of the emulsifier would change the surface charge density of the particles. To avoid this, it was necessary to remove the adsorbed emulsifier as completely as possible, relying on the sulfate end groups to give the particles the required stability.

A mixed-bed ion exchange method (35) was used to remove the adsorbed emulsifier. The rigorously-purified DOWEX mixed resin was prepared from separate batches of DOWEX 50W-X4 and DOWEX 1-X4. DOWEX 50W-X4 resin is the sulfonate salt (H^+ form) of a 96:4 styrene-divinylbenzene copolymer, and DOWEX 1-X4 resin is the analogous trimethylammonium salt (OH^- form). Each resin was eluted consecutively with 3N NaOH, hot water, methanol, cold water, 3N HCl, hot water, methanol, and cold water. The cycle was repeated until the wash water from the resin showed no adsorption at 224 μm, indicating no polyelectrolytes had leached from the resins. The DOWEX 50W-X4 resin was transformed to the H^+ form by washing with an excess of 3N HCl, then with distilled deionized water until the pH of the wash water was neutral. The DOWEX 1-X4 was transformed to the OH^- form only shortly prior to use by washing with an excess of 3N NaOH, then with distilled deionized water as previously mentioned. The mixed resin was prepared from equal weights of both resins and washed three times prior to use with distilled deionized water.

Each PSL particle size was agitated slowly with a 5-fold excess (w/w) of resin for four hours. The latex/ion exchange resins were then filtered

on a Buchner funnel, and an aliquot of the filtrate was titrated with 0.01N NaOH. The exchange was repeated with fresh resin until a constant charge was obtained.

TITRATION OF POLYSTYRENE LATEX PARTICLES

After ion exchange, the PSL particles are stabilized by the sulfate end groups of the polymer chain. Above pH 2 all of the sulfate end groups are dissociated and in the H^+ form (15). The surface charge densities of the PSL particles were determined by the hydrogen ion titration technique described by Kenchington (60) and Tanford (61).

The method involves a blank titration of solvent where the $[OH^-]$ added as a function of pH is determined. A known amount of PSL is titrated in the same solvent and the $[OH^-]$ added as a function of pH is again determined. The amount of $[H^+]$ bound to PSL at a given pH is calculated by subtracting the amount of $[OH^-]$ required by the blank at the given pH from the amount added to the PSL solution. The errors in measurement are the same for separate titration of solution and solvent when their ionic strengths are essentially the same.

The titrations were carried out in a stirred Plexiglas cell similar to that used by Clapp (62) at room temperature in a CO_2-free nitrogen atmosphere. The pH of the blank was adjusted to that of the PSL solution. Both solution and solvent were then acidified with a known amount of 0.6N HCl. Fifty ml of known PSL concentration was titrated with 0.01N NaOH. Five-minute intervals were used for successive points. A 5.000 ml buret was used to deliver accurate volumes of titrant. A Corning Research pH meter, readable to 0.001 pH unit and believed reliable to the 0.01 pH unit, was used for pH measurements.

ZETA POTENTIALS

The zeta potentials of the five PSL particle sizes were determined at 25°C in 10^{-2}M NaCl and in 5×10^{-4}M NaCl at pH 6. The pH of each solution was adjusted by addition of 0.01N HCl or 0.01N NaOH in the respective salt concentration. The electrophoretic mobilities were determined on a Zeta meter made by Zeta Meter Inc. by averaging seven readings that were within one second of each other. Zeta potential values were calculated from the Helmholtz-Smoluchowski equation.

EXPERIMENTAL RESULTS AND DISCUSSION

SURFACE CHARGE DENSITY

The original titration data, pH versus milliliters of base for PSL particles in water and for the respective blanks are shown in Fig. 29. The titration curves are similar to those found by Van den Hul and Vanderhoff (35) in their investigation of the surface charge density of ion-exchanged polystyrene latexes. The inflection on the curves near pH 6 is indicative of the pKa of surface sulfate groups. Ottewill and Shaw (63) found a large proportion of carboxyl groups on latex particles prepared with hydrogen peroxide initiator and sodium laurate emulsifier and cleaned by dialysis. Surface carboxylic acid groups have an apparent pKa in the range of 4.0-4.6. Their presence would be noted by an inflection in this range on the potentiometric curve. In summary, the sulfate end groups are present on the surface in sufficient number to stabilize the PSL particles.

The equivalence points of the potentiometric curves were determined by plotting the first derivative curve shown in Fig. 30. The position of the maximum on the first derivative curves corresponds to the inflection point

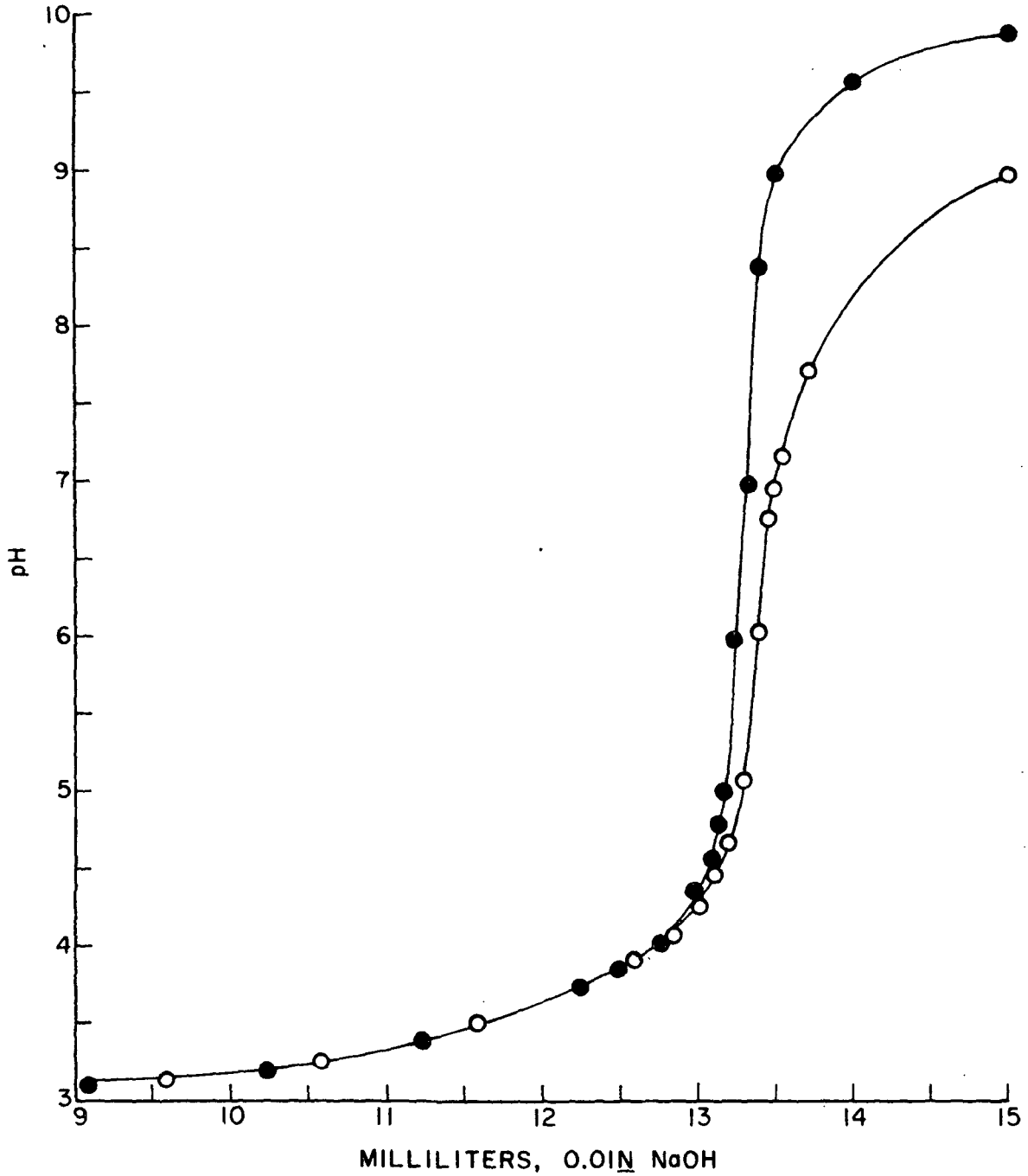

Figure 29. Titration Curve of PSL Sol, Particle Size 0.481 μm (Open Circles) and Solvent (Solid Circles)

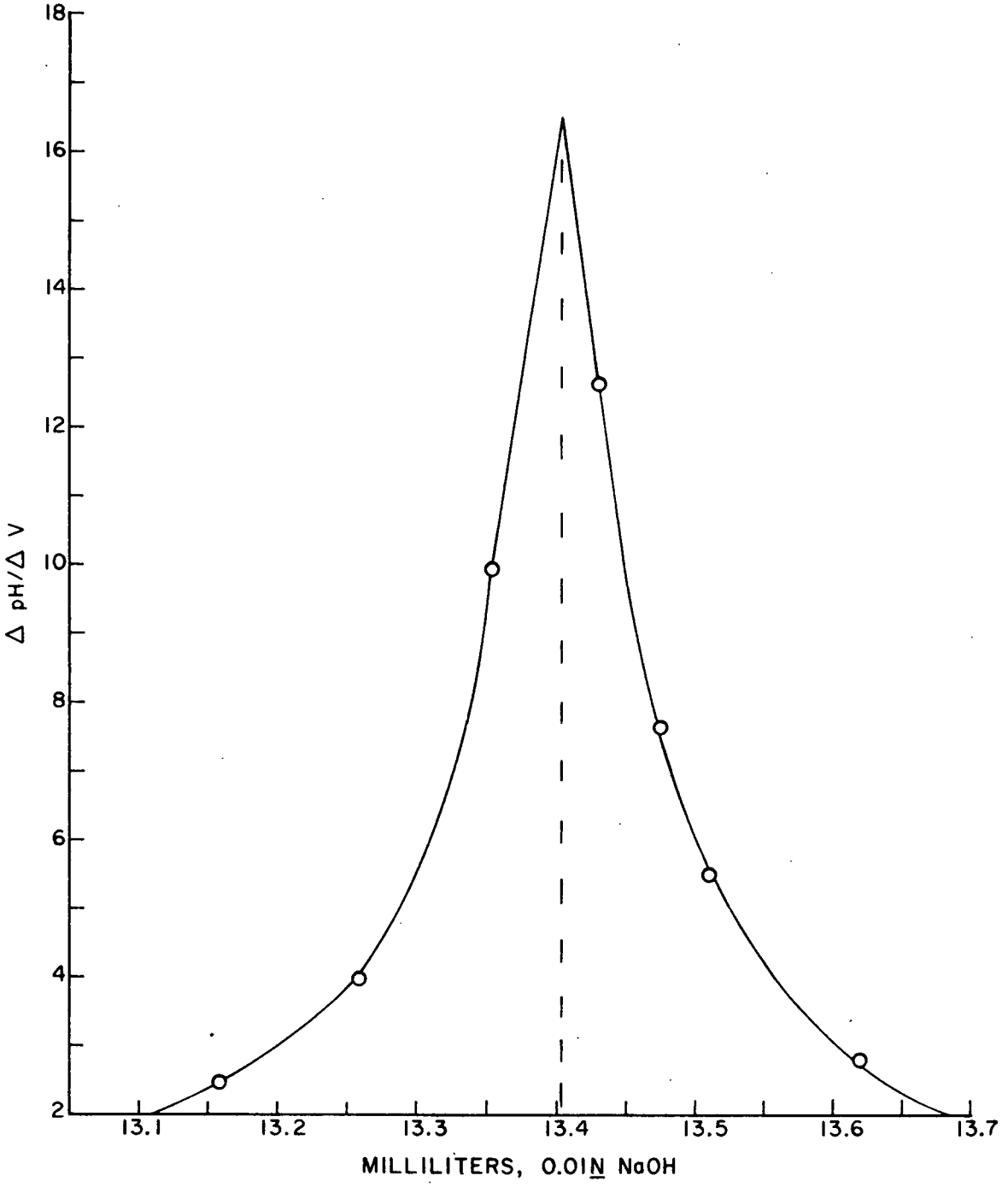

Figure 30. First Derivative Curve. Particle Size 0.481 μm

on the normal titration curve. The difference between the PSL equivalence point and its respective blank at the corresponding pH was easily converted into the surface charge density of the PSL particles. Table XIV completely describes the surface charge densities of the PSL particles. The uncertainties in the determination of the surface charge densities originated from duplicate measurements and the determination of PSL concentration by a freeze-drying method. These surface charge densities are within the range found by Van den Hul and Vanderhoff (35) and Kasper (15). With the Dow PSL particles, the surface charge density increases as the particle increases (Table XIV). The relationship seen in Fig. 31 suggests that the residual particle charge consists of sulfate end groups rather than adsorbed emulsifier. Since the number of sulfate end groups increases as the mass of the particle size increases, and since the mass to surface area ratio increases as the particle size increases, then the number of sulfate end groups per unit area increases with particle size. This is based on the assumption that the sulfate end groups are located on the surface of the particle. This is a reasonable assumption; Ottewill (63) has shown experimentally that such surface groups do exist.

TABLE XIV

SURFACE CHARGE DENSITY OF PSL PARTICLES

Particle Size, μm	Surface Charge Density, $\mu C/cm^2$	Charges/100 A^2
0.109	1.71 ± 0.24	0.12
0.234	4.93 ± 0.71	0.31
0.330	3.45 ± 0.50	0.22
0.481	6.87 ± 1.00	0.43
0.794	12.86 ± 1.66	0.80
1.101	16.47 ± 1.93	1.03

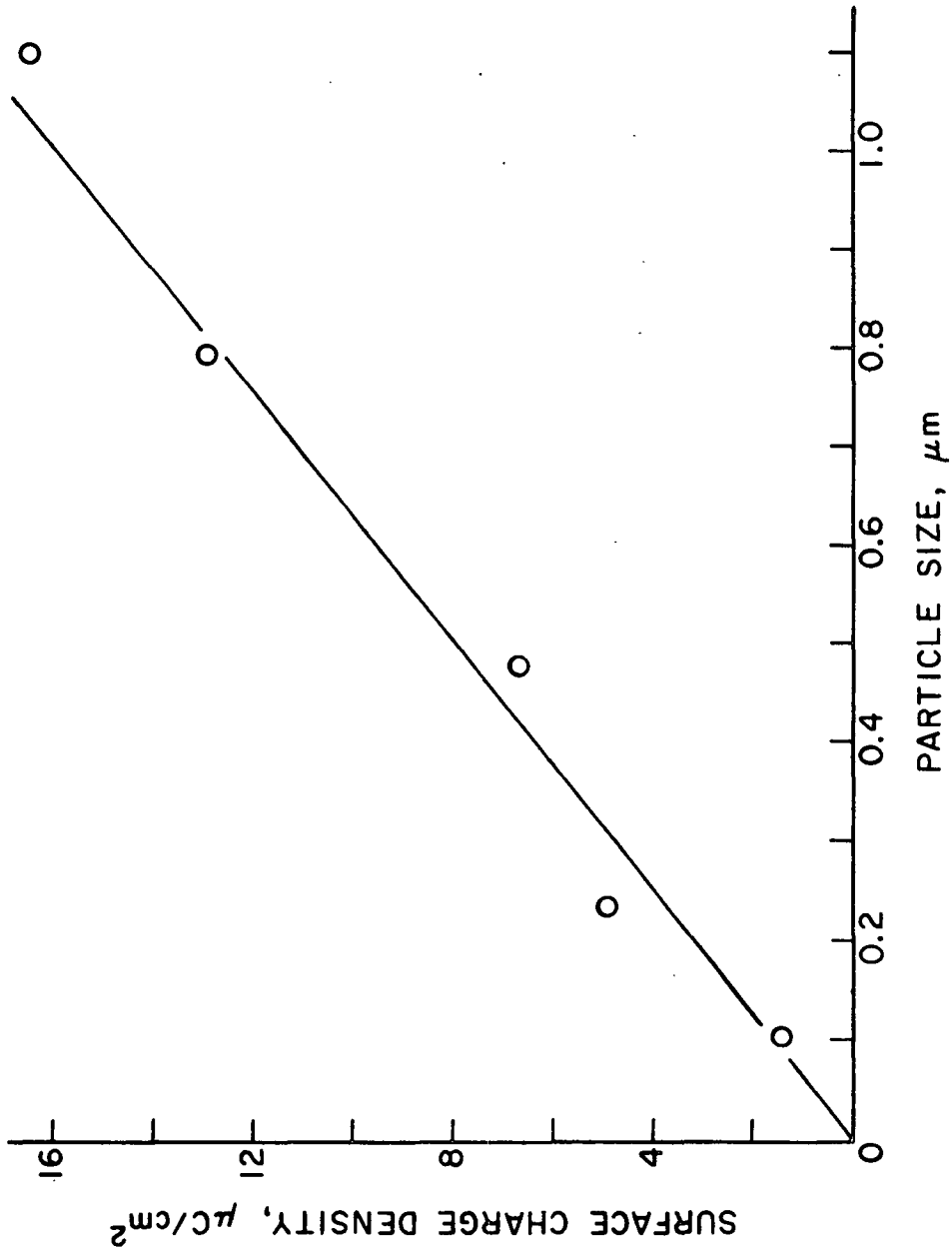

Figure 31. Surface Charge Density Versus Particle Size

TITRATION DATA

The difference between the amounts of OH^- ions that produce a given pH in the PSL suspension and the corresponding pH in the blank sample gives the relative amount of H^+ released by the surface. The relative charge density is then given by:

$$\sigma = -\frac{A \times F}{S} \times 10^{-2}, \qquad (9)$$

where σ = charge density in μcoulombs/cm^2

$\underline{A}$ = relative amount of H^+ released in meq H^+/g

F = Faraday constant, 96,500 coulombs/eq

$\underline{S}$ = geometric surface area, cm^2/g

Titration data of PSL particle sizes and data of blank for PSL particle sizes are included in Tables XV through XXII.

TABLE XV

TITRATION DATA OF PSL PARTICLE SIZE 0.109 μm, 0.27 g

Vol. of Titrant	pH	Vol. of Titrant	pH
10.000	3.470	10.000	3.500
10.500	3.585	11.000	3.910
11.000	3.790	11.500	4.160
11.500	4.080	11.750	4.510
11.750	4.435	11.900	4.915
11.900	4.885	12.000	5.980
12.000	5.955	12.040	6.500
12.100	7.180	12.100	7.200
12.600	8.680	12.200	7.630
13.000	9.630	13.000	9.200

TABLE XVI

TITRATION DATA OF PSL PARTICLE SIZE 0.234 μm, 0.23 g

Vol. of Titrant	pH	Vol. of Titrant	pH
10.500	3.575	10.510	3.585
11.000	3.765	11.010	3.775
11.500	4.075	11.510	4.095
11.800	4.475	11.710	4.315
11.900	4.740	11.810	4.490
12.000	5.240	11.910	4.765
12.100	6.860	12.010	5.300
12.200	7.765	12.110	6.925
12.300	8.260	12.210	7.800
12.510	8.630	12.510	8.690
13.000	9.000		

TABLE XVII

TITRATION DATA OF PSL PARTICLE SIZE 0.481 μm, 0.15 g

Vol. of Titrant	pH	Vol. of Titrant	pH
10.600	3.280	9.905	3.160
11.600	3.505	10.905	3.344
12.600	3.905	11.905	3.660
13.010	4.275	12.855	4.105
13.115	4.450	13.105	4.343
13.210	4.690	13.205	4.650
13.310	5.090	13.305	5.115
13.404	6.025	13.405	6.085
13.462	6.760	13.455	6.690
13.490	6.975	13.505	7.005
13.530	7.195	13.605	7.315
13.715	7.716		
15.000	9.000		

TABLE XVIII

TITRATION DATA OF PSL PARTICLE SIZE 0.794 μm, 0.28 g

Vol. of Titrant	pH	Vol. of Titrant	pH
12.000	3.540	12.000	3.570
13.000	4.015	13.000	4.030
13.100	4.115	13.100	4.125
13.195	4.240	13.200	4.265
13.273	4.360	13.300	4.460
13.340	4.510	13.400	4.780
13.400	4.680	13.500	5.230
13.460	4.940	13.550	6.090
13.500	5.180	13.600	6.840
13.540	5.960	13.700	7.350
13.581	6.705	13.800	7.755
13.671	7.205	14.000	8.325
13.790	7.735		
13.903	8.115		

TABLE XIX

TITRATION DATA OF PSL PARTICLE SIZE 1.101 μm, 0.24 g

Vol. of Titrant	pH	Vol. of Titrant	pH
9.770	3.395	9.920	3.480
11.270	3.935	10.920	3.720
11.520	4.130	11.420	3.970
11.770	4.520	11.670	4.410
11.850	4.825	11.920	5.250
11.897	5.055	11.970	5.885
11.930	5.360	12.020	6.635
11.990	6.135	12.120	7.590
12.012	6.490	12.220	8.075
12.060	6.980		
12.125	7.545		
12.210	7.975		
12.920	8.500		

TABLE XX

TITRATION DATA OF BLANK FOR PSL PARTICLE SIZES 0.109, 0.234 AND 1.101 μm

Vol. of Titrant	pH	Vol. of Titrant	pH
10.050	3.620	10.060	3.625
10.550	3.870	10.560	3.865
11.050	4.033	11.060	4.020
11.300	4.383	11.310	4.355
11.550	4.858	11.560	4.905
11.650	5.290	11.760	6.085
11.750	5.938	11.810	6.540
11.800	6.370	11.850	7.420
11.850	7.465	11.910	8.020
11.950	8.184	12.060	8.760
12.050	8.820	13.060	9.750
13.050	9.780		

TABLE XXI

TITRATION DATA OF BLANK FOR PSL PARTICLE SIZES 0.481 AND 0.794 μm

Vol. of Titrant	pH	Vol. of Titrant	pH
10.230	3.195	10.060	3.160
11.230	3.390	11.060	3.365
12.230	3.710	12.060	3.765
12.480	3.840	12.560	4.055
12.800	4.055	12.810	4.240
12.910	4.170	13.060	4.610
13.010	4.330	13.160	4.870
13.160	4.775	13.260	5.770
13.210	5.030	13.310	6.520
13.270	5.950	13.360	7.990
13.320	6.950	13.460	8.850
13.392	8.410		
13.462	9.060		
14.000	9.200		

TABLE XXII

TITRATION DATA OF PARTICLE SIZE 0.330 μm, 0.16 g (A)
AND RESPECTIVE BLANK (B)

(A)		(B)	
Vol. of Titrant	pH	Vol. of Titrant	pH
10.000	4.065	10.000	4.490
11.000	4.400	11.000	4.590
11.250	4.530	11.100	4.630
11.500	4.705	11.350	4.825
11.600	4.755	11.500	5.000
12.000	5.005	11.600	5.080
12.100	5.075	11.700	5.280
12.200	5.135	11.900	5.410
12.300	5.255	12.100	5.520
12.400	5.450	12.200	5.615
12.500	5.670	12.300	5.690
12.600	6.015	12.400	5.805
12.650	6.260	12.500	6.000
12.700	6.500	12.600	6.555
12.750	6.700	12.700	7.060
12.800	6.910	12.800	7.370
12.900	7.155	13.000	7.940
13.210	7.720	13.350	8.300

ZETA POTENTIALS

The zeta potentials of the PSL particles in 5×10^{-4}M NaCl and 10^{-2}M NaCl are shown in Table XXIII. The calculation of the zeta potential is based on the Helmholtz-Smoluchowski equation (64). In the case of a spherical colloid particle, corrections, which increase with increasing zeta potential, are necessary for moderate values of κa ($0.2 < \kappa a < 50$) (65). Calculations indicated that no correction in zeta potential was necessary for the larger particles and that only a slight difference (<3 mv) is found for the smaller

particles when the zeta potential is recalculated. At a specific charge density, the zeta potential becomes less negative with increasing electrolyte concentration. The addition of the electrolyte decreases the zeta potential by compressing the electrical double layer.

TABLE XXIII

ZETA POTENTIALS OF THE PSL PARTICLES

Particle Size, μm	5×10^{-4} M NaCl	10^{-2} M NaCl
0.109	-39.0	-32.0
0.234	-48.0	-37.0
0.330	-44.0	-34.0
0.481	-52.0	-43.0
0.794	-62.0	-49.0
1.101	-70.0	-54.0

APPENDIX II

POLYMER SYNTHESIS AND CHARACTERIZATION

SYNTHESIS OF POLY(1,2-DIMETHYL-5-VINYLPYRIDINIUM BROMIDE)

The reaction scheme of poly(DMVPB) is shown in Fig. 32. Poly(DMVPB) was synthesized according to the procedure of Shyluk (66) with minor modifications.

MONOMER SYNTHESIS

A solution of distilled 2-methyl-5-vinylpyridine in anhydrous acetone (1 g/4 ml) was stirred magnetically in a beaker placed in an ice water bath. An equimolar amount of dimethyl sulfate in anhydrous acetone (1 g/2 ml) was added. The reaction temperature was maintained at 25-35°C by the rate of dimethyl sulfate addition and by stirring. After one hour, the ice bath was removed and the stirring was continued for another forty-five minutes. The pyridinium salt was then washed three times with anhydrous acetone and dried overnight in a vacuum oven at 35°C. The monomer was recrystallized by dissolving it in boiling absolute ethanol (1 g/4 ml) and immediately stirring the solution in an ice water bath. Absolute ether was used to wash the crystals which were then dried for one day in a vacuum oven at 35°C: m.p. 137-140°C. Literature: m.p. 137-138°C. The 1,2-dimethyl-5-vinylpyridinium methyl sulfate was stored in a sealed bottle at 4°C.

POLYMER SYNTHESIS

Apparatus (Fig. 33) was constructed in order for polymerization of the monomer to take place in an oxygen-free atmosphere. After placing monomer and initiator solution separately in glove bag, the glove bag was sealed and filled with nitrogen. The monomer and initiator solution were then placed in

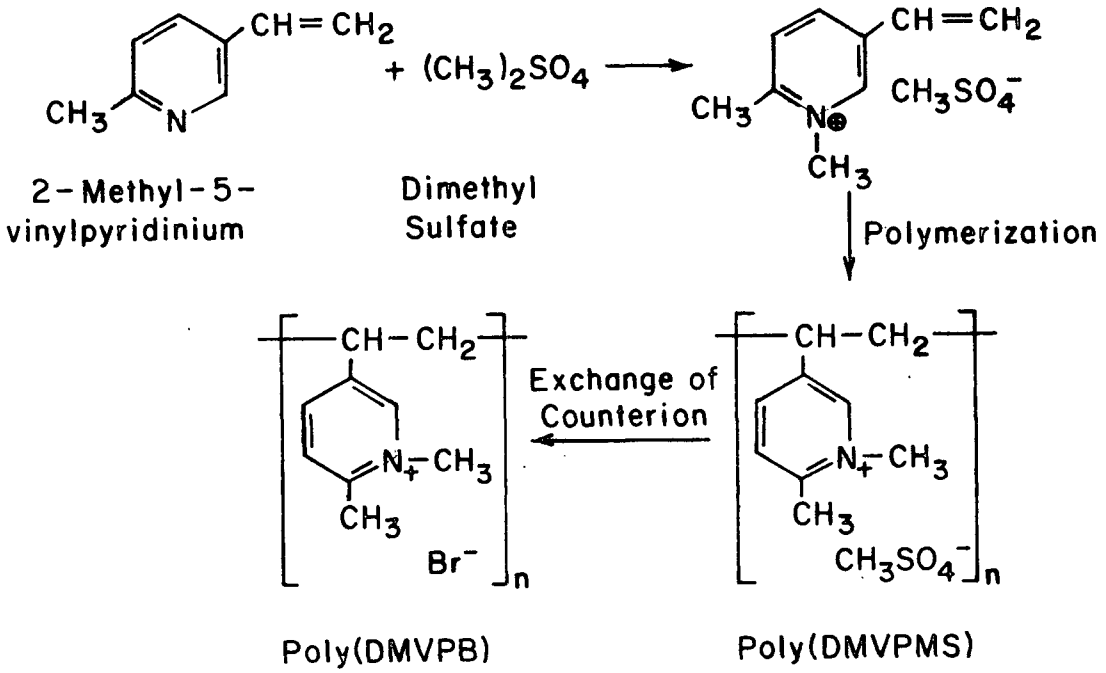

Figure 32. Reaction Scheme of Poly(DMVPB) Synthesis

the reaction flask in a 35°C water bath and the mixture was shaken until all of the monomer had dissolved. A three way stopcock permitted the reaction solution to be degassed by vacuum, followed by repressurization with nitrogen. This cycle was repeated four times. After the final repressurization with nitrogen, the reaction flask was immediately sealed with dental dam and kept in the bath until the desired amount of polymerization occurred. The monomer-polymer solution was then dialyzed on the Amicon Stirred Cell Model 202 Ultrafiltration System to remove the monomer. A complete description including operation and performance of the system has been described by Lindquist (17). Counterion exchange was achieved by dialysis with 0.4M KBr in the same manner.

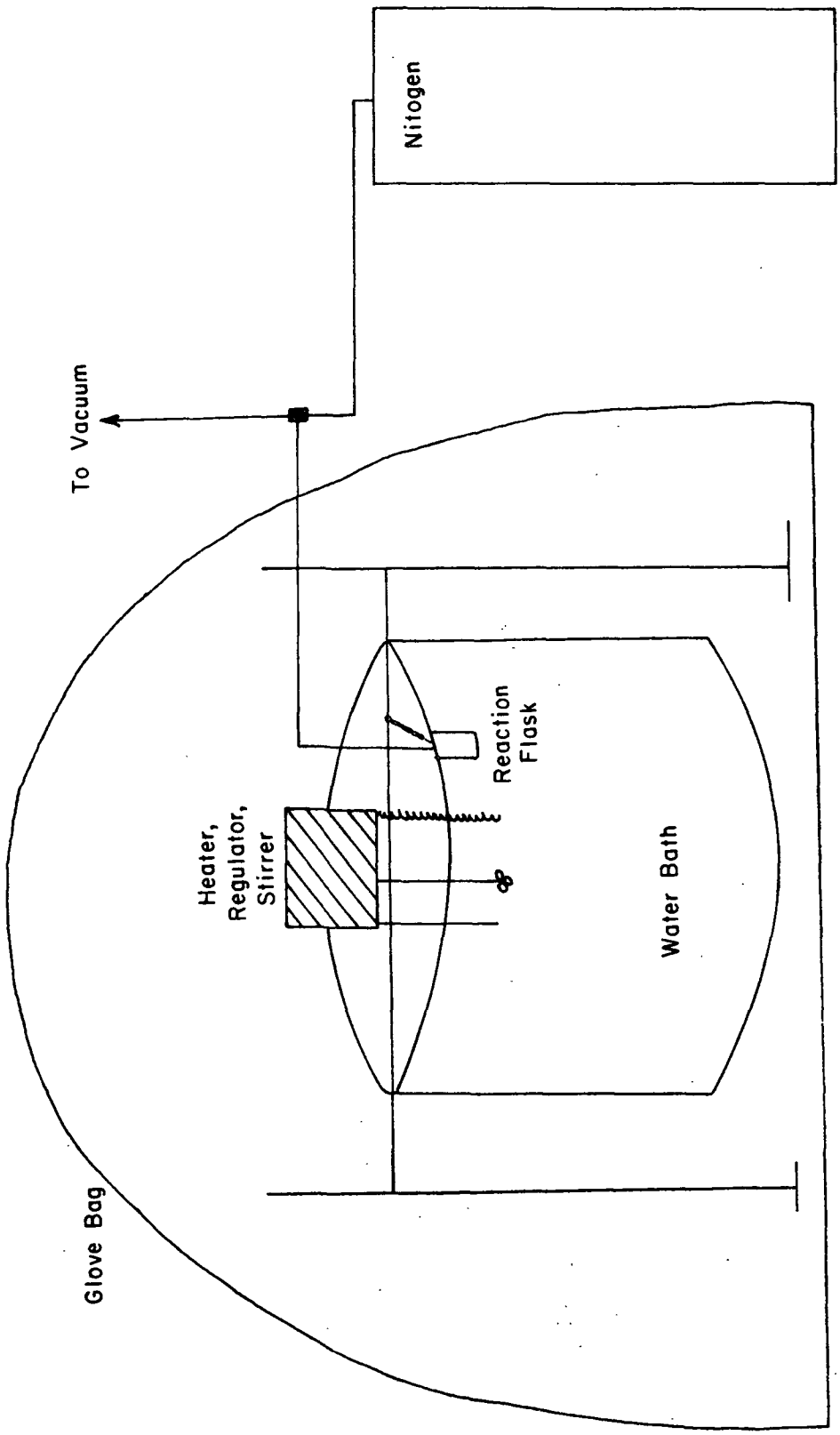

Figure 33. Schematic Diagram of Polymerization Equipment

TABLE XXIV

POLYMERIZATION OF 1,2-DIMETHYL-5-VINYLPYRIDINIUM METHYL SULFATE IN AQUEOUS SOLUTION

Monomer Concn., %	Initiator Concn., %	Reaction Temp.	Reaction Time	Conversion to Polymer, %	Approx. $\overline{M}_w$
35	0.005	35°C	120 min	15	10^6
20	2.000	35°C	35 min	20	10^4

QUANTITATIVE ANALYSIS OF POLY(DMVPB)

The concentration of poly(DMVPB) was determined by ultraviolet adsorption at a wavelength of 274 nm. A standard curve of poly(DMVPB) concentration *versus* adsorbance was prepared by determining the organic nitrogen content by the Hengar technique (67).

FRACTIONATION OF POLY(DMVPB)

DESCRIPTION OF SYSTEM

The column and solvent supply system was the same as described by Lindquist (17). The exception in this system was that the fraction collector operated on a constant volume basis rather than a constant time. The solvent was 0.4*M* KBr, and ultraviolet adsorption at 274 nm was employed to determine the concentration of poly(DMVPB) in each fraction.

PREPARATION OF COLUMN

Bio-Glas 2500 (100 cc) was added slowly with continuous stirring to 500 ml of a 1% solution of polyethylene glycol ($\overline{M}_w$ 20,000). This mixture was deaerated with a vacuum pump and filtered. The treated Bio-Glas was washed eight times with 100 ml portions of distilled water, poured into the column and allowed to settle. This procedure was repeated with Bio-Glas 1500, 1000, and 500, respectively. Solvent was then eluted through the column for two days.

FRACTIONATION PROCEDURES

The sample loading process was begun by draining 0.4M KBr down to the top of the Bio-Glas. Thirty ml of 2.0% high molecular weight poly(DMVPB) solution was loaded on the top of the column with a syringe. The column was filled to the top with solvent and connected to the solvent supply system. The column was eluted at a flow rate of 1.00 ml/min at 28.5°C. The low molecular weight polymer was fractionated in a similar manner. The exceptions were a polymer loading of 4.0%, a water jacket temperature of 25.5°C and the use of 0.4M NaCl as the solvent.

Thirty-two samples of each molecular weight were fractionated. Sixteen fractions of 20 ml each were collected from each fractionation run. Like fractions from separate fractionations were combined. The salt was removed from the polymer solutions by the previously mentioned dialysis method.

DETERMINATION OF MOLECULAR WEIGHT BY THE MENISCUS DEPLETION SEDIMENTATION EQUILIBRIUM METHOD

This method, first suggested by Wales, Adler and Van Holde (68) and treated extensively by Yphantis (69), is also called the high speed method or zero meniscus concentration method. This method is the same as the conventional (slow speed) sedimentation equilibrium method in principle, only varying in the procedure of calibrating the fringe system. The centrifuge is operated at speeds two to three times greater than the conventional method to sediment the macromolecular solute out of the region of the cell near the meniscus. The interference fringe count through the cell image then becomes a direct measure of the absolute concentration of solute at any position in the cell. This method has the advantage of requiring only a single run and less machine time. A limitation of this procedure is that it cannot be used for molecular weights in the order of 10,000 or smaller.

The weight-average molecular weight can be derived from the concentration distribution of the polymer in a centrifugal field by means of the following classical equation:

$$M_w = 2RT/\omega^2(1-vp) \times 2.303\ d\log c/d(r^2), \qquad (10)$$

where R = universal gas constant

T = absolute temperature

ω = angular velocity of the rotor

v = partial specific volume of the polymer

p = solvent density

c = polymer concentration at a distance r from the axis of rotation

A plot of log c versus r^2 will exhibit a slope which is proportional to the molecular weight. For a monodisperse, ideal system the plot will be linear along the whole cell. For the nonideal monodispersed case, the plot is a line of decreasing slope. For the polydispersed ideal case, the plot shows a line of increasing slope.

Both fractions were dialyzed against solvent and filtered prior to an experimental run. All measurements were performed at 25°C in 0.10M NaCl. Each fraction was run at a number of concentrations on a Beckman Spinco Model E ultracentrifuge equipped with a Rayleigh optical system.

The Rayleigh interference patterns produced by the polymer solutions and the pure solvent were photographed at intervals of time and tested against one another to assure that equilibrium conditions were met. Fringe numbers and positions were determined from these photographs with the aid of an x-y microcomparator fitted with digital and punched-card readout devices. The weight average and number average molecular weight (69) were obtained by

extrapolating the reciprocal of the apparent molecular weight to zero polymer concentration.

DIFFUSION COEFFICIENTS

The diffusion coefficients of solutes are most conveniently calculated with data obtained from free-diffusion experiments. This type of experiment is initiated by creating a boundary between two solutions having different concentrations of the soluted species under investigation. Observation of the solute concentration as a function of distance from the initial boundary and elapsed time permits the calculation of the diffusion coefficient. Gosting (70) gives a comprehensive review of the analysis of diffusion coefficients.

The use of a Rayleigh optical system is an appropriate method of following the solute concentration with respect to distance and time. The difference in the refractive index between solvent and solute produces an interference fringe pattern which is related to the distribution of solute within the cell. The relative positions of interference fringes are the primary information required for diffusion measurements.

Diffusion coefficients were determined on fractions F_1-6 and F_2-7 in 5×10^{-4}M NaCl and 10^{-2}M NaCl. The polymer fractions were dialyzed against the solvent to assure that there would be no Donnan effect. Dust was removed from the solution by filtration. A Beckman Spinco Model E ultracentrifuge was employed in the free diffusion experiments. Rayleigh optics were used to monitor the solute concentration across the boundary region as a function of time. From these data the apparent diffusion coefficients were calculated based on Fick's second law.

LIGHT SCATTERING

STANDARD EQUATIONS

Ideally the light scattering from a dilute polymer solution may be expressed in the following general form:

$$(Hc/T) = [1/M_w P(\theta)] + 2A_2c + 3A_3c^2 \cdots, \qquad (11)$$

where H = a constant

c = concentration expressed as g/ml

M_w = weight average molecular weight

$P(\theta)$ = particle scattering function in terms of angle θ

A_2, A_3 = second and third virial coefficients

T = absolute turbidity expressed as

$$T = [16TD/3\ (1.045)h](n_o^2 R_w/R_c)(a)(r/r')[\sin\theta/(1+\cos^2)]$$
$$X[(FG_\theta/G_o)_{solution} - (FG_\theta/G_o)_{solvent}], \qquad (12)$$

where TD = experimentally determined product of the diffuse transmittance of an opal glass reference standard and a diffuser correction factor

h = diaphram width

a = working standard constant

n_o = refractive index of the solvent

R_w/R_c = correction factor for incomplete compensation of refraction effects

r/r' = calibration factor for narrow slit system and circular cell

$\sin\theta$ = correction factor for the volume change on viewing the solution at different angles

$1/(1+\cos^2\theta)$ = correction factor applied when unpolarized light is used

F = filter factor

G_θ = galvanometer reading at angle θ

G_o = galvanometer reading at angle $\theta = 0$

DETERMINATION OF WEIGHT AVERAGE MOLECULAR WEIGHT, SECOND VIRIAL COEFFICIENT AND MEAN SQUARE RADIUS OF GYRATION

The Zimm treatment (71) affords the most accurate graphical procedure for the derivation of light scattering parameters when angular dependence comes into play. Turbidity measurements are made at a series of angles for different concentrations. A double extrapolation procedure is employed, plotting $\underline{Hc}/\underline{T}$ against $\sin^2\theta/2 + \underline{kc}$, where $\underline{k}$ is an arbitrary constant chosen so as to suitably spread out the concentration values, and extrapolating at constant concentration and constant angle. The resulting Zimm plot is a gridlike graph with two limiting lines — $(\underline{Hc}/\underline{T})_{\theta,\underline{c}=0}$ versus $\sin^2(\theta/2)$ and $(\underline{Hc}/\underline{T})_{\theta=0,\underline{c}}$ versus $\underline{kc}$. Ideally, the two extrapolations would cut the $\underline{Hc}/\underline{T}$ axis at the same point. The reciprocal of the intercept $(\underline{Hc}/\underline{T})_{\theta=0,\underline{c}=0}$ is equal to the weight average molecular weight of the polymer. The slope of the line $(\underline{Hc}/\underline{T})_{\theta=0,\underline{c}}$ is equal to twice the second virial coefficient divided by the arbitrary constant $\underline{k}$. The mean square radius of gyration $(\underline{s}^2)_{\underline{z}}$ is given by the intercept and initial slope of the line $\underline{c}=0$;

$$(s^2)_z = (3\lambda^2/16\pi^2)[\text{initial slope of line } c=0/\text{intercept}(Hc/T)_{\theta=0,c=0}] \quad (13)$$

EXPERIMENTAL PROCEDURES

Solution Preparation

Polymer solutions of fraction F_1-6 were prepared at a concentration of $5 \times 10^{-4}\underline{M}$ NaCl and $10^{-2}\underline{M}$ NaCl. To assure that the concentrations of the simple ionic species in the solvent were equal to those in the polymer solutions, the two were dialyzed against each other prior to light scattering measurements. Dust was removed from the solutions by filtration through 4500 A and 6500 A Millipore filters. The solutions were transferred to the

light scattering cell, Brice-Phoenix C-101, with a pipet. Dilution was accomplished by adding filtered solvent to the cell by pipet.

Light-Scattering Apparatus and Working Equations

Light scattering measurements were made at 25°C using a Brice-Phoenix Universal Light Scattering Photometer (Series 1937). For the particular instrument used, Equation (12) becomes:

$$T = 1.21(n_o^2 R_w/R_c)a(r/r')\frac{(\sin\theta)}{(1+\cos^2\theta)}[(FG_\theta/G_0)_{solution}-(FG_\theta/G_0)_{solvent}] \quad (14)$$

at wavelength 5461 A. The value of a was found to be 0.0502, (r/r') was equal to 1.057 and the appropriate value of $(n_o^2 R_w/R_c)$ was obtained from the Brice-Phoenix operation manual (72).

Depolarization Correction

The light scattered transversely from small isotropic particles is completely polarized. If the particles are anisotropic, additional scattering will arise from the differences in polarizability along different axes of the molecule and a correction must be applied to the turbidity. The correction for this effect has been related to the depolarization ratio, P_u, by Cabannes and Rocard (73) through the following ratio:

$$C_u = (6-7P_u)/(6+6P_u), \quad (15)$$

where C_u, the Cabannes factor, is multiplied by the observed molecular weight to obtain the true average molecular weight. The depolarization ratio is given by

$$(P_u)_c = \frac{(FG_{90}^H/G_0^H)_{solution} - (FG_{90}^H/G_0^H)_{solvent}}{(FG_{90}^V/G_0^V)_{solution} - (FG_{90}^V/G_0^V)_{solvent}}, \quad (16)$$

where $(P_u)_c$ is the value at a given concentration and must be extrapolated to zero concentration to obtain P_u. The superscripts H and V, respectively, refer to the horizontal and vertical components of the scattered light. They are measured by placing a polaroid lens in the proper position between the cell and the photomultiplier tube.

The value of C_u for the large M_w polymer in both 5×10^{-4}M NaCl and 10^{-2}M NaCl was 0.85 ± 0.02. Fluorescence was negligible.

VISCOSITY

The intrinsic viscosity, $[\eta]$, of a solution can be defined in the following manner:

$$[\eta] = \lim_{c\to 0}(\eta_{sp}/c) = \lim_{c\to 0}[(\eta_{rel}-1)/c] = \lim_{c\to 0}[(\ln\eta_{rel})/c], \qquad (17)$$

where the relative viscosity, η_{rel}, is the ratio of the efflux time of the solution, t, to that of the solvent, t_o. The specific viscosity, η_{sp}, is given by

$$\eta_{sp} = (\eta_{rel}-1) = (t-t_o)/t_o \qquad (18)$$

The concentration, c, is expressed in grams per deciliter of solution. Therefore, the intrinsic viscosity may be determined by extrapolation of η_{sp}/c as a function of concentration to zero concentration.

KINETIC ENERGY CORRECTION

The fact that some of the pressure drop between the ends of the viscometer tube represents conversion of potential energy to the kinetic energy of the stream leaving the capillary necessitates a correction applied to the flow times to account for this kinetic energy loss. This correction may be applied

to the specific viscosity by using the following relationship (74):

$$\eta_{sp} = \eta'_{sp}\{(F_o/(1-F))[((t+t_o)/t)+1]\} \qquad (19)$$

In this expression, η_{sp} is the corrected specific viscosity, η'_{sp} is the observed specific viscosity and F_o is defined as

$$F_o = m_e \rho_o V/8\eta_o t_o L, \qquad (20)$$

where m_e = kinetic energy coefficient or end correction

ρ_o = solvent density

V = bulb volume

η_o = absolute solvent viscosity expressed in poises

L = length of the capillary

NON-NEWTONIAN BEHAVIOR

If viscosity is independent of the rate of shear, the liquid is said to be Newtonian or to exhibit ideal flow behavior. A non-Newtonian behavior commonly observed in polymer solutions where the degree of polymerization is greater than 2200 is shear thinning. Shear thinning results from the tendency of the applied force to disturb the long chains from their favored equilibrium conformation, causing elongation in the direction of shear. This results in a decrease of viscosity. To correct for this effect, η_{sp}/c as a function of shear stress must be extrapolated to zero shear stress.

EXPERIMENTAL PROCEDURES

Viscosity determinations were performed for the low molecular weight polymer in 5×10^{-4}M NaCl and 10^{-2}M NaCl solutions at 25.00 ± 0.01°C. Both polymer solutions and solvents were filtered through 2000 A Millipore filters prior to viscosity determinations. Duplicate viscosity determinations were

made using two Cannon 50 Ubbelohde dilution viscometers at a number of solution concentrations by dilution in the viscometer. Twenty minutes were allowed for equilibration after a dilution was made. Dilutions were made using a microsyringe equipped with a 10-inch stainless steel needle. Efflux times were recorded until 3 successive times differed by less than 0.3 sec; efflux times were greater than 200 sec making kinetic energy corrections unimportant (74). A negligible shear rate dependence is assumed for low molecular weight polymer.

A modified Ubbelohde variable shear viscometer, Cannon 75 S109 was used for viscometric measurements for fraction F_1-6 in 5×10^{-4}M NaCl and 10^{-2}M NaCl solutions. Solution preparation and the experimental conditions and procedures were the same as described for fraction F_2-7. The one exception was that the polymer solutions in 5×10^{-4}M NaCl and 10^{-2}M NaCl were filtered through 6500 A and 4500 A Millipore filters, respectively. The maximum kinetic energy corrections were found to be less than 1% and were neglected.

After each viscosity determination, a small sample was removed and the poly(DMVPB) concentration determined by UV adsorption. The solvent efflux times were also redetermined. The intrinsic viscosities were calculated by the least squares method for the best fit of reduced specific viscosity (η_{sp}/c) as a function of poly(DMVPB) concentration.

EXPERIMENTAL RESULTS AND DISCUSSION

QUANTITATIVE ANALYSIS OF POLY(1,2-DIMETHYLVINYLPYRIDINIUM BROMIDE)

The concentration of poly(DMVPB) was determined spectrophotometrically. Poly(DMVPB) has an absorbance peak at 274 nm. Figure 34 shows a standard

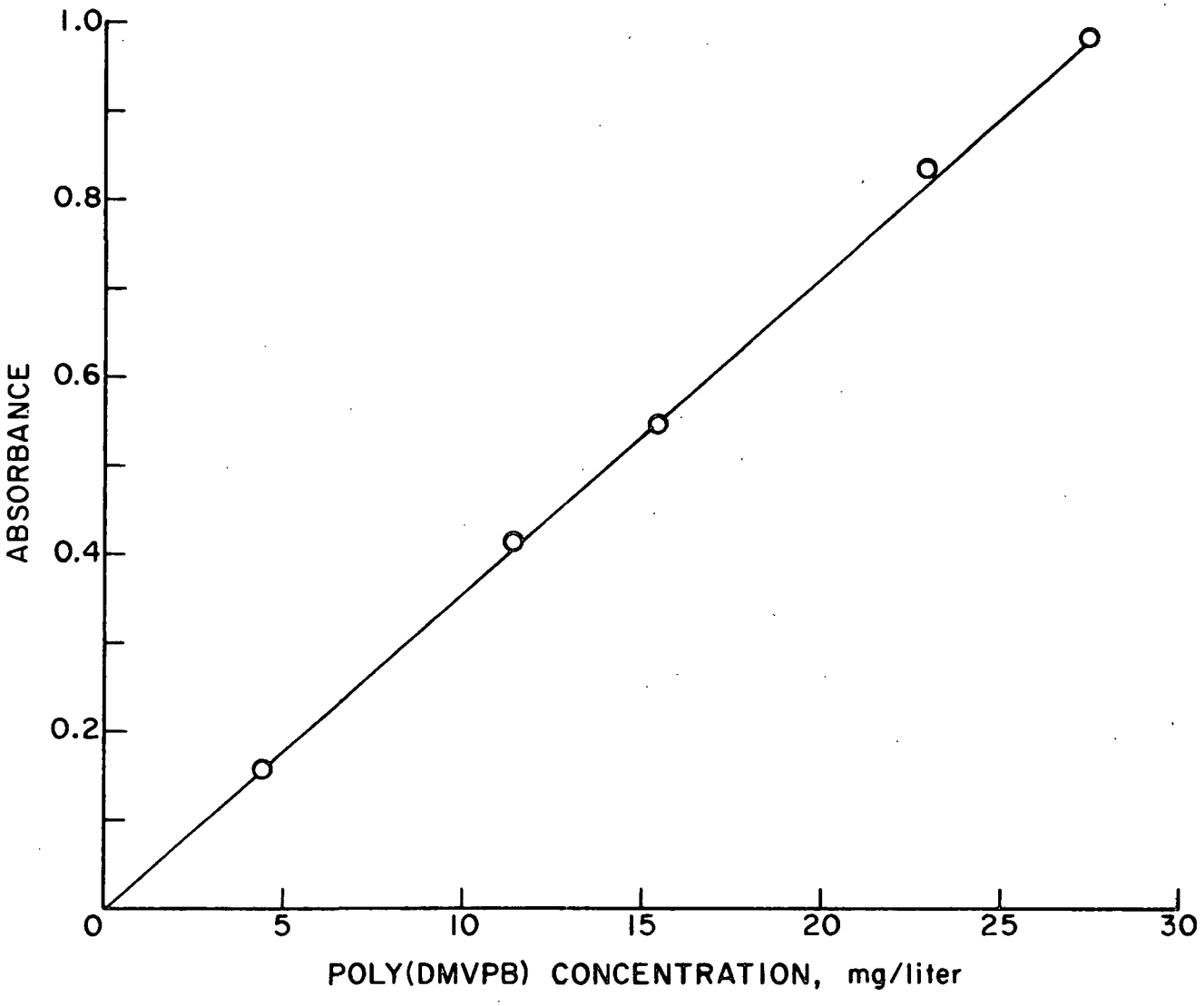

Figure 34. Absorbance at 274 nm Versus Poly(DMVPB) Concentration

curve of poly(DMVPB) concentration versus absorbance. The standard curve obeys Beer's Law.

FRACTIONATION

The elution volume-concentration distribution of the combined fractions is shown in Fig. 35 and 36. The values plotted are the average values for the combined fractions from 1-16 for the first ten fractionations.

MOLECULAR WEIGHT OF FRACTIONS

The weight and number average molecular weight data of fractions F_1-6 and F_2-7 were determined by a sedimentation equilibrium technique. Table XXV is a summary of these results.

TABLE XXV

SEDIMENTATION EQUILIBRIUM MOLECULAR WEIGHT DATA

Fraction	Rotor rpm's	$\underline{M}_w$	$\underline{M}_n$	$\underline{M}_w/\underline{M}_n$
1	6,995	841,600	741,400	1.14
	8,766	749,650	632,200	1.19
	12,590	611,800	525,900	1.16
2	2,041	30,700	26,300	1.17
	3,560	35,100	30,900	1.14
	4,204	33,100	25,800	1.28

From Table XXV it is seen that the large molecular weight varies with rotor speed. The final weight-average molecular weight was determined by plotting $1/\underline{M}_w$ versus λ^2 as suggested by Utiyama, et al. (75) where λ is

$$\lambda = (1-vp)(\omega^2)(r_b^2-r_a^2)/2RT, \qquad (21)$$

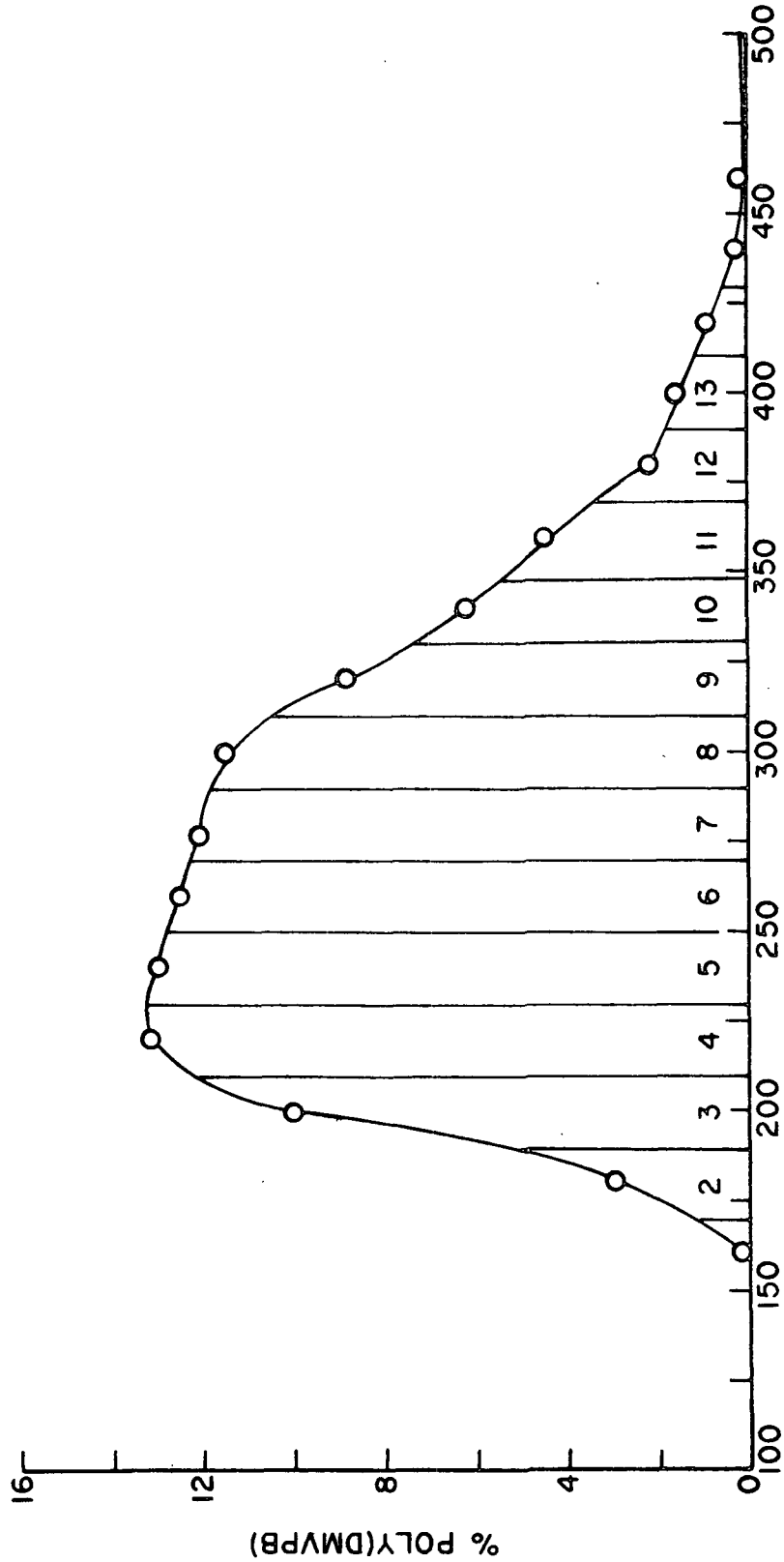

Figure 35. Elution Volume Versus Poly(DMVPB) Concentration for Large Molecular Weight Polymer. Average Values for 10 Fractionations

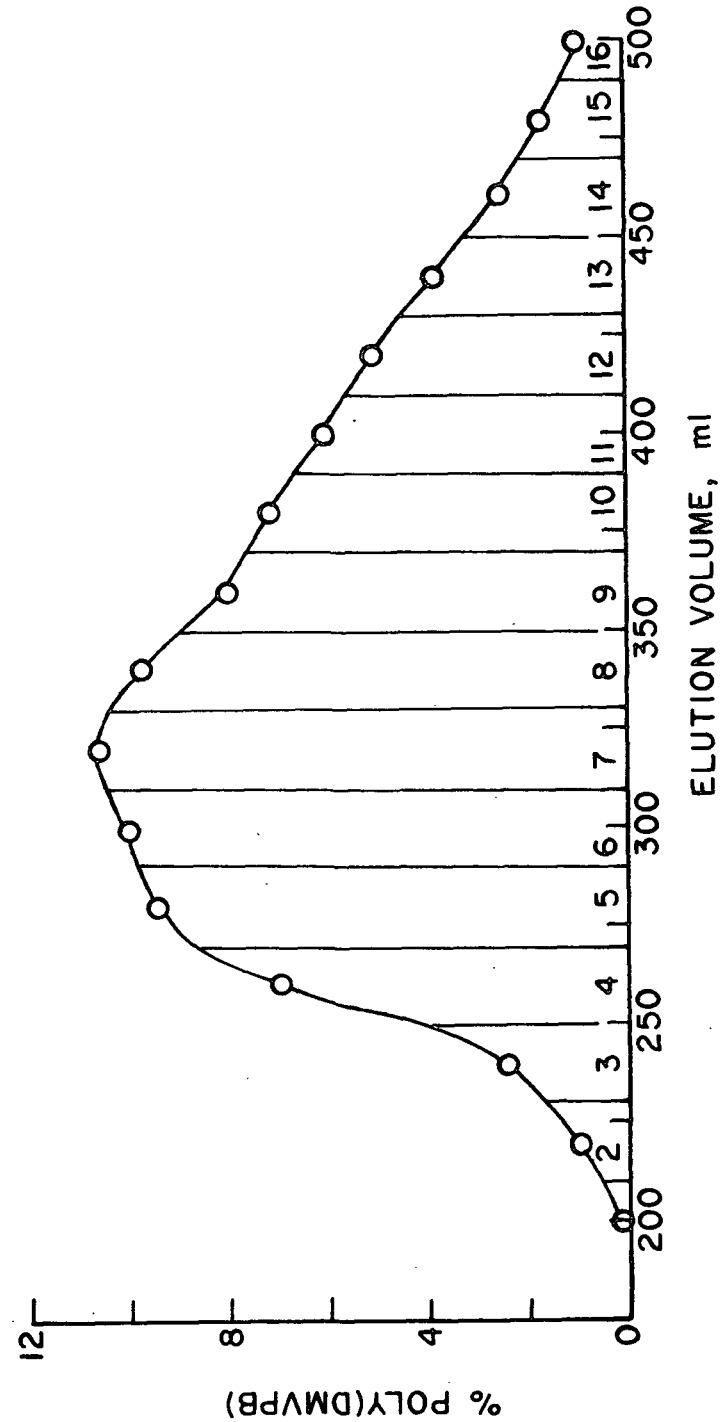

Figure 36. Elution Volume Versus Poly(DMVPB) Concentration for Low Molecular Weight Polymer. Average Values for 10 Fractionations

where $\underline{v}$ = partial specific volume of solute at infinite dilution

$\underline{\rho}$ = density of the solvent

ω = angular speed of the rotor

$\underline{r_a}, \underline{r_b}$ = radial distances from the center of rotation to the meniscus and bottom of the solution column

$\underline{R}$ = gas constant

$\underline{T}$ = absolute temperature

The final weight and number average molecular weights of fractions F_1-6 and F_2-7 are presented in Table XXVI. The molecular weight of fraction F_2-7 is an average value of those molecular weights presented in Table XXV. The molecular weights listed are for infinite dilution.

TABLE XXVI

WEIGHT AND NUMBER AVERAGE MOLECULAR WEIGHTS

Fraction	$\underline{M_w}$	$\underline{M_n}$	$\underline{M_w}/\underline{M_n}$
F_1-6	885,000	763,000	1.16
F_2-7	33,000	27,700	1.20

DIFFUSION COEFFICIENTS

The concentration-diffusion coefficient curves for fractions F_1-6 and F_2-7 in the 5×10^{-4} M NaCl are shown in Fig. 34. The diffusion coefficients were calculated according to the Creeth method (76) and thus the concentration is expressed as the average concentration in the cell. A concentration of thirty fringes corresponds approximately to 5000 mg/liter.

Two trends are readily apparent in Fig. 37. The diffusion coefficients of the higher molecular weight samples are much more sensitive to concentration changes than are those for the smaller molecules. The effect of polymer

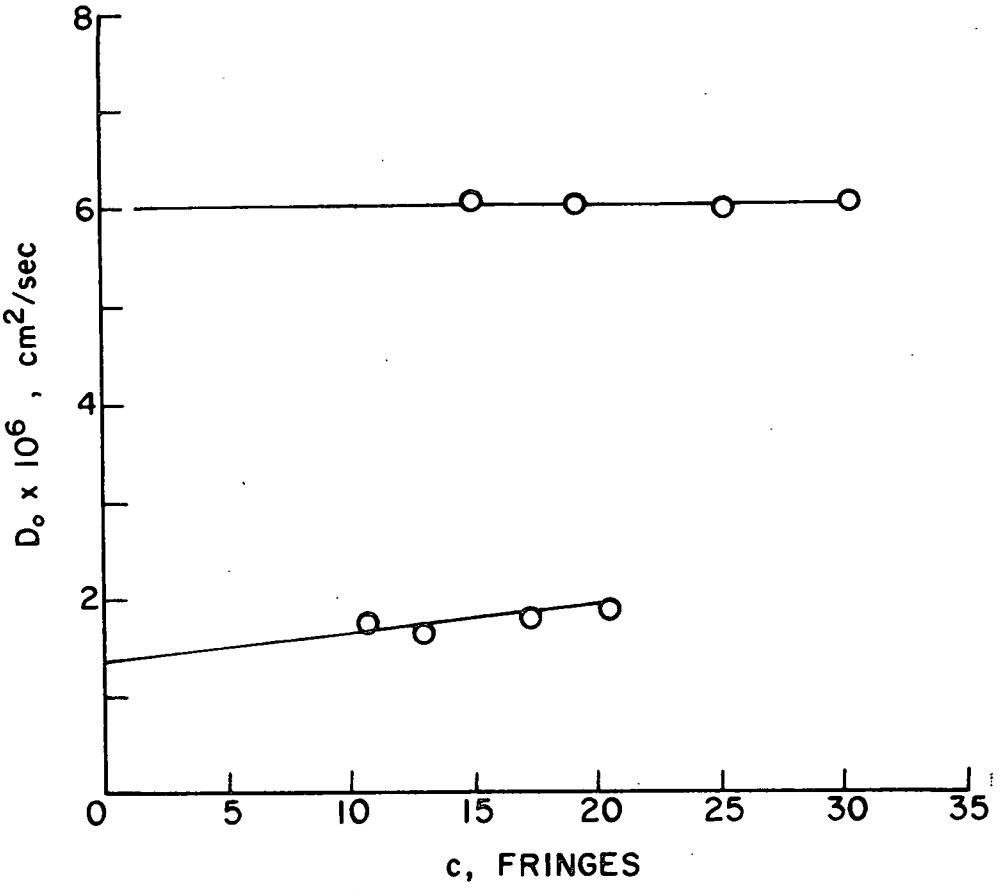

Figure 37. Diffusion Coefficients of F_1-6 (Bottom) and F_2-7 (Top) in 5×10^{-4} M NaCl

concentration on the diffusion coefficient may be due to either a thermodyamic or a hydrodynamic factor. The thermodyamic factor reflects deviation from solution ideality and, in general, causes the diffusion coefficient to increase with concentration. The hydrodynamic factor is a result of interaction between the motion of particles. This interaction has the effect of increasing the friction factor and thus decreasing the diffusion coefficient with concentration. Apparently it is the thermodynamic factor which predominates over the range of conditions studied.

The second trend is the decrease in the diffusion coefficient at infinite dilution with increasing molecular weight. This is a result of the larger friction coefficient for the higher molecular weight species. In a study of

the diffusion behavior of poly-L-lysine, Daniel and Alexandrowicz (77) found a linear relationship between the logarithm of the degree of polymerization and the logarithm of the diffusion coefficient. This relationship was also determined by others for polyethylenimine (17,78).

Effect of Ionic Strength

The concentration-diffusion coefficient curves for fractions F_1-6 and F_2-7 in 0.01M NaCl are shown in Fig. 38. The effect of salt concentration on the diffusion coefficient is not well defined in the literature. One theory (77) proposed is based on the charge effect. In a system where a polymer has a large degree of ionization, the counterions exert a strong drag effect on the macromolecule. The more mobile counterions tend to diffuse ahead of the charged macroion and, in the process, create an unstable separation of charge. This charge separation causes the macromolecule to diffuse more rapidly than if it were uncharged. The two motions are "locked," one to another. In the presence of a dissociating low molecular weight salt, the counterions will no longer be completely locked to that of the macroion; the byions of the salt prevent the macroion from "seeing" the counterions. The result is that the diffusion coefficients at infinite dilution should increase with decreasing salt concentration until a maximum value in salt-free solutions is reached asymptotically. This trend was found by Alexandrowicz and Daniel (77).

Another theory used to interpret diffusion data is based on the friction model. This model is well known and has been clearly defined by others (79,80). Whereas the charge effect theory centers on the dragging of small ions, the friction model is centered on the influence of the macroion's friction coefficient. The greater the frictional coefficient, the smaller the diffusion coefficient.

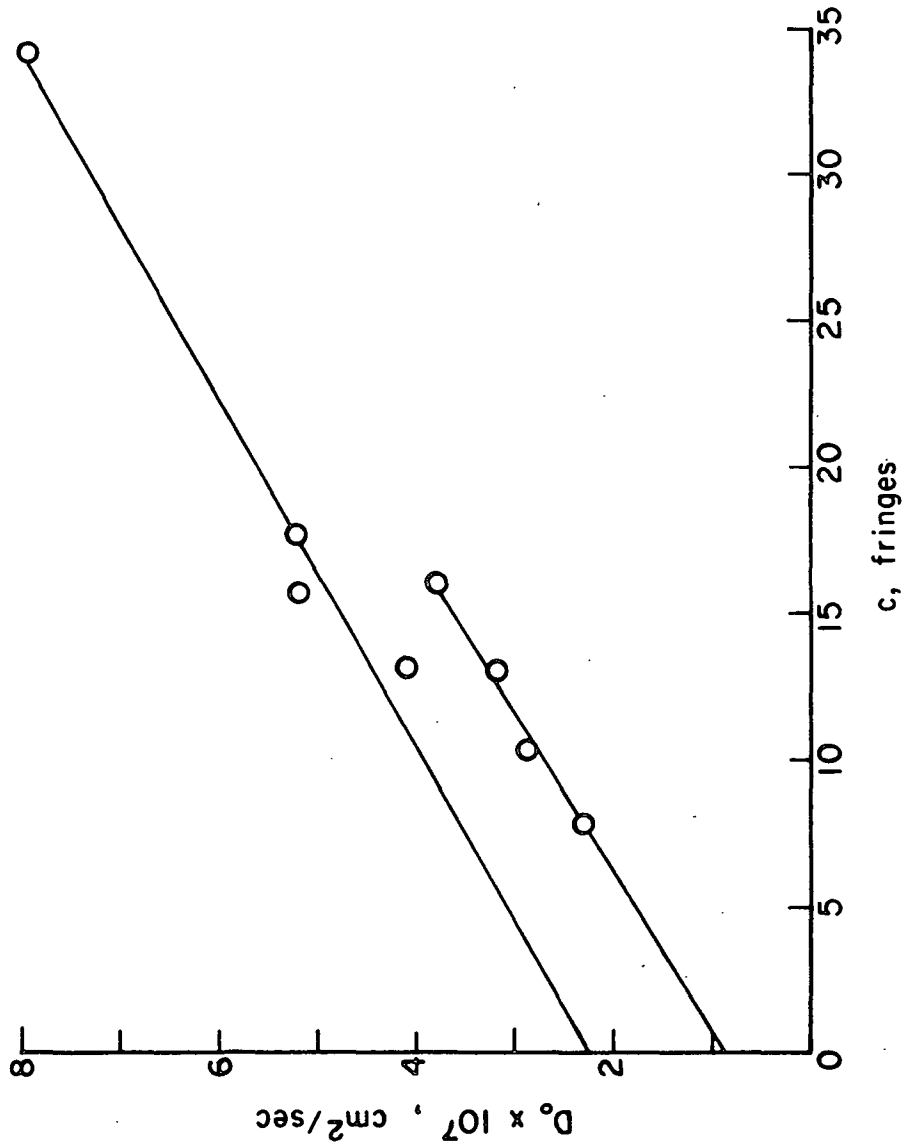

Figure 38. Diffusion Coefficients of F_1-6 (Bottom) and F_2-7 (Top) in 10^{-2} M NaCl

The diffusion coefficients at infinite dilution are tabulated in Table XXVII. The diffusion coefficients can be related to molecular size by the Stokes equation (81):

$$R_e = kT/6\pi\eta_o D_o, \tag{22}$$

where k = Boltzmann constant

T = absolute temperature

η_o = solvent viscosity

D_o = limiting diffusion coefficient

This concept implies that the macroion behaves as an impermeable sphere in solution. The radius of the hydrodynamic equivalent sphere (R_e) is related to the radius of gyration (R_G) in the following manner (82):

$$\frac{R_e}{R_G} = 0.665 = \varepsilon_F \tag{23}$$

For a number of other polymers, values of ε_F ranging from 0.55 to 0.75 have been observed (82). In each of these instances fairly good solvents were used. However, it has not been established whether or not ε_F varies with the nature of the solvent. Mandelkern (83) shows a trend that ε_F is dependent on molecular weight; however, insufficient work has been done in this area to say anything definite. Table XXVIII presents R_G as calculated from the results in Table XXIX and Equations (22) and (23).

TABLE XXVII

DIFFUSION COEFFICIENTS

Fraction	Solvent	$\underline{D}_o \times 10^7$, cm^2/sec
F_1-6	$5 \times 10^{-4}\underline{M}$ NaCl	13.50
	$10^{-2}\underline{M}$ NaCl	0.93
F_2-7	$5 \times 10^{-4}\underline{M}$ NaCl	60.05
	$10^{-2}\underline{M}$ NaCl	2.25

TABLE XXVIII

RADIUS OF GYRATION FROM DIFFUSION COEFFICIENT

Fraction	Solvent	$\underline{R}_G$
F_1-6	$10^{-2}\underline{M}$ NaCl	390 A
F_2-7	$10^{-2}\underline{M}$ NaCl	140 A

TABLE XXIX

DIFFUSION COEFFICIENTS

Fraction	Solvent, $\underline{M}$ NaCl	Average Fringe Number	Apparent $\underline{D} \times 10^6$, cm^2/sec at $\underline{t} = \infty$	Limiting $\underline{D}_o \times 10^6$, cm^2/sec at $\underline{t} = \infty, \underline{c} = 0$
F_1-6	5×10^{-4}	10.94	1.75	1.350
		12.94	1.65	
		17.24	1.78	
		20.42	1.87	
F_2-7	5×10^{-4}	15.00	6.07	6.050
		19.36	6.08	
		25.53	6.00	
		30.49	6.07	
F_2-7	10^{-2}	13.13	0.41	0.225
		15.77	0.52	
		16.74	0.52	
		34.22	0.79	
F_1-6	10^{-2}	7.85	0.23	0.093
		10.30	0.29	
		13.10	0.32	
		15.82	0.38	

It has generally been recognized that aqueous solutions of polyelectrolytes display a strongly nonideal behavior. In the classical studies the deviations from ideal behavior were interpreted in terms of polyion-polyion interactions and polyion-ionic atmosphere interactions, the ionic atmosphere including the small ions in the overall vicinity of the polyion. The strong electrostatic forces between the charges on individual macroions are not suppressed at the experimentally attainable low polymer concentrations and furthermore the polyion-ionic atmosphere interactions persist at infinite dilution. To overcome some of these difficulties, measurements are carried out in the presence of an excess of a low molecular weight salt. The radii of gyration obtained from the diffusion coefficients of the weak salt polymer solutions were unrealistic and are not included in Table XXVIII. The error may be attributed to one of two sources: 1) the difficulty of obtaining realistic diffusion data from polyelectrolytes in very weak salt solutions, or 2) the inapplicability of Stokes equation in calculating the radius of gyration. If the charge effect is modifying the diffusion mechanism of polyelectrolytes in weak salt solutions, and since Stokes Law does not include this effect, it might be expected that the simple calculation based on the latter would be in error.

LIGHT SCATTERING

The results of the experimental light-scattering investigation are presented in the form of Zimm plots in Fig. 39 and 40. The weight average molecular weight of fraction F_1-6 in 5×10^{-4}M NaCl and 10^{-2}M NaCl is found to be 1,042,000 ± 78,000. The uncertainty can be attributed to the experimental difficulty of satisfactorily separating high molecular weight solutes from extraneous impurities (dust) which are inevitably introduced into the system. As the size of the dissolved macromolecules is increased beyond a

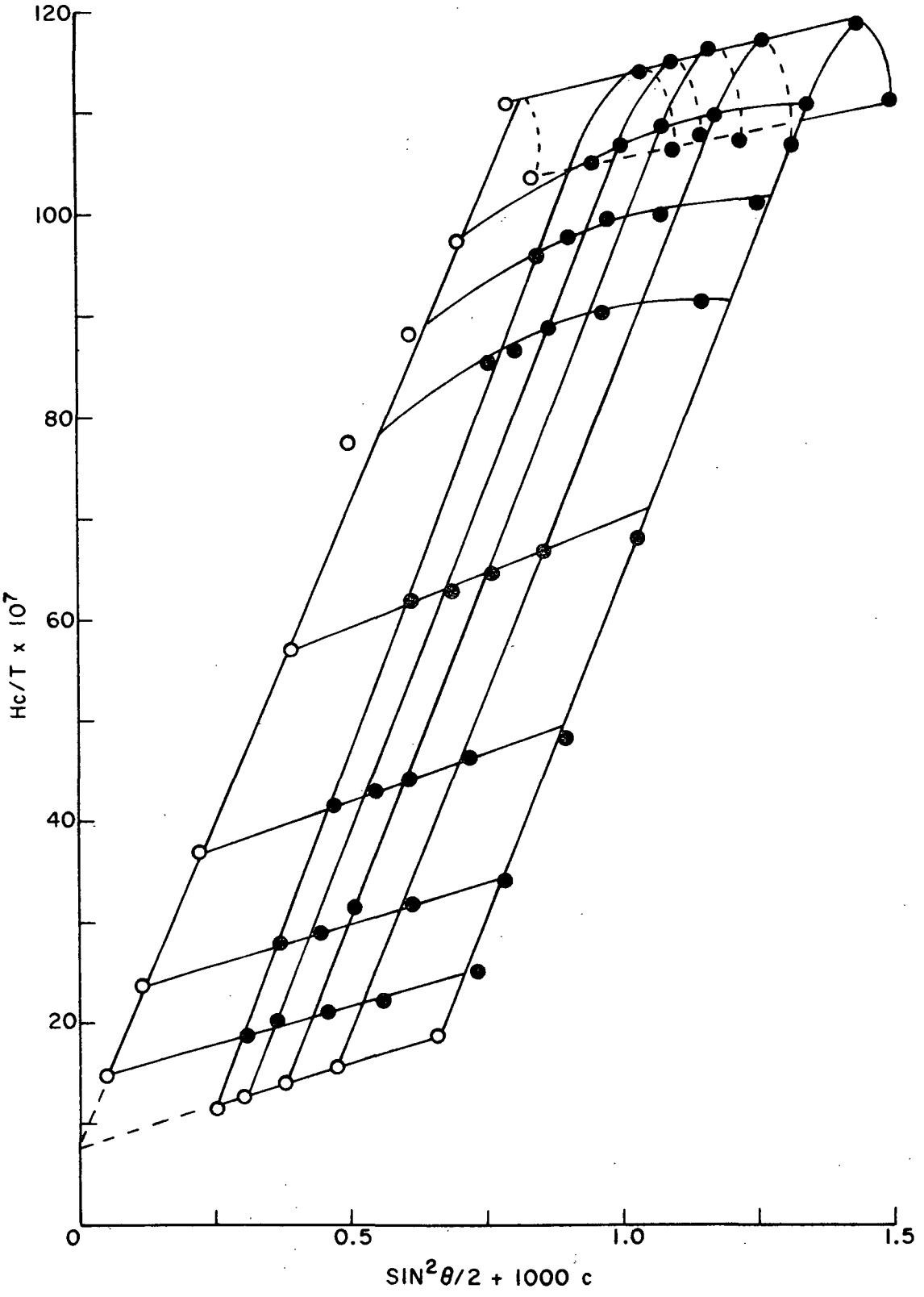

Figure 39. Zimm Plot for Poly(DMVPB), F_1-6 in 5×10^{-4} M NaCl. $\lambda = 5461$ A; $\underline{M}_w = 1.1 \times 10^6$; $(\underline{s}^2_z)^{1/2} = 2757$ A; $A_2 = 9.01 \times 10^{-4}$ moles cc g^{-2}

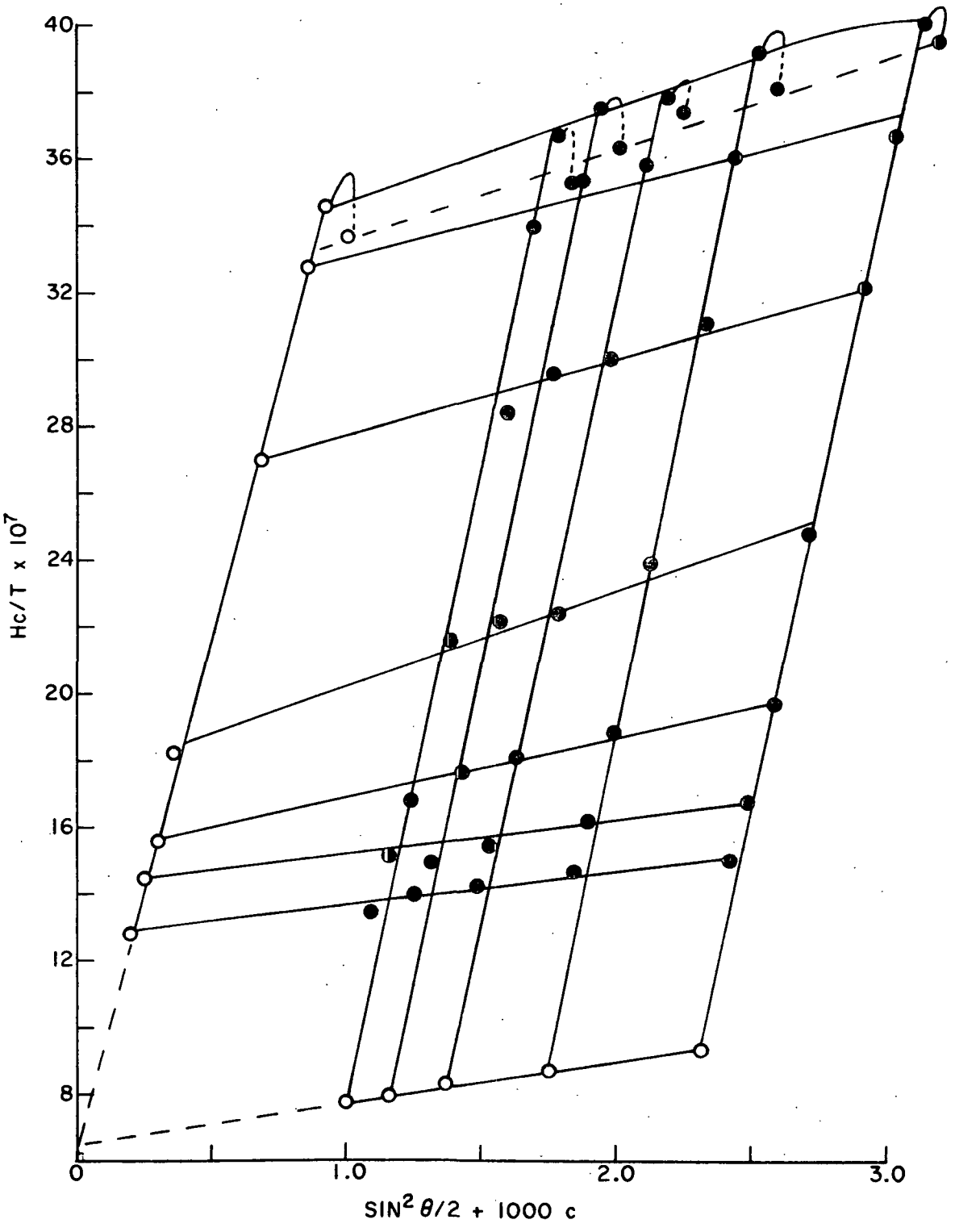

Figure 40. Zimm Plot for Poly(DMVPB), Fraction F_1-6 in 10^{-2} M NaCl. λ = 5461 A; $\underline{M}_w$ = 0.97 × 10^6; $(\underline{s}^2_z)^{1/2}$ = 1304 A; A_2 = 0.58 × 10^{-4} moles cc g^{-2}

certain limit (0.2 μm), any procedure to "clean" the solution becomes either inadequate to remove all the dust or else it removes with it the highest molecular weight fraction of the sample under investigation.

From the data, one trend is readily apparent: as the salt concentration increases, the mean square radius of gyration and the second virial coefficient decrease. The mean square radius of gyration of polyelectrolytes is determined by the long range electrostatic interaction among fixed charges along the polyion backbone. In a salt-free system, the repulsion between the fixed charges will give a relatively high free energy to compact configurations and a relatively lower free energy to expanded ones. As salt is added to the polymer solution, the byions shield the fixed charges, decreasing the electrostatic interaction between the fixed charges and allowing for a more compact configuration. This change in configuration is reflected as a decrease in the slope of the plot $(\underline{Hc}/\underline{T})_{\underline{c}=0}$ versus $\sin^2(\theta/2)$ and has been observed by numerous workers (84,85) in a number of different polyelectrolyte systems.

The second virial coefficient of polyelectrolytes in salt solutions is governed by the distribution of the diffusible ions (polymer-solvent interactions). As the solvent becomes better, i.e., the concentration of the added salt is decreased, the second virial coefficient increases. This is in agreement with previous findings. Takahashi, et al. (86) observed that A_2 is linear with respect to the reciprocal of the salt concentration if the salt concentration is lower than 0.1M. At higher concentrations, A_2 was found to be linear with the reciprocal of the square root of the salt concentration.

VISCOSITY

Low Molecular Weight

When 5×10^{-4} M NaCl was used as the solvent, the slope of intrinsic viscosity versus concentration increased negatively upon dilution (Fig. 41) preventing extrapolation to obtain a reliable value for the intrinsic viscosity. This characteristic is typical for polyelectrolytes in weak salt solutions. Fuoss and Strauss (87) suggest the use of the following relationship to interpret these data.

$$\eta_{sp}/c = A/(1+B\sqrt{c}), \qquad (24)$$

where A is the limiting value of η_{sp}/c as c approaches zero. A is obtained by plotting c/η_{sp} versus $\sqrt{c}$ where the intercept at $\sqrt{c} = 0$ is $1/A$ (i.e., $1/\eta_{sp}$). If poly(DMVPB) follows this relationship, the plot will be linear. Figure 42 shows the plot.

Large Molecular Weight

Determination of the intrinsic viscosity at zero shear stress proceeded in the following manner. The reduced specific viscosity at each concentration was plotted against the calculated shear stress (Fig. 43). Since the plot is nonlinear and extrapolation to $T_R = 0$ would lead to large uncertainties for the intrinsic viscosity, another method was employed. The plot of c/η_{sp} versus $T_R^{1/2}$ showed a linear relationship (Fig. 44). The intrinsic viscosity was determined by extrapolating $(\eta_{sp}/c)_{T_R=0}$ to infinite dilution (Fig. 45). The complete viscosity data are summarized in Tables XXX-XXXIII. The intrinsic viscosity values based on 95% confidence limits have an average error of about ±3.4%.

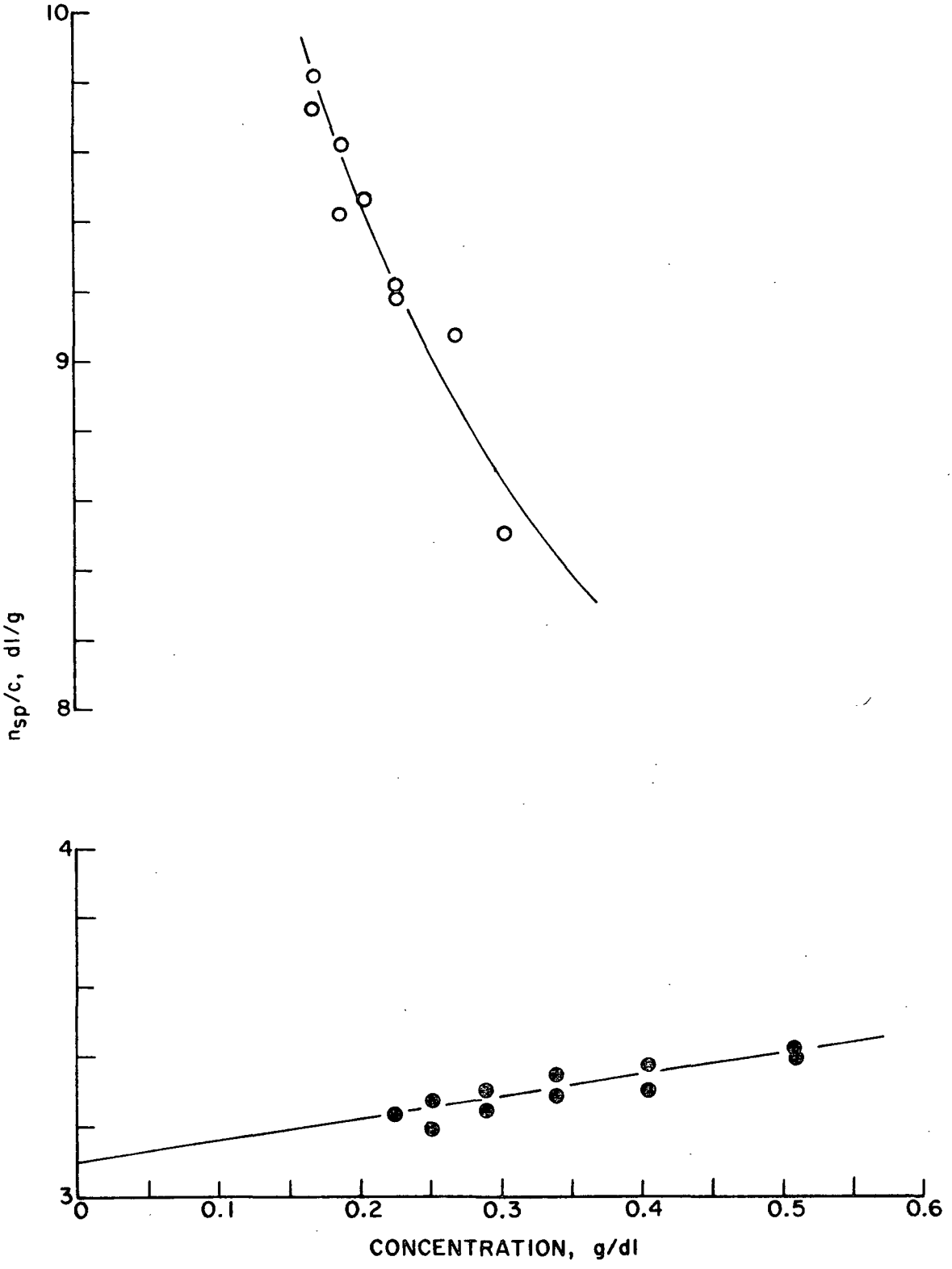

Figure 41. Viscosity as a Function of Concentration, Fraction F_2-7 in 5×10^{-4} M NaCl (Open Circles) and 10^{-2} M NaCl (Solid Circles) at 25.00 ± 0.01° C

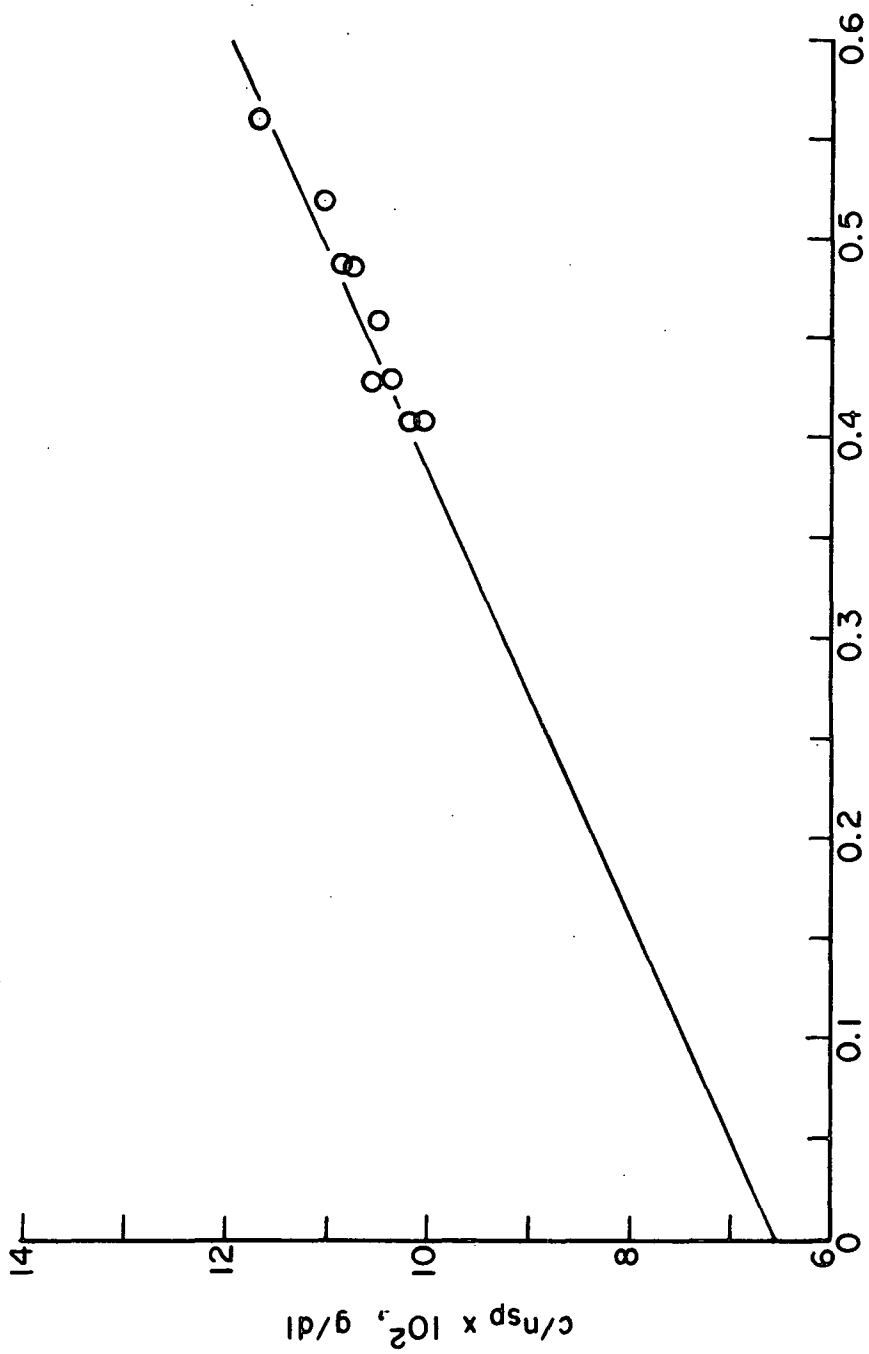

Figure 42. c/η_{sp} Versus $c^{1/2}$, Fraction F_2-7 in 5×10^{-4} M NaCl at 25.00 ± 0.01°C

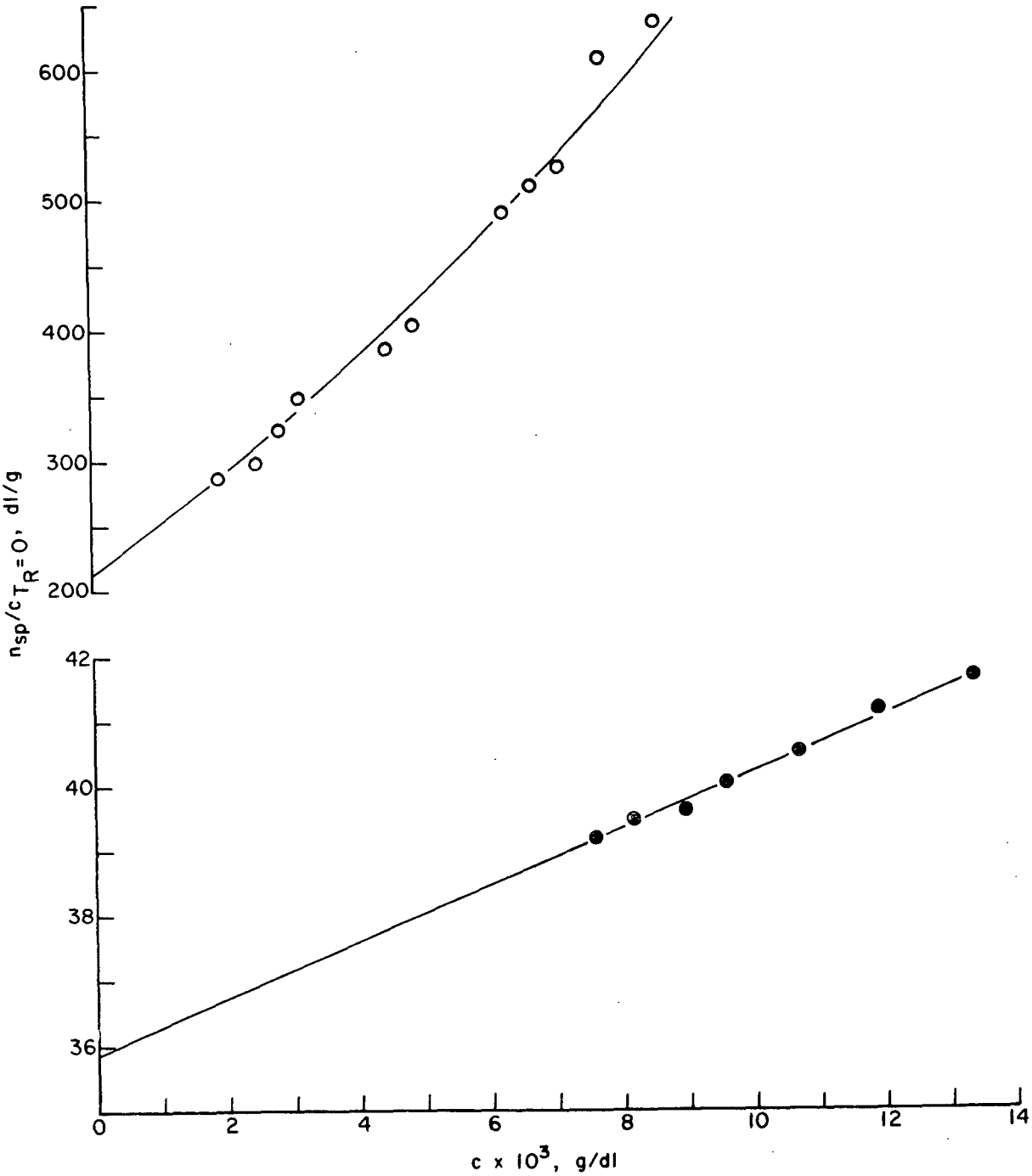

Figure 43. $\underline{\eta}_{sp}/\underline{c}$ Versus $\underline{T}_R$, Fraction F_1-6 in 5×10^{-4} M NaCl (Open Circles) and 10^{-2} M NaCl (Solid Circles) at 25.00 ± 0.01°C. Polymer Concentration 0.013%

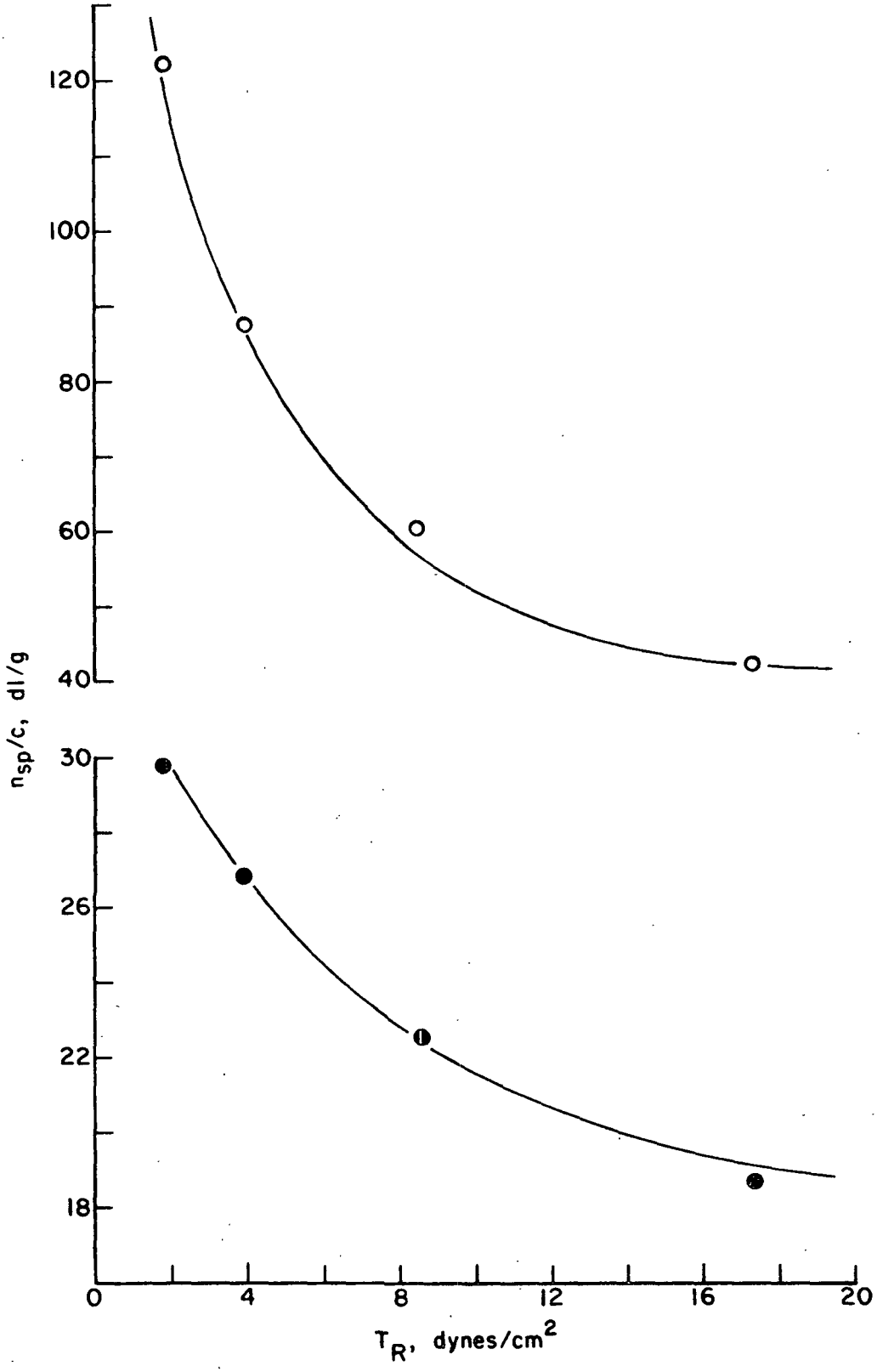

Figure 44. $\underline{c}/\underline{n}_{sp}$ Versus $\underline{T}_R^{1/2}$, Fraction F_1-6 in $5 \times 10^{-4}\underline{M}$ NaCl (Open Circles) and $10^{-2}\underline{M}$ NaCl (Solid Circles) at $25.00 \pm 0.01^{\circ}$C. Polymer Concentration 0.013%

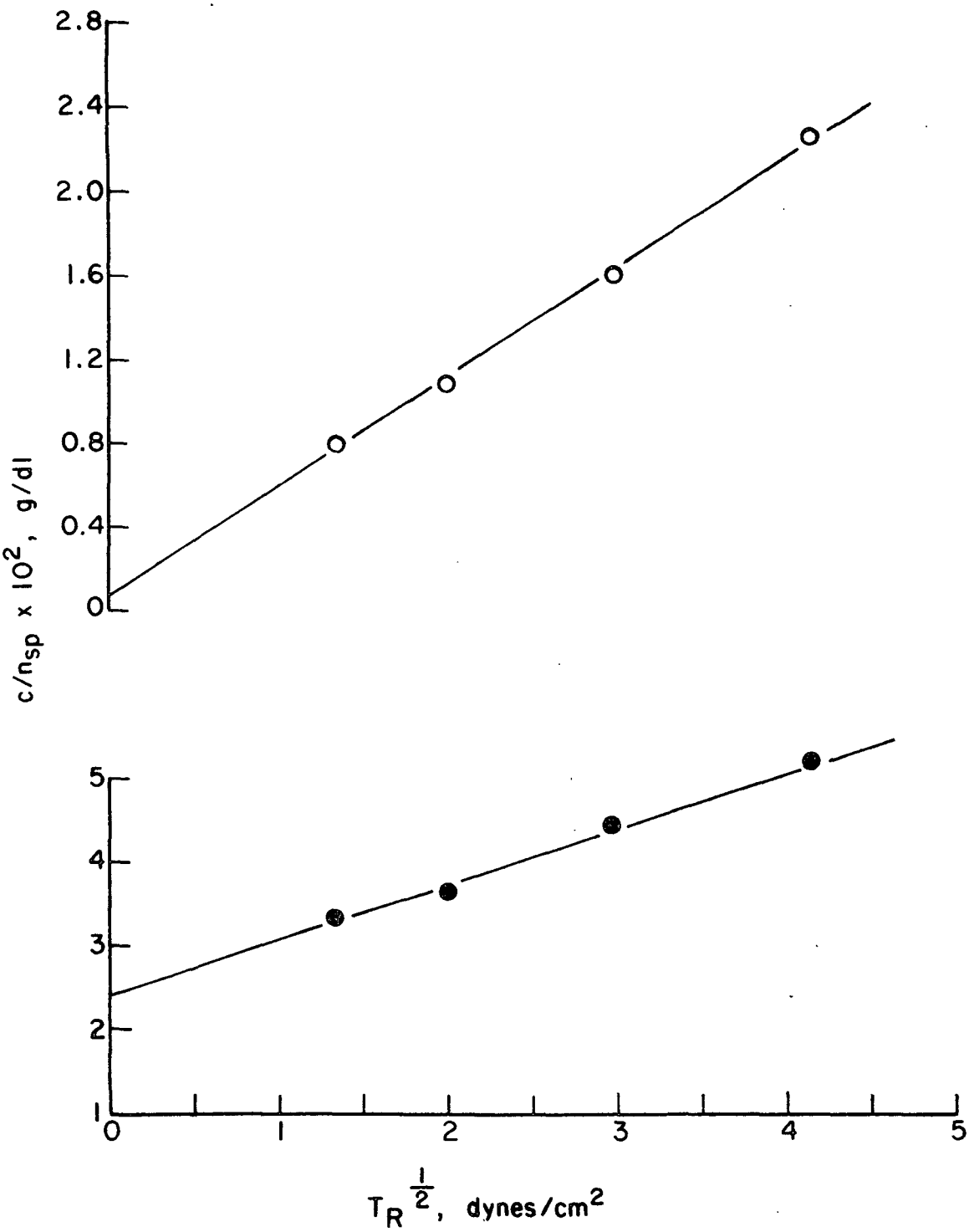

Figure 45. Viscosity as a Function of Concentration, Fraction F_1-6 in 5×10^{-4} M NaCl (Open Circles) and 10^{-2} M NaCl (Solid Circles) at 25.00 ± 0.01°C

TABLE XXX

VISCOSITY DATA FOR F_1-6 IN 5×10^{-4} M NaCl

pH	Concentration, %	Reduced Viscosity, $(\eta_{sp}/c)_{T_R=0}$, dl/g	Intrinsic Viscosity, $[\eta]$, dl/g
6.0	0.0098	700.0	215.0
	0.0086	635.0	
	0.0078	610.0	
	0.0072	525.0	
	0.0067	510.0	
	0.0063	490.0	
	0.0049	405.0	
	0.0045	385.0	
	0.0032	350.0	
	0.0028	325.0	
	0.0025	300.0	
	0.0019	277.0	

TABLE XXXI

VISCOSITY DATA FOR F_1-6 IN 10^{-2} M NaCl

pH	Concentration, %	Reduced Viscosity, $(\eta_{sp}/c)_{T_R=0}$, dl/g	Intrinsic Viscosity, $[\eta]$, dl/g
6.0	0.0134	41.60	35.85
	0.0118	41.10	
	0.0107	40.50	
	0.0096	40.00	
	0.0089	39.60	
	0.0082	39.45	
	0.0076	38.70	

TABLE XXXII

VISCOSITY DATA FOR F_2-7 IN 10^{-2}M NaCl

pH	Concentration, %	Reduced Viscosity, (η_{sp}/c), dl/g	Intrinsic Viscosity, $[\eta]$, dl/g
6.0	0.506	3.40	3.07
	0.405	3.31	
	0.338	3.29	
	0.289	3.25	
	0.253	3.20	
	0.225	3.24	
6.0	0.506	3.42	3.13
	0.405	3.38	
	0.338	3.35	
	0.289	3.32	
	0.253	3.28	
	0.225	3.24	

TABLE XXXIII

VISCOSITY DATA FOR F_2-7 IN 5×10^{-4}M NaCl

pH	Concentration, %	Reduced Viscosity, (η_{sp}/c), dl/g	Intrinsic Viscosity, $[\eta]$, dl/g
6.0	0.313	8.56	16.04
	0.268	9.05	
	0.235	9.20	
	0.209	9.48	
	0.188	9.63	
	0.171	9.84	
6.0	0.315	8.54	14.52
	0.270	9.04	
	0.236	9.28	
	0.189	9.42	
	0.172	9.73	

The intrinsic viscosity increases as the concentration of the added salt decreases. The increase in intrinsic viscosity is caused by an increase in the radius of gyration of the polyion with decreasing concentration of added salt. Many theories have been published on the expansion of polyions due to electrostatic repulsion among fixed polymer charges. In brief, as the salt concentration increases, the fixed charges become shielded from each other by the additional byions. The repulsion between the fixed charges is less, resulting in a more compact configuration.

By determining the viscosity of a polymer in solution under various conditions, one can relate the viscosity and molecular weight of a polymer to its molecular dimensions under these same conditions. One relationship between the intrinsic viscosity and the size of a polymer molecule in solution is the well known Einstein-Stokes equation (88):

$$\eta = 2.5(N/M)(4/3)R_e^3, \qquad (25)$$

where N = Avogadro's number

M = molecular weight

R_e = hydrodynamic molecular radius

This model assumes that the polymer molecule acts essentially as an impermeable sphere. A more correct assumption would be to introduce an equivalent hydrodynamic sphere to represent the polymer molecule. The density of the polymeric material in solution is greatest at the center of mass and decreases with distance away from it. Solvent which lies at the center of mass is "trapped" and is forced to travel with the velocity of the polymer molecule. Solvent which lies further away from the center of mass will become progressively less restricted until it is free to travel at its own velocity. This concept is

applicable to flexible coils as well as rigid macroions. From the work of Kirkwood and Riseman (89) the following equation is proposed:

$$R_e/R_G = 0.875 = \varepsilon \qquad (26)$$

Tanford (82) is in agreement with this concept; however he believes that the value of the parameter ε lies between 0.775 and 0.875. Table XXXIV gives the calculated radius of gyration using an ε of 0.875. The relative expansion factor is defined here as the ratio of the radius of gyration of a fraction in the weak salt solution to that in the strong salt solution.

TABLE XXXIV

RADIUS OF GYRATION FROM INTRINSIC VISCOSITY DATA
BASED ON POLYMER MOLECULAR WEIGHTS OF 1×10^6 AND 3.3×10^4

Fraction	Solvent, M NaCl	R_G, A	Relative Expansion Factor
F_1-6	5×10^{-4}	1730	1.82
	10^{-2}	950	
F_2-7	5×10^{-4}	220	1.69
	10^{-2}	130	

It is noted that the relative expansion factors are approximately the same, even though there is a large difference in molecular weight. This is in accordance with theoretical predictions and experimental results. Theoretically, Morawetz (90) predicts the same expansion factor for chains of different length, as long as the density on ionized groups along the chain is kept constant. The experimental data of Arnold and Overbeek reinforce this prediction (91).

MOLECULAR SIZE

Table XXXV summarizes the experimental data and theoretical predictions on the molecular size of poly(DMVPB) in solution. For a rigid rod the radius of gyration is theoretically equal to $1/\sqrt{12}$ the length (here the contour length of the polymer chain).

TABLE XXXV

RADIUS OF GYRATION OF POLY(DMVPB) IN SOLUTION
BASED ON POLYMER MOLECULAR WEIGHTS OF 1×10^6 AND 3.3×10^4

Technique	Fraction	Solvent, M NaCl	R_G, A
Theoretical, based on			
rigid rod configuration	F_1-6		3580
random coil configuration	F_1-6		100
Light scattering	F_1-6	5×10^{-4}	2760
Viscosity	F_1-6	5×10^{-4}	1730
Light scattering	F_1-6	10^{-2}	1300
Viscosity	F_1-6	10^{-2}	950
Diffusion	F_1-6	10^{-2}	390
Theoretical, based on			
rigid rod configuration	F_2-7		110
random coil configuration	F_2-7		16
Viscosity	F_2-7	5×10^{-4}	220
Viscosity	F_2-7	10^{-2}	130
Diffusion	F_2-7	10^{-2}	140

The molecular size determined from light scattering data will be considered the more valid. Light scattering is a physical measurement of the dimensions of a macromolecule without any assumption regarding its general form (rod, ellipsoid, random coil, etc.). With both viscosity and diffusion data,

it is necessary to postulate a molecular configuration when calculating molecular size.

In general, the radii of gyration are in good agreement considering the various assumptions made in calculating the molecular size from the various techniques. A comparison between the theoretical predictions and the actual experimental findings indicates that the polymer in solution behaves more like a stiff rod rather than a random coil. The electrostatic repulsion between the polyelectrolyte's fixed charges is responsible for the expanded configuration. It can also be noted that the lower molecular weight polymer acts as a "stiffer" particle than the higher molecular weight polymer. This observation is consistent with the findings of Koleske (92) and other workers (93,94).

APPENDIX III

ADSORPTION DATA

Table XXXVI lists the kinetic data of the adsorption of poly(DMVPB) on PSL. The poly(DMVPB) concentration, $\underline{C}_o$, is 0.44 mg/liter in all cases. $\underline{Ce}$ is equal to $\underline{C}_o$ minus $\underline{C}_*$, the amount of polymer adsorbed. The concentration of PSL particle size 0.794 μm is 260 mg/liter. The reaction temperature is 25.0 ± 0.1°C and the agitation rate is 5.5 rpm.

TABLE XXXVI

ADSORPTION CHARACTERISTICS OF POLY(DMVPB)

$\underline{C}_o$, mg/liter	$\underline{C}_*$, mg/liter	$\underline{Ce}$, mg/liter	Time, min
0.44	--	0.44	0
	0.36	0.08	6
	0.35	0.09	18
	0.39	0.05	30
	0.38	0.06	60
	0.38	0.06	86
	0.38	0.06	356
	0.38	0.06	1056

APPENDIX IV

ADSORPTION AND FLOCCULATION DATA

The following tables (XXXVII-XXXVIII) contain the adsorption and flocculation data for the poly(DMVPB)-water-PSL system studied under various experimental conditions. Constant agitation temperature and pH are maintained. The turbidity data were taken after one and one-half hours adsorption time, zeta potentials after two hours, and adsorption data after four hours. The symbols have the same meaning as in the text; $\underline{C}_o$ is the initial poly(DMVPB) and $\underline{C}_*$ is the poly(DMVPB) concentration adsorbed.

TABLE XXXVII

ADSORPTION AND FLOCCULATION DATA FOR CONSTANT SURFACE AREA DATA ($0.0445\ m^2$)

$\underline{M}_w$: 10^6
$\underline{NaCl}$: $10^{-2}\underline{M}$
Particle Size: 1.101 μm
PSL Concentration: 341 mg/liter

$\underline{C}_o$, mg/liter	$\underline{C}_*$, mg/liter	Relative Turbidity, %[a]	Zeta Potential, mv
0.0018	0.0018	89	-58
0.0037	0.0037	89	-54
0.0184	0.0184	89	-48
0.0263	0.0263	63	
0.0307	0.0307	49	-43
0.0368	0.0368	15	
0.0920	0.0920	7	
0.1840	0.1840	6	
0.2400	0.2400	5	-16
0.3200	0.3200	11	+19
0.4000	0.3600	31	+29
1.2400	0.8500	70	+48
1.5800	0.9000	72	
2.0600	1.0000	73	
6.8300	1.2700	78	
10.2200	1.3600	78	+48
20.9200	1.5000	78	+48

[a]Turbidity of PSL solution with polymer/turbidity of PSL solution without polymer.

TABLE XXXVII (Continued)

ADSORPTION AND FLOCCULATION DATA FOR CONSTANT SURFACE AREA DATA
($0.0445\ m^2$)

$\underline{M}_w$: 3.3×10^4
$\underline{NaCl}$: $10^{-2}\underline{M}$
Particle Size: 1.101 μm
PSL Concentration: 341 mg/liter

$\underline{C}_o$, mg/liter	$\underline{C}_*$, mg/liter	Relative Turbidity, %	Zeta Potential, mv
0.0018	0.0018	88	-54
0.0037	0.0037	89	
0.0184	0.0184	88	
0.0368	0.0368	88	
0.0460	0.0460	89	
0.0580	0.0580	87	
0.0920	0.0920	51	-35
0.1227	0.1227	20	
0.1840	0.1840	17	-15
0.2500	0.2500	13	-13
0.3300	0.3300	39	+14
0.4100	0.3700	65	+23
1.2400	0.9600	85	+45
1.6500	1.0000	90	
2.0600	1.0300	93	
2.4500	1.0600	92	
3.2700	1.1400	92	+48
4.0900	1.1900	92	
6.8700	1.3200	92	
12.5900	1.4100	92	
16.7800	1.4400	92	
20.9800	1.4700	92	+48

TABLE XXXVII (Continued)

ADSORPTION AND FLOCCULATION DATA FOR CONSTANT SURFACE AREA DATA
($0.0445\ m^2$)

M_w: 10^6
NaCl: $5 \times 10^{-4} M$
Particle Size: 1.101 μm
PSL Concentration: 341 mg/liter

C_o, mg/liter	C_*, mg/liter	Relative Turbidity, %	Zeta Potential, mv
0.0019	0.0019	87	-54
0.0038	0.0038	87	
0.0192	0.0192	89	
0.0213	0.0213	89	
0.0240	0.0240	90	
0.0274	0.0274	90	-50
0.0320	0.0320	88	
0.0384	0.0384	81	
0.0480	0.0480	75	-43
0.0960	0.0960	9	-27
0.1920	0.1920	7	-24
0.2500	0.2500	10	-15
0.3300	0.3300	45	+12
0.4100	0.3700	68	
1.2700	0.6600	82	+30
2.1100	0.7300	85	+62
4.1700	0.8700	85	
6.8100	1.0200	85	
11.8980	1.1500	85	
19.830	1.2200	85	+62

TABLE XXXVII (Continued)

ADSORPTION AND FLOCCULATION DATA FOR CONSTANT SURFACE AREA DATA
($0.0445\ m^2$)

$\underline{M}_w$: 3.3×10^4
NaCl: $5 \times 10^{-4}\underline{M}$
Particle Size: 1.101 μm
PSL Concentration: 341 mg/liter

$\underline{C}_o$, mg/liter	$\underline{C}_*$, mg/liter	Relative Turbidity, %	Zeta Potential, mv
0.0033	0.0033	87	-62
0.0066	0.0066	90	
0.0332	0.0332	90	
0.0664	0.0664	87	-51
0.1328	0.1328	87	-30
0.1660	0.1660	61	
0.2320	0.2320	61	
0.2990	0.2990	71	≈0
0.3987	0.3400	78	+22
0.4984	0.4200	85	
1.0200	0.8200	95	+25
2.0400	1.0400	95	
4.0000	1.1200	95	+54
6.5400	1.2800	95	+54
9.8100	1.3500	95	
19.6200	1.3800	95	+54

TABLE XXXVII (Continued)

ADSORPTION AND FLOCCULATION DATA FOR CONSTANT SURFACE AREA DATA
($0.0445\ m^2$)

$\underline{M}_w$: 10^6
NaCl: $10^{-2}\underline{M}$
Particle Size: 0.794 μm
PSL Concentration: 245 mg/liter

$\underline{C}_o$, mg/liter	$\underline{C}_*$, mg/liter	Relative Turbidity, %	Zeta Potential, mv
0.0159	0.0159	93	
0.0175	0.0175	86	
0.0194	0.0194	86	-54
0.0219	0.0219	87	
0.0250	0.0250	84	-48
0.0291	0.0291	74	
0.0350	0.0350	44	-43
0.0437	0.0437	40	
0.0583	0.0583	21	-33
0.0874	0.0874	12	
0.1748	0.1748	8	-23
0.2280	0.2280	9	-17
0.3040	0.2700	15	+10
0.4000		48	
1.0300	0.8300	93	+43
4.0800	0.9500	90	+45
6.8300	1.1000	92	+48
10.2400	1.2700	92	+48
20.4800	1.3300	92	+48

TABLE XXXVII (Continued)

ADSORPTION AND FLOCCULATION DATA FOR CONSTANT SURFACE AREA DATA
($0.0445\ m^2$)

$\underline{M}_w$: 3.3×10^4
NaCl: $10^{-2}\underline{M}$
Particle Size: 0.794 μm
PSL Concentration: 245 mg/liter

$\underline{C}_o$, mg/liter	$\underline{C}_*$, mg/liter	Relative Turbidity, %	Zeta Potential, mv
0.0159	0.0159	88	-51
0.0175	0.0175	87	
0.0194	0.0194	87	
0.0219	0.0219	87	
0.0250	0.0250	87	-48
0.0291	0.0291	88	
0.0350	0.0350	89	
0.0437	0.0437	88	
0.0583	0.0583	84	
0.0874	0.0874	69	
0.1748	0.1748	18	-26
0.2417	0.2417	15	≈0
0.3222	0.2900	35	+13
0.4028		73	+29
1.0000	0.8000	95	+43
2.0000	0.9000	97	+45
4.0101	1.2300	97	+48
6.8700	1.3600	96	+48
20.6000	1.3600	96	+48

TABLE XXXVII (Continued)

ADSORPTION AND FLOCCULATION DATA FOR CONSTANT SURFACE AREA DATA
($0.0445\ m^2$)

$\underline{M}_w$: 10^6
NaCl: 5×10^{-4} M
Particle Size: 0.794 μm
PSL Concentration: 245 mg/liter

C_o, mg/liter	C_*, mg/liter	Relative Turbidity, %	Zeta Potential, mv
0.0166	0.0166	94	
0.0182	0.0182	93	
0.0203	0.0203	91	-62
0.0228	0.0228	92	
0.0260	0.0260	93	-58
0.0302	0.0302	94	
0.0365	0.0365	74	-54
0.0456	0.0456	40	
0.0608	0.0608	30	-48
0.0912	0.0912	14	
0.1824	0.1824	14	-25
0.2348	0.2348	20	≈0
0.3131	0.2800	61	+30
0.3914		70	+41
1.0300	0.7000	84	+54
2.0600	0.7600	89	+58
4.0700	0.8500	89	+62
6.8100	0.9900	90	+62
10.2100	1.1200	90	+62
20.4200	1.1400	90	+62

TABLE XXXVII (Continued)

ADSORPTION AND FLOCCULATION DATA FOR CONSTANT SURFACE AREA DATA
($0.0445\ m^2$)

$\underline{M}_w$: 3.3×10^4
NaCl: $5 \times 10^{-4}\underline{M}$
Particle Size: 0.794 μm
PSL Concentration: 245 mg/liter

$\underline{C}_o$, mg/liter	$\underline{C}_*$, mg/liter	Relative Turbidity, %	Zeta Potential, mv
0.0287	0.0287	93	-58
0.0315	0.0315	93	
0.0350	0.0350	92	-56
0.0394	0.0394	90	
0.0451	0.0451	92	-54
0.0526	0.0526	92	
0.0631	0.0631	93	-52
0.0789	0.0789	93	-48
0.1051	0.1051	92	-31
0.1200	0.1200	92	-20
0.1577	0.1577	84	+16
0.2213	0.2213	70	+34
0.3154	0.2800	60	
0.3787	0.3100	74	
0.4734		82	+58
1.0200	0.8200	97	+58
2.0400	0.9900	97	+58
4.0000	1.1500	97	
6.5400	1.2000	97	+58
9.8100	1.2900	97	
19.6200	1.3500	97	+58

TABLE XXXVII (Continued)

ADSORPTION AND FLOCCULATION DATA FOR CONSTANT SURFACE AREA DATA
($0.0445\ m^2$)

$\underline{M}_w$: 10^6
NaCl: $10^{-2}\underline{M}$
Particle Size: 0.481 μm
PSL Concentration: 150 mg/liter

$\underline{C}_o$, mg/liter	$\underline{C}_*$, mg/liter	Relative Turbidity, %	Zeta Potential, mv
0.0103	0.0103	89	-45
0.0137	0.0137	89	
0.0206	0.0206	89	-43
0.0249	0.0249	20	
0.0257	0.0257	15	-39
0.1412	0.1412	9	
0.1680	0.1680	20	
0.1820	0.1820	23	
0.2120	0.2120	23	-25
0.3030	0.2700	53	+16
0.4000	0.3400	82	
1.0300	0.7500	88	+37
2.0500	0.9400	87	+45
10.2400	1.2900	88	
20.4800	1.4200	87	+48

TABLE XXXVII (Continued)

ADSORPTION AND FLOCCULATION DATA FOR CONSTANT SURFACE AREA DATA
($0.0445\ m^2$)

$\underline{M}_w$: 3.3×10^4
NaCl: $10^{-2}\underline{M}$
Particle Size: 0.481 μm
PSL Concentration: 150 mg/liter

$\underline{C}_o$, mg/liter	$\underline{C}_*$, mg/liter	Relative Turbidity, %	Zeta Potential, mv
0.0104	0.0104	89	-48
0.0130	0.0130	89	-48
0.0260	0.0260	89	-45
0.0519	0.0519	80	-45
0.0578	0.0578	54	
0.0650	0.0650	23	
0.0743	0.0743	14	-36
0.0984	0.0984	9	-19
0.2800	0.2500	43	+6
0.4000	0.3400	68	+18
1.0000	0.8000	85	+25
2.0000	1.0000	85	
4.0000	1.1700	83	+45
10.3000	1.4500	85	+45
20.6000	1.4300	83	+45

TABLE XXXVII (Continued)

ADSORPTION AND FLOCCULATION DATA FOR CONSTANT SURFACE AREA DATA
($0.0445\ m^2$)

$\underline{M}_w$: 10^6
NaCl: $5 \times 10^{-4}\underline{M}$
Particle Size: 0.481 μm
PSL Concentration: 150 mg/liter

$\underline{C}_o$, mg/liter	$\underline{C}_*$, mg/liter	Relative Turbidity, %	Zeta Potential, mv
0.0100	0.0100	95	-49
0.0149	0.0149	95	
0.0298	0.0298	95	-49
0.0331	0.0331	95	
0.0372	0.0372	80	
0.0425	0.0425	59	
0.0500	0.0500	38	
0.0595	0.0595	22	-42
0.0744	0.0744	12	-30
0.1700	0.1700	16	-21
0.2490	0.2100	54	+15
0.2975		75	+36
0.5950	0.5100	86	
1.0300	0.6300	91	
2.0600	0.7500	91	+54
4.0700	0.9300	90	
6.8100	1.0000	91	+54
10.2100	1.0900	91	
20.4200	1.2600	91	+54

TABLE XXXVII (Continued)

ADSORPTION AND FLOCCULATION DATA FOR CONSTANT SURFACE AREA DATA
($0.0445\ m^2$)

$\underline{M}_w$: 3.3×10^4
NaCl: $5 \times 10^{-4}\underline{M}$
Particle Size: 0.481 μm
PSL Concentration: 150 mg/liter

$\underline{C}_o$, mg/liter	$\underline{C}_*$, mg/liter	Relative Turbidity, %	Zeta Potential, mv
0.0119	0.0119	94	-54
0.0149	0.0149	94	
0.0199	0.0199	95	-49
0.0299	0.0299	95	
0.0598	0.0598	94	
0.0664	0.0664	94	-45
0.0747	0.0747	94	
0.0854	0.0854	95	
0.0996	0.0996	95	
0.1195	0.1195	95	-28
0.1494	0.1494	87	
0.1992	0.1992	48	-19
0.2988	0.2600	73	+25
0.5976		81	+36
1.0200	0.8000	96	+45
2.0400	1.0500	96	
4.0000	1.1700	96	
6.5400	1.2900	96	+45
9.8100	1.3800	96	
19.6200	1.3900	96	+45

TABLE XXXVII (Continued)

ADSORPTION AND FLOCCULATION DATA FOR CONSTANT SURFACE AREA DATA
($0.0445\ m^2$)

$\underline{M}_w$: 10^6
NaCl: $10^{-2}\underline{M}$
Particle Size: 0.330 μm
PSL Concentration: 102 mg/liter

$\underline{C}_o$, mg/liter	$\underline{C}_*$, mg/liter[a]	Relative Turbidity, %	Zeta Potential, mv
0.0167		87	
0.0184		86	
0.0204		85	
0.0263		85	
0.0307		79	
0.0368		72	
0.0460		68	
0.0613		42	
0.0920		35	
0.1227		30	-30.0
0.1415		25	-29.0
0.1840		14	-15.0
0.2000		14	+10.0
0.2353		22	+26.0
0.2667		39	
0.4000		73	
0.5250		73	+39.0
0.7000		75	
1.0500		86	

[a]Adsorption not measured.

TABLE XXXVII (Continued)

ADSORPTION AND FLOCCULATION DATA FOR CONSTANT SURFACE AREA DATA
($0.0445\ m^2$)

$\underline{M}_w$: 3.3×10^4
NaCl: 5×10^{-4} M
Particle Size: 0.330 μm
PSL Concentration: 102 mg/liter

C_o, mg/liter	C_*, mg/liter[a]	Relative Turbidity, %	Zeta Potential, mv
0.0204		83	
0.0263		86	
0.0368		84	
0.0460		86	
0.0613		75	
0.0920		36	
0.1082		37	
0.1227		17	
0.1840		12	-20.0
0.2494		38	+10.0
0.2830		68	+19.0
0.4240		73	+36.0
0.5250		77	+45.0
0.7000		75	
1.0500		82	

[a]Adsorption not measured.

TABLE XXXVII (Continued)

ADSORPTION AND FLOCCULATION DATA FOR CONSTANT SURFACE AREA DATA
($0.0445\ m^2$)

$\underline{M}_w$: 10^6
NaCl: 5×10^{-4} M
Particle Size: 0.330 μm
PSL Concentration: 102 mg/liter

$\underline{C}_o$, mg/liter	$\underline{C}_*$, mg/liter[a]	Relative Turbidity, %	Zeta Potential, mv
0.0287		88	
0.0344		87	
0.0430		81	
0.0491		75	
0.0860		47	
0.1157		28	-27.0
0.1720		23	0
0.2000		81	+29.0
0.4000		84	
0.4666		88	
0.5250		88	
1.0500		95	

[a] Adsorption not measured.

TABLE XXXVII (Continued)

ADSORPTION AND FLOCCULATION DATA FOR CONSTANT SURFACE AREA DATA
($0.0445\ m^2$)

$\underline{M}_w$: 3.3×10^4
NaCl: 5×10^{-4} M
Particle Size: 0.330 μm
PSL Concentration: 102 mg/liter

C_o, mg/liter	C_*, mg/liter[a]	Relative Turbidity, %	Zeta Potential, mv
0.0560		88	
0.0840		88	
0.1120		87	
0.1292		45	
0.1527		37	
0.1680		43	-20.0
0.2000		76	-14.0
0.2350		74	+19.0
0.2666		89	
0.5200		94	
0.6800		92	
1.0500		94	+42.0

[a] Adsorption not measured.

TABLE XXXVII (Continued)

ADSORPTION AND FLOCCULATION DATA FOR CONSTANT SURFACE AREA DATA
($0.0445\ m^2$)

$\underline{M}_w$: 10^6
NaCl: $10^{-2}\underline{M}$
Particle Size: 0.234 μm
PSL Concentration: 73 mg/liter

$\underline{C}_o$, mg/liter	$\underline{C}_*$, mg/liter	Relative Turbidity, %	Zeta Potential, mv
0.0179	0.0179	81	-43
0.0205	0.0205	80	
0.0239	0.0239	76	
0.0287	0.0287	69	-39
0.0359	0.0359	41	
0.0478	0.0478	27	
0.0718	0.0718	24	-27
0.1435	0.1435	12	-16
0.1872	0.1600	27	+6
0.2496	0.2200	71	+28
0.3120	0.2500	74	
1.0200	0.7000	80	
2.0400	0.9000	85	+41
4.0800	1.0700	97	
6.6000	1.2100	97	+45
9.9000	1.4400	97	
19.8000	1.5000	97	+45

TABLE XXXVII (Continued)

ADSORPTION AND FLOCCULATION DATA FOR CONSTANT SURFACE AREA DATA
($0.0445\ m^2$)

$\underline{M}_w$: 3.3×10^4
NaCl: $10^{-2}\underline{M}$
Particle Size: 0.234 μm
PSL Concentration: 73 mg/liter

$\underline{C}_o$, mg/liter	$\underline{C}_*$, mg/liter	Relative Turbidity, %	Zeta Potential, mv
0.0239	0.0239	82	-41
0.0287	0.0287	81	
0.0359	0.0359	81	
0.0478	0.0478	42	-37
0.0718	0.0718	16	
0.1435	0.1435	29	-10
0.1984	0.1700	57	+31
0.2675	0.2400	70	
0.3307	0.3000	75	+35
1.0000	0.7000	86	
2.0000	0.9200	86	+41
4.0100	1.0700	86	+43
6.7900	1.1400	86	+45
10.1800	1.2800	86	
20.3600	1.3500	86	+45

TABLE XXXVII (Continued)

ADSORPTION AND FLOCCULATION DATA FOR CONSTANT SURFACE AREA DATA
($0.0445\ m^2$)

$\underline{M}_w$: 10^6
NaCl: $5 \times 10^{-4}\underline{M}$
Particle Size: 0.234 μm
PSL Concentration: 73 mg/liter

$\underline{C}_o$, mg/liter	$\underline{C}_*$, mg/liter	Relative Turbidity, %	Zeta Potential, mv
0.0213	0.0213	95	-45
0.0240	0.0240	95	
0.0274	0.0274	97	
0.0320	0.0320	95	
0.0384	0.0384	70	-43
0.0480	0.0480	17	-37
0.0640	0.0640	12	
0.0960	0.0960	15	-29
0.1920	0.1600	65	+24
0.2472	0.2200	69	+29
0.3296	0.2900	81	
0.4120	0.3500	84	+43
1.0300	0.5500	84	
2.0600	0.7700	89	+51
4.0600	0.9200	89	+58
6.7500	1.0500	94	+58
10.1300	1.1000	94	+58
20.2600	1.1700	94	+58

TABLE XXXVII (Continued)

ADSORPTION AND FLOCCULATION DATA FOR CONSTANT SURFACE AREA DATA
($0.0445\ m^2$)

$\underline{M_w}$: 3.3×10^4
$\underline{NaCl}$: $5 \times 10^{-4}\underline{M}$
Particle Size: 0.234 μm
PSL Concentration: 73 mg/liter

$\underline{C_o}$, mg/liter	$\underline{C_*}$, mg/liter	Relative Turbidity, %	Zeta Potential, mv
0.0553	0.0553	97	
0.0664	0.0664	95	-30
0.0830	0.0830	96	
0.1106	0.1106	76	
0.1660	0.1660	46	-11
0.2320	0.2000	61	+7
0.2987	0.2700	67	+15
0.4984	0.4300	77	+30
1.0200	0.7700	77	+35
2.0400	1.0000	77	
4.0000	1.1200	82	+39
6.5400	1.2100	99	
9.8100	1.2600	99	+41
19.6200	1.3200	99	+43

TABLE XXXVII (Continued)

ADSORPTION AND FLOCCULATION DATA FOR CONSTANT SURFACE AREA DATA
($0.0445\ m^2$)

$\underline{M}_w$: 10^6
NaCl: $10^{-2}\underline{M}$
Particle Size: 0.109 μm
PSL Concentration: 34 mg/liter

$\underline{C}_o$, mg/liter	$\underline{C}_*$, mg/liter	Relative Turbidity, %	Zeta Potential, mv
0.0015	0.0015	77	
0.0029	0.0029	78	-35
0.0134	0.0134	78	-33
0.0210	0.0210	75	
0.0245	0.0245	22	
0.0491	0.0491	19	-31
0.0736	0.0736	11	-22
0.1472	0.1200	10	+6
0.1920	0.1600	19	
0.2560	0.2260	96	+34
0.3200	0.2900	99	
1.0200	0.6700	99	+39
2.0400	0.9200	98	+41
4.0000	1.1000	98	
6.6000	1.2000	98	+41
9.9000	1.3500	98	
19.8000	1.4300	98	+41

TABLE XXXVII (Continued)

ADSORPTION AND FLOCCULATION DATA FOR CONSTANT SURFACE AREA DATA
($0.0445\ m^2$)

$\underline{M}_w$: 3.3×10^4
NaCl: $10^{-2}\underline{M}$
Particle Size: 0.109 μm
PSL Concentration: 34 mg/liter

$\underline{C}_o$, mg/liter	$\underline{C}_*$, mg/liter	Relative Turbidity, %	Zeta Potential, mv
0.0184	0.0184	77	
0.0210	0.0210	79	-31
0.0245	0.0245	77	
0.0294	0.0294	77	-26
0.0335	0.0335	79	
0.0368	0.0368	25	
0.0491	0.0491	19	
0.0736	0.0736	12	-15
0.1472	0.1200	16	+6
0.2045	0.1700	82	+23
0.2713	0.2400	83	
0.3392	0.3100	93	+36
1.0000	0.7300	93	+43
2.0000	0.8800	93	
4.0100	1.0500	92	
6.7900	1.1900	92	
10.1800	1.3100	92	
20.3600	1.3700	92	+43

TABLE XXXVII (Continued)

ADSORPTION AND FLOCCULATION DATA FOR CONSTANT SURFACE AREA DATA
($0.0445\ m^2$)

$\underline{M}_w$: 10^6
NaCl: $5 \times 10^{-4}\underline{M}$
Particle Size: 0.109 μm
PSL Concentration: 34 mg/liter

$\underline{C}_o$, mg/liter	$\underline{C}_*$, mg/liter	Relative Turbidity, %	Zeta Potential, mv
0.0240	0.0240	94	
0.0274	0.0274	96	-29
0.0320	0.0320	98	
0.0384	0.0384	82	-27
0.0480	0.0480	71	
0.0640	0.0640	27	-23
0.0960	0.0960	16	-19
0.1920	0.1600	74	+21
0.2472	0.2100	91	
0.3296	0.2900	95	+26
0.4120	0.3500	95	+32
1.0300	0.5500	94	+37
2.0600	0.7000	94	
4.0600	0.8800	94	+37
6.7500	1.0000	94	+37
10.1300	1.1300	95	
20.2600	1.2400	94	+37

TABLE XXXVII (Continued)

ADSORPTION AND FLOCCULATION DATA FOR CONSTANT SURFACE AREA DATA
($0.0445\ m^2$)

$\underline{M}_w$: 3.3×10^4
NaCl: 5×10^{-4} M
Particle Size: 0.109 μm
PSL Concentration: 34 mg/liter

C_o, mg/liter	C_*, mg/liter	Relative Turbidity, %	Zeta Potential, mv
0.0474	0.0474	94	-28
0.0553	0.0553	93	
0.0664	0.0664	94	-29
0.0830	0.0830	94	
0.0930	0.0930	80	
0.1106	0.1106	45	-24
0.1660	0.1300	67	
0.3320	0.3000	86	+21
0.3987	0.3700	92	
0.4984	0.4400	93	+24
1.0200	0.8200	94	
2.0400	1.0500	94	
4.0000	1.1400	94	+35
6.5400	1.1900	94	+37
9.8100	1.2300	94	+39
19.6200	1.3200	94	+39

TABLE XXXVIII

ADSORPTION AND FLOCCULATION DATA FOR CONSTANT PARTICLE EXPERIMENT

$\underline{M}_w$: 10^6
NaCl: $10^{-2}\underline{M}$
Particle Size: 1.101 μm
PSL Concentration: 1796 mg/liter

$\underline{C}_o$, mg/liter	$\underline{C}_*$, mg/liter	Relative Turbidity, %	Zeta Potential, mv
0.0307	0.0307	91	
0.0460	0.0460	90	-58
0.0613	0.0613	89	
0.0920	0.0920	90	-48
0.0968	0.0968	90	
0.1082	0.1082	88	-45
0.1234	0.1234	88	
0.1415	0.1415	51	-38
0.1840	0.1840	32	
0.4000	0.4000	16	-28
1.0520	1.0520	9	
1.4100	1.4100	8	-16
1.6185	1.6185	26	≈0
2.1040	1.9040	29	+26
4.0960	2.9100	51	
10.2550	3.8750	66	
16.4080	4.2680	88	+37
20.5100	5.0700	92	
40.6800	6.1200	98	+48

TABLE XXXVIII (Continued)

ADSORPTION AND FLOCCULATION DATA FOR CONSTANT PARTICLE EXPERIMENT

$\underline{M}_w$: 3.3×10^4
NaCl: $10^{-2}\underline{M}$
Particle Size: 1.101 μm
PSL Concentration: 1796 mg/liter

$\underline{C}_o$, mg/liter	$\underline{C}_*$, mg/liter	Relative Turbidity, %	Zeta Potential, mv
0.1840	0.1840	91	-39
0.2544	0.2544	87	
0.3028	0.3028	83	-29
0.3392	0.3392	87	
0.3816	0.3816	54	-28
0.4240	0.4240	25	
1.2576	1.2576	9	-24
1.4971	1.4971	12	≈0
1.8864	1.7886	42	
2.0960	1.8560	65	+33
4.1040	3.4440	91	
10.3000	4.0400	92	+41
16.4800	4.6900	93	
20.6000	5.6000	90	
41.4800	6.4400	91	+51

TABLE XXXVIII (Continued)

ADSORPTION AND FLOCCULATION DATA FOR CONSTANT PARTICLE EXPERIMENT

$\underline{M}_w$: 10^6
NaCl: $5 \times 10^{-4}\underline{M}$
Particle Size: 1.101 μm
PSL Concentration: 1796 mg/liter

$\underline{C}_o$, mg/liter	$\underline{C}_*$, mg/liter	Relative Turbidity, %	Zeta Potential, mv
0.1000	0.1000	91	-63
0.1330	0.1330	91	
0.1538	0.1538	91	
0.2000	0.2000	31	-58
0.3200	0.3200	11	
0.4000	0.4000	5	-51
1.2360	1.2360	7	
1.3802	1.3802	9	-37
1.5848	1.5848	5	-37
2.0600	1.7500	19	+40
4.0700	2.4500	20	
10.2100	3.2000	62	+58
16.3400	3.6900	72	
20.4200	4.2900	84	+68
43.3400	4.8100	86	+68

TABLE XXXVIII (Continued)

ADSORPTION AND FLOCCULATION DATA FOR CONSTANT PARTICLE EXPERIMENT

$\underline{M}_w$: 3.3×10^4
NaCl: 5×10^{-4} M
Particle Size: 1.101 μm
PSL Concentration: 1796 mg/liter

$\underline{C}_o$, mg/liter	$\underline{C}_*$, mg/liter	Relative Turbidity, %	Zeta Potential, mv
0.3320	0.3320	89	
0.5000	0.5000	88	-48
0.6834	0.6834	89	
0.8160	0.8160	50	-35
1.0200	1.0200	73	
1.2240	1.2240	87	-28
1.3668	1.3668	83	-16
1.6320	1.6000	93	+24
2.0400	1.9400	87	
4.0000	3.1700	93	+34
9.8120	4.6000	96	
19.6240	5.3200	99	+51
34.6400	6.1000	97	
43.3000	6.3500	93	+54

TABLE XXXVIII (Continued)

ADSORPTION AND FLOCCULATION DATA FOR CONSTANT PARTICLE EXPERIMENT

$\underline{M}_w$: 10^6
$\underline{NaCl}$: $10^{-2}\underline{M}$
Particle Size: 0.794 μm
PSL Concentration: 677 mg/liter

$\underline{C}_o$, mg/liter	$\underline{C}_*$, mg/liter	Relative Turbidity, %	Zeta Potential, mv
0.0368	0.0368	89	
0.0613	0.0613	93	-48
0.0657	0.0657	93	
0.0708	0.0708	82	-48
0.0767	0.0767	70	
0.0836	0.0836	48	-43
0.4000	0.4000	13	-27
0.5130	0.5130	11	
0.5857	0.5857	20	
0.6833	0.6500	33	≈0
0.8200		45	+36
1.0300		54	
2.0500	1.0800	65	+45
4.0800	1.5700	79	
16.3800	1.7700	93	+48
20.4800	2.2500	96	+48
40.6900	3.1300	96	+48

TABLE XXXVIII (Continued)

ADSORPTION AND FLOCCULATION DATA FOR CONSTANT PARTICLE EXPERIMENT

$\underline{M}_w$: 3.3×10^4
NaCl: $10^{-2}\underline{M}$
Particle Size: 0.794 μm
PSL Concentration: 677 mg/liter

$\underline{C}_o$, mg/liter	$\underline{C}_*$, mg/liter	Relative Turbidity, %	Zeta Potential, mv
0.1325	0.1325	89	-48
0.1433	0.1433	82	
0.1720	0.1720	16	-45
0.2400	0.2400	8	
0.3200	0.3200	9	-45
0.4000	0.4000	7	-29
0.6667	0.6667	14	-21
1.0000	0.9000	67	+20
1.6000	1.3200	79	+30
2.0000	1.3900	80	
4.0100	1.6000	85	
10.3000	1.8300	89	+45
20.6000	2.5500	87	
41.4800	3.3100	88	+51

TABLE XXXVIII (Continued)

ADSORPTION AND FLOCCULATION DATA FOR CONSTANT PARTICLE EXPERIMENT

$\underline{M}_w$: 10^6
NaCl: 5×10^{-4} M
Particle Size: 0.794 μm
PSL Concentration: 677 mg/liter

$\underline{C}_o$, mg/liter	$\underline{C}_*$, mg/liter	Relative Turbidity, %	Zeta Potential, mv
0.0508	0.0508	87	
0.0664	0.0664	87	
0.0800	0.0800	87	
0.0886	0.0886	26	-48
0.1020	0.1020	19	
0.1133	0.1133	9	
0.1457	0.1457	9	-37
0.1700	0.1700	8	
0.2040	0.2040	5	-35
0.4000	0.4000	31	-34
0.5025	0.5025	34	-16
0.7000	0.6500	51	+26
1.0500	0.8100	59	
10.2100	1.5500	76	+51
20.4200	2.1000	79	+54
43.5400	2.5700	93	+62

TABLE XXXVIII (Continued)

ADSORPTION AND FLOCCULATION DATA FOR CONSTANT PARTICLE EXPERIMENT

$\underline{M}_w$: 3.3×10^4
NaCl: 5×10^{-4} M
Particle Size: 0.794 μm
PSL Concentration: 677 mg/liter

C_o, mg/liter	C_*, mg/liter	Relative Turbidity, %	Zeta Potential, mv
0.0664	0.0664	89	-48
0.1660	0.1660	90	
0.3320	0.3320	90	-35
0.3750	0.3750	51	
0.4000	0.4000	52	-19
0.4167	0.4167	50	
0.4500	0.4500	58	-15
0.5000	0.5000	61	-13
0.6800	0.6500	68	+15
1.0200	0.9500	82	
2.0400	1.4200	87	+21
4.0000	1.5700	90	
9.9200	1.8000	93	+26
19.8300	2.4000	94	+39
43.3000	3.2000	89	+49

TABLE XXXVIII (Continued)

ADSORPTION AND FLOCCULATION DATA FOR CONSTANT PARTICLE EXPERIMENT

$\underline{M}_w$: 10^6
NaCl: $10^{-2}\underline{M}$
Particle Size: 0.234 μm
PSL Concentration: 17 mg/liter

$\underline{C}_o$, mg/liter	$\underline{C}_*$, mg/liter[a]	Relative Turbidity, %	Zeta Potential, mv
0.0037		88	-20
0.0041		89	
0.0046		90	
0.0053		88	
0.0061		90	
0.0074		85	
0.0092		80	-14
0.0123		78	
0.0184		71	
0.0368		63	-6
0.0460		68	+6
0.0613		72	+10
0.0920		81	
0.1840		87	
0.4000		90	
2.0520		95	
4.0800		97	

[a]Adsorption not measured.

TABLE XXXVIII (Continued)

ADSORPTION AND FLOCCULATION DATA FOR CONSTANT PARTICLE EXPERIMENT

$\underline{M}_w$: 3.3×10^4
NaCl: $10^{-2}\underline{M}$
Particle Size: 0.234 μm
PSL Concentration: 17 mg/liter

$\underline{C}_o$, mg/liter	$\underline{C}_*$, mg/liter[a]	Relative Turbidity, %	Zeta Potential, mv
0.0034		88	-
0.0042		87	-
0.0066		91	-
0.0082		89	-
0.0108		89	-
0.0123		85	-
0.0156		79	-
0.0287		78	-
0.0344		79	-
0.0430		75	≈0
0.0491		79	+
0.0573		84	+
0.1720		87	+
0.0573		84	+
0.1720		87	+
0.4000		94	+
2.0000		93	+
4.0120		93	+

[a]Adsorption not measured.

TABLE XXXVIII (Continued)

ADSORPTION AND FLOCCULATION DATA FOR CONSTANT PARTICLE EXPERIMENT

$\underline{M}_w$: 10^6
NaCl: 5×10^{-4} M
Particle Size: 0.234 μm
PSL Concentration: 17 mg/liter

C_o, mg/liter	C_*, mg/liter[a]	Relative Turbidity, %	Zeta Potential, mv
0.0040		87	-
0.0050		87	-
0.0079		88	-
0.0097		82	-
0.0128		79	-
0.0186		75	-
0.0340		74	-16
0.0408		77	+16
0.0453		82	+
0.0510		88	+
0.0680		89	+
0.2040		92	+
0.4000		91	+
2.0640		94	+

[a]Adsorption not measured.

TABLE XXXVIII (Continued)

ADSORPTION AND FLOCCULATION DATA FOR CONSTANT PARTICLE EXPERIMENT

$\underline{M}_w$: 3.3×10^4
NaCl: 5×10^{-4} M
Particle Size: 0.234 μm
PSL Concentration: 17 mg/liter

C_o, mg/liter	C_*, mg/liter[a]	Relative Turbidity, %	Zeta Potential, mv
0.0158		90	-27
0.0175		90	-
0.0208		89	
0.0221		90	
0.0237		89	
0.0255		85	
0.0277		83	
0.0302		79	-23
0.0369		82	
0.0415		83	+
0.3320		88	+
0.4743		88	
0.5000		93	+
2.0400		96	+

[a] Adsorption not measured.

APPENDIX V

DUPLICATED FLOCCULATION RUNS

Figures 46-48 represent flocculation curves drawn from duplication runs.

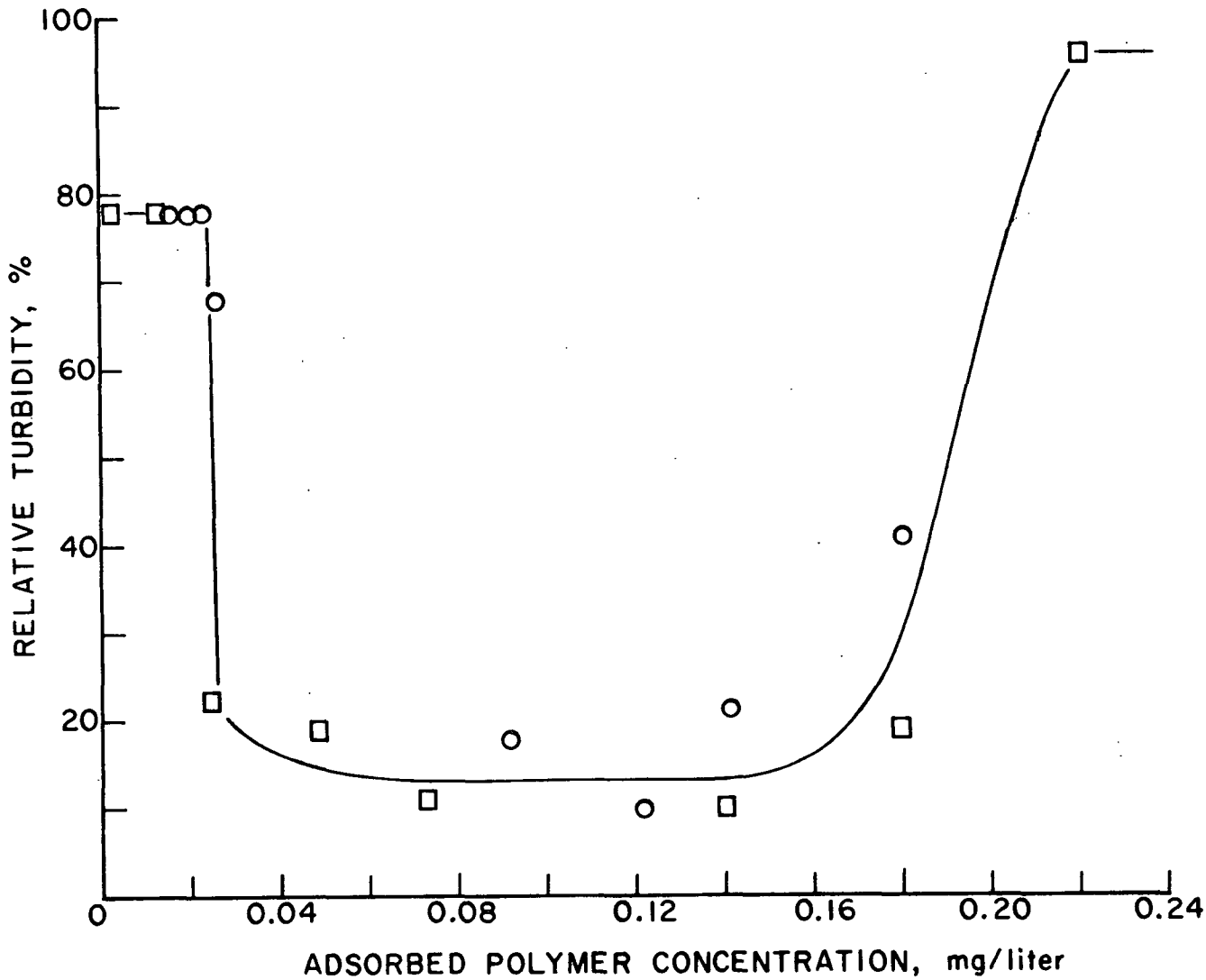

Figure 46. Relative Turbidity Versus Adsorbed Polymer Concentration for PSL Particle Size 0.109 μm with Fraction F_1-6 in 10^{-2}M NaCl. Original (□) and Duplicated (0) Runs. PSL Concentration: 34 mg/Liter

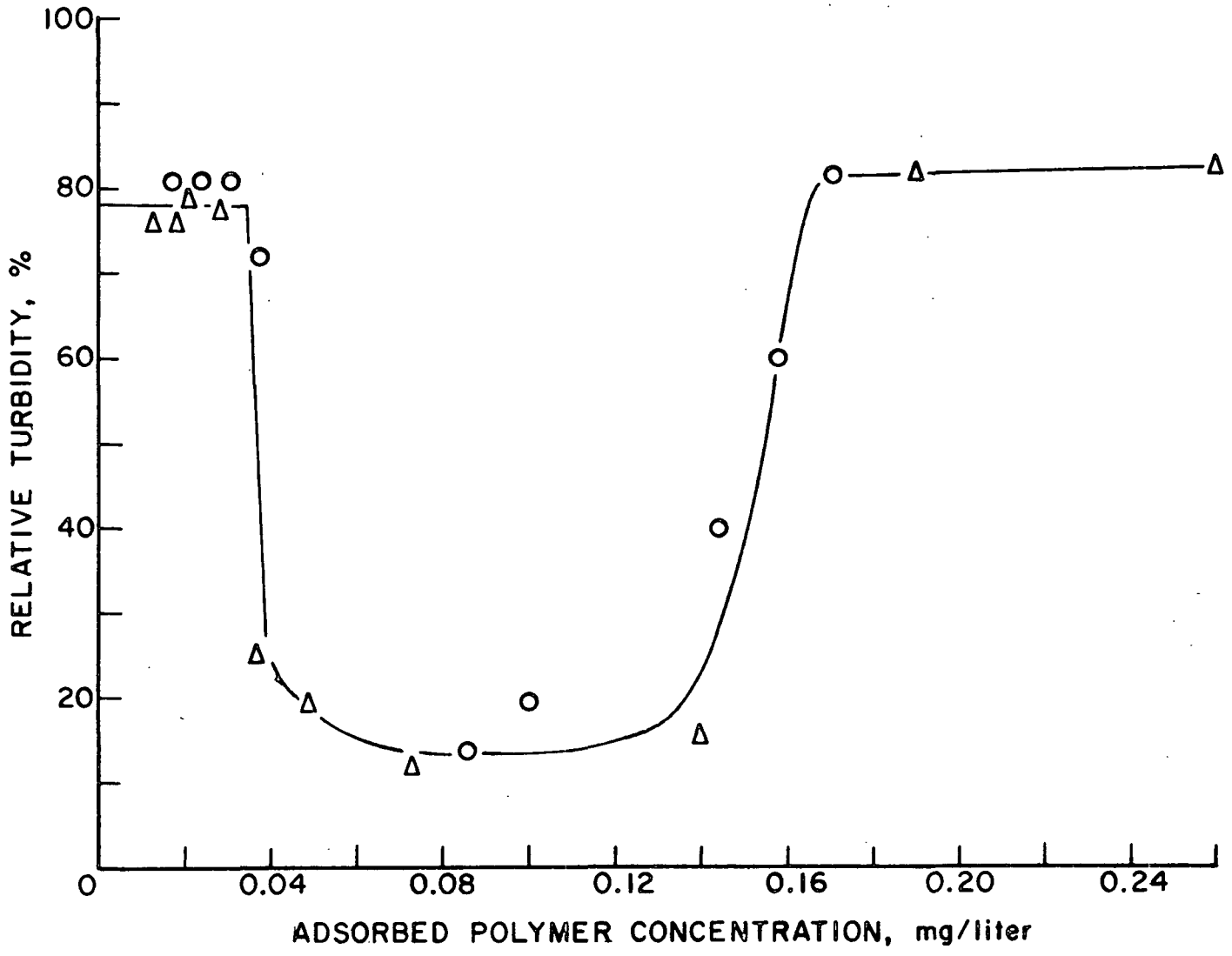

Figure 47. Relative Turbidity Versus Adsorbed Polymer Concentration for PSL Particle Size 0.109 μm with Fraction F_2-7 in 10^{-2}M NaCl. Original (Δ) and Duplicated (o) Runs. PSL Concentration: 34 mg/Liter

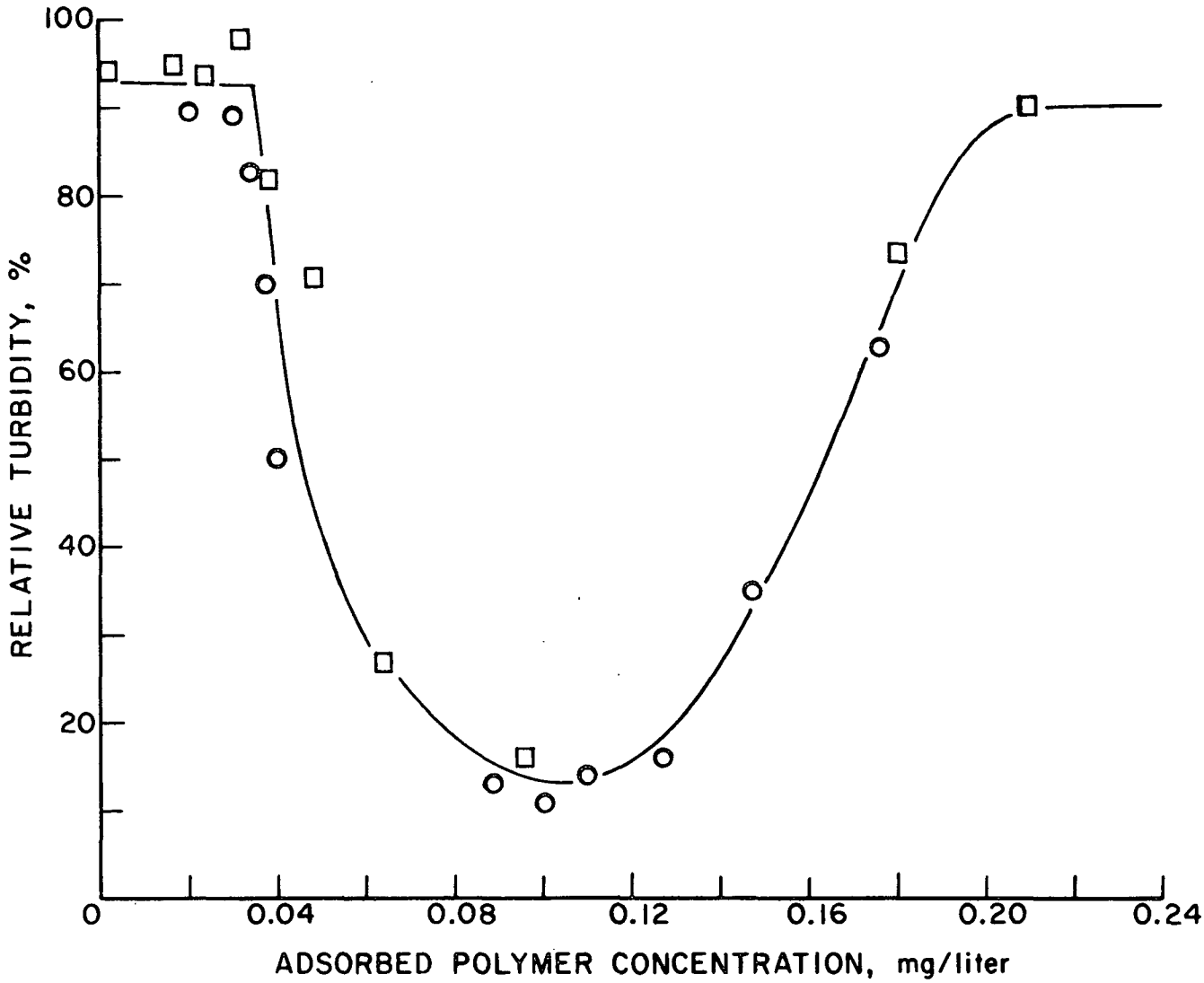

Figure 48. Relative Turbidity Versus Adsorbed Polymer Concentration for PSL Particle Size 0.109 μm with Fraction F_1-6 in 5×10^{-4} M NaCl. Original (□) and Duplicated (0) Runs. PSL Concentration: 34 mg/Liter

APPENDIX VI

THE CFC AND OFC VALUES FOR THE CONSTANT PARTICLE EXPERIMENT

Table XXXIX presents the CFC and OFC values of the constant particle experiment.

TABLE XXXIX

THE CFC AND OFC VALUES FOR THE CONSTANT PARTICLE EXPERIMENT

Particle Size, μm	Fraction	Salt Concn., M	CFC, mg/liter	OFC, mg/liter
1.101	F_1-6	10^{-2}	0.135	1.05
		5×10^{-4}	0.178	1.00
	F_2-7	10^{-2}	0.355	1.10
		5×10^{-4}	0.741	0.88
0.794	F_1-6	10^{-2}	0.069	0.42
		5×10^{-4}	0.084	0.30
	F_2-7	10^{-2}	0.141	0.44
		5×10^{-4}	0.355	0.42
0.234	F_1-6	10^{-2}	0.006	0.034
		5×10^{-4}	0.008	0.028
	F_2-7	10^{-2}	0.012	0.033
		5×10^{-4}	0.025	0.034